Effects of Unburned-Gas Temperature and Heat Loss on the Intrinsic Instabilities of Premixed Flames

予混合火炎の固有不安定性における未燃ガス温度と熱損失の影響

THWE THWE AUNG

Information, Science and Control Engineering

Department of Mechanical Engineering

Graduate School of Engineering

Nagaoka University of Technology

August 2015

Effects of Unburned-Gas Temperature and Heat Loss on the Intrinsic Instabilities of Premixed Flames

予混合火炎の固有不安定性における未燃ガス温度と熱損失の影響

by

THWE THWE AUNG

Dissertation

Presented to the Graduate School of Engineering

Nagaoka University of Technology

in Partial Fulfillment

of the Requirements

for the Degree of

Doctor of Engineering

(Information, Science and Control Engineering)

Nagaoka University of Technology

August 2015

Dedication

This dissertation is dedicated to all my teachers, past and present, and my loving family.

Acknowledgements

First and foremost, I wish like to offer my sincerest and deepest gratitude to my academic advisor, Prof. Satoshi KADOWAKI, for his guidance, valuable suggestions and constant supervising throughout my study with his patience and knowledge. This study would not have been successfully completed without his effort, encouragement and mentoring.

I would like to extend my gratitude to Prof. Seiji KAMIMURA, Prof. Masajiro ABE, Assoc Prof. Wataru YAMAZAKI and Lect. Toshikazu FUJINO for their support, guidance and valuable comments which enable me to improve my dissertation.

I would like to acknowledge the Ministry of Education, Culture, Sports, Science and Technology, Japan for financial support during my study in Nagaoka University of Technology.

Further, I wish to thank the members of Environment, Safety and Energy Laboratory and all my friends, past and present, for their assistance, support and encouragements at all times. I would also like to give my thanks to International Student Affair and Employment Support Office of NUT for their kindly supports.

Finally, my special thanks go to my loving parents, sisters and brothers, who are always supporting and encouraging me with their warmest and best wishes.

Abstract

The effects of unburned-gas temperature and heat loss on the intrinsic instabilities of premixed flames were studied numerically based on the diffusive-thermal model equation and compressible Navier-Stokes equation. The characteristics of cellular premixed flames generated by intrinsic instability, i.e. the burning velocity, unstable behavior and flame structure, were examined. The instability intensity became stronger (weaker) as the unburned-gas temperature became lower (higher). This was due to thermal expansion and apparent activation energy. When radiative heat loss was considered, the normalized burning velocity of a cellular flame increased at small Lewis numbers. This was because of the destabilizing influence of heat loss on small Lewis number flames. The dissertation consists of five chapters:

Chapter 1 describes the introduction about the importance of energy from combustion for environment and human, and the background of research study field. After that, related works are reviewed. In a wide range of the application of combustion processes, to reduce the pollutant emissions from the combustion of fossil fuel is essential. The research in the field of finding the possible ways in the reduction of emissions while increasing of the efficiency of combustion processes has been carried out since many decades. This research is one of the contributing works not only for finding the available energy source in low temperature environment but also for reduction of pollutant emissions from combustion process.

Chapter 2 presents the numerical calculation procedures in detail consisting of theoretical model, assumptions, governing equations and numerical method to elucidate the characteristics of the intrinsic instabilities of premixed flames.

Chapter 3 describes the results of numerical calculations based on the diffusive-thermal model equation on the elucidations of the characteristics of diffusive-thermal instability which is dominant in hydrogen-air or methane-air premixed combustion at sufficiently small Lewis numbers. At first, high-temperature unburned gas is considered for adiabatic and non-adiabatic premixed flames, and then premixed flames with low-temperature unburned gases are simulated. The results include the effects of unburned-gas temperature and heat loss on the characteristics of the premixed flames, such as burning velocities of planar and cellular flames, unstable behavior and structure of cellular flame fronts.

Chapter 4 presents the investigations on both diffusive-thermal and hydrodynamic instabilities especially for premixed flames with low-temperature unburned gases under the adiabatic and non-adiabatic conditions at Lewis numbers equal to and less than unity. The numerical calculation is based on the compressible Navier-Stokes equation with chemical reaction. The numerical results include the characteristics premixed flames, such as burning velocities, unstable behavior and formation of cellular flame fronts. The analytical and numerical results for burning velocity of planar flames and dispersion relations at Lewis number unity are also compared in this chapter.

Chapter 5 consists of the conclusions on the research calculations, and the future works including the different methods for extensive studies to evaluate the characteristics of the lean premixed flames of hydrogen-air or methane-air or hydrogen-hydrocarbon-air with various equivalence ratios and different unburned-gas temperatures.

Table of Contents

Dedication **ii**

Acknowledgements **iii**

Abstract **iv**

Table of Contents **vi**

List of Tables **x**

List of Figures **xii**

List of Symbols **xviii**

Chapter 1: Overview **1**

1.1 Introduction 1

1.2 Background 3

1.2.1 Instabilities in Premixed Flames 3

1.2.2 Heat Loss in Premixed Flames 7

1.3 Related Works 7

1.4 Research Objectives 11

1.5 Structure of the Thesis 11

Chapter 2: Research Methodology **13**

2.1 Introduction 13

2.1.1 General Structure of a Theoretical Model 13

2.1.2 Assumptions for Governing Equations 14

2.2 Governing Equations 15

2.2.1 Diffusive-Thermal Model Equation 15
2.2.1.1 Non-Dimensionalized Equation 16
2.2.1.2 Boundary Conditions 19
2.2.2 Compressible Navier-Stokes Equation 19
2.2.2.1 Non-Dimensionalized Equations 20
2.2.2.2 Boundary Conditions 24
2.2.3 Numerical Method 25
2.2.4 Calculation Domain 26
2.2.5 Characteristics of Dimensionless Parameter 27
2.2.6 Initial Conditions 28

Chapter 3: Diffusive-Thermal Instability of Premixed Flames 30
3.1 Introduction 30
3.2 Numerical Results for High Temperature Unburned-Gas Premixed Flames 31
3.2.1 Effect of Unburned-Gas Temperature 31
3.2.1.1 Numerical results for adiabatic stationary planar flame 31
3.2.1.2 Dispersion relations 33
3.2.1.2 Formation of cellular flame fronts 38
3.2.1.4 Burning velocities of cellular flame 46
3.2.2 Effect of Heat Loss 46
3.2.2.1 Numerical results for non-adiabatic planar flame 47
3.2.2.2 Dispersion relations 50
3.2.2.3 Formation of cellular flame fronts 51
3.2.2.4 Burning velocities of non-adiabatic cellular flames 58
3.3 Numerical Results for Low Temperature Unburned-Gas Premixed Flames 59
3.3.1 Effect of Unburned-Gas Temperature 59

3.3.1.1 Numerical results for adiabatic stationary planar flame 59
3.3.1.2 Dispersion relations 60
3.3.1.3 Formation of cellular flame fronts 62
3.3.1.4 Burning velocities of cellular flames 68
3.3.2 Effect of Heat Loss 68
3.3.2.1 Numerical results for non-adiabatic stationary planar flame 69
3.3.2.2 Dispersion relations 70
3.3.2.3 Formation of cellular flame fronts 72
3.3.2.4 Burning velocities of non-adiabatic cellular flames 77
3.4 Concluding Remarks 78

Chapter 4: Diffusive-Thermal and Hydrodynamic Instabilities of Premixed Flames 79

4.1 Introduction 79
4.2 Numerical Results for Low Temperature Unburned-Gas Premixed Flames 79
4.2.1 Effect of Unburned-Gas Temperature 80
4.2.1.1 Numerical results for adiabatic stationary planar flame 80
4.2.1.2 Dispersion relations 82
4.2.1.3 Formation of cellular flame fronts 86
4.2.1.4 Burning velocities of cellular flames 93
4.2.2 Effect of Heat Loss 94
4.2.2.1 Numerical results for non-adiabatic stationary planar flame 94
4.2.2.2 Dispersion relations 98
4.2.2.3 Formation of cellular flame fronts 100
4.2.2.4 Burning velocities of cellular flames 107
4.3 Comparison of Theoretical and Numerical Results 108

4.4 Concluding Remarks 110

Chapter 5: Conclusions 111

5.1 Conclusions 111

5.2 Future Work 113

References 115

List of Tables

Table 3.1: Frequency factors for Le = 0.3 and 0.5. 30

Table 3.2: Burning velocity of adiabatic planar flame at Le = 0.3 and 0.5. 32

Table 3.3: Critical wavelengths at Le = 0.3 and 0.5, T_u = 1.0~2.5. 36

Table 3.4: Zeldovich numbers for T_u = 1.0~2.5. 38

Table 3.5: D_{cell}, L_{cf} and D_{cell}/λ_c of cellular flames at Le = 0.3 and 0.5. 41

Table 3.6: Burning velocities of cellular flames and normalized values at Le = 0.3 and 0.5. 46

Table 3.7: Maximum heat loss parameter at Le = 0.3 and 0.5. 48

Table 3.8: Burning velocities of non-adiabatic planar flames at Le = 0.3 and 0.5, A = 1×10^{-4}. 48

Table 3.9: Critical wavelengths at Le = 0.3 and 0.5 ($A = 1\times10^{-4}$). 51

Table 3.10: D_{cell}, L_{cf} and D_{cell}/λ_c at Le = 0.3 and 0.5, and T_u = 1.0~2.5 ($A = 1\times10^{-4}$). ... 53

Table 3.11: Burning velocities of cellular flames and normalized values at Le =0.3 and 0.5 ($A = 1\times10^{-4}$). 58

Table 3.12: Burning velocity of a planar flame for Le = 0.3 and 0.5, T_u = 1.0~0.6. 60

Table 3.13: Critical wavelengths at Le = 0.3 and 0.5. 61

Table 3.14: D_{cell}, L_{cf} and D_{cell}/λ_c at Le = 0.3 and 0.5, and T_u = 1.0~0.6. 63

Table 3.15: Burning velocities of cellular flames and normalized values at Le =0.3 and 0.5. 68

Table 3.16: Burning velocities of planar flames depend on A at Le = 0.3. 70

Table 3.17: Burning velocities of planar flames depend on A at Le = 0.5. 70

Table 3.18: Critical wavelengths at Le = 0.3 and 0.5 ($A = 4\times10^{-5}$). 72

Table 3.19: D_{cell}, L_{cf} and D_{cell}/λ_c at Le = 0.3 and 0.5, and T_u = 1.0~0.6 ($A = 4\times10^{-5}$). ... 77

Table 3.20: Burning velocities of cellular flames and normalized values at Le = 0.3 and 0.5, and T_u = 1.0~0.6 (A = 4×10^{-5}). 77

Table 4.1: Burning velocity of adiabatic planar flame at Le = 0.5~1.0. 80

Table 4.2: Critical wavelengths at Le = 0.5~1.0. 84

Table 4.3: Zeldovich numbers for T_u = 1.0~0.6. 86

Table 4.4: D_{cell}, L_{cf} and D_{cell}/λ_c of cellular flames at Le = 0.5~1.0 and T_u = 1.0~0.6. ... 86

Table 4.5: Burning velocities and normalized values of cellular flames at Le = 0.5~1.0 and T_u = 1.0~0.6. 94

Table 4.6: Burning velocity of planar flame depends on A at Le = 0.5. 96

Table 4.7: Burning velocity of planar flame depends on A at Le = 0.7. 96

Table 4.8: Burning velocity of planar flame depends on A at Le = 1.0. 96

Table 4.9: Critical wavelengths at Le = 0.5~1.0 (A = 4×10^{-5}). 100

Table 4.10: D_{cell}, L_{cf} and D_{cell}/λ_c of cellular flames at Le = 0.5~1.0 and T_u = 1.0~0.6 (A = 4×10^{-5}). 104

Table 4.11: Burning velocities and normalized values of cellular flames at Le = 0.5~1.0 and T_u = 1.0~0.6 (A = 4×10^{-5}). 107

Table 4.12: Theoretical and numerical results of burning velocities of planar flames at Le = 1.0. 109

List of Figures

Figure 1.1: World population and energy demand growth. [6] 2

Figure 1.2: CO_2 emission trend from combustion of fossil fuels. [3] 3

Figure 1.3: Illustration of the mechanism of the diffusive-thermal instability (a) *Le* <1 and (b) *Le* >1. [11] 5

Figure 1.4: Illustration of the mechanism of DL instability. 6

Figure 1.5: Temperature profiles of adiabatic and non-adiabatic premixed flames. 7

Figure 2.1: General structure of a theoretical model 13

Figure 2.2: Calculation domain and coordinate system. 27

Figure 2.3: Distribution of Y and T in a stationary planar flame, D-T model. 28

Figure 2.4: Distribution of ρ, e, p, Y and T in a stationary planar flame, N-S model. 29

Figure 2.5: Disturbance on a stationary planar flame. 29

Figure 3.1: Distribution of temperature at *Le* = 0.3 and 0.5. 32

Figure 3.2: Distribution of mass fraction at *Le* = 0.3 and 0.5. 32

Figure 3.3: Reaction rate at *Le* = 0.3 and 0.5. 33

Figure 3.4: Evolution of disturbed flame front at *Le* = 0.5, T_u = 1.0. 34

Figure 3.5: Amplitude growth rate of disturbance at *Le* = 0.5, T_u = 1.0. 34

Figure 3.6: Dispersion relations at *Le* = 0.3 and T_u = 1.0~2.5. 35

Figure 3.7: Dispersion relations at *Le* = 0.5 and T_u = 1.0~2.5. 36

Figure 3.8: Normalized dispersion relations at *Le* = 0.3 and T_u = 1.0~2.5. 37

Figure 3.9: Normalized dispersion relations at *Le* = 0.5 and T_u = 1.0~2.5. 38

Figure 3.10(a) (b): Evolution of disturbed flame fronts at *Le* = 0.3, T_u = 1.0 and 1.5. 40

Figure 3.10(c) (d): Evolution of disturbed flame fronts at *Le* = 0.3, T_u=2.0 and 2.5. 41

Figure 3.11 (a) (b) (c): Temperature distribution of cellular flame fronts at *Le* = 0.3 and T_u =1.0~2.0. 42

Figure 3.11 (d): Temperature distribution of cellular flame fronts at Le = 0.3 and T_u =2.5. 43

Figure 3.12 (a) (b): Evolution of disturbed flame fronts at Le = 0.5, T_u=1.0 and 1.5..... 43

Figure 3.12 (c) (d): Evolution of disturbed flame fronts at Le = 0.5, T_u=2.0 and 2.5..... 44

Figure 3.13 (a): Temperature distribution of cellular flame fronts at Le = 0.5 and T_u =1.0. 44

Figure 3.13 (b) (c) (d): Temperature distribution of cellular flame fronts at Le = 0.5 and T_u =1.5~2.5. 45

Figure 3.14: Relation between heat loss parameter and burning velocity at Le = 0.3... 47

Figure 3.15: Relation between heat loss parameter and burning velocity at Le = 0.5... 48

Figure 3.16: Distribution of temperature at Le = 0.3 and 0.5 ($A = 1\times10^{-4}$). 49

Figure 3.17: Distribution of mass fraction at Le = 0.3 and 0.5 ($A = 1\times10^{-4}$). 49

Figure 3.18: Reaction rate at Le = 0.3 and 0.5 ($A = 1\times10^{-4}$). 49

Figure 3.19: Dispersion relation (a) and normalized dispersion relation (b) at Le = 0.3 and T_u = 1.0~2.5 ($A = 1\times10^{-4}$). 50

Figure 3.20: Dispersion relation (a) and normalized dispersion relation (b) at Le = 0.5 and T_u = 1.0~2.5 ($A = 1\times10^{-4}$). 51

Figure 3.21 (a) (b): Evolution of disturbed flame fronts at Le = 0.3, T_u = 1.0 and 1.5..... 52

Figure 3.21 (c) (d): Evolution of disturbed flame fronts at Le = 0.3, T_u = 2.0 and 2.5..... 53

Figure 3.22 (a) (b) (c): Evolution of disturbed flame fronts at Le = 0.5, T_u = 1.0~2.0..... 54

Figure 3.22 (d): Evolution of disturbed flame fronts at Le = 0.5, T_u = 2.5..... 55

Figure 3.23 (a) (b): Temperature distribution of cellular flames at Le = 0.3, T_u = 1.0, 1.5. 55

Figure 3.23 (c) (d): Temperature distribution of cellular flames at Le = 0.3, T_u = 2.0, 2.5. 56

Figure 3.24 (a): Temperature distribution of cellular flames at Le = 0.5, T_u = 1.0..... 56

Figure 3.24 (b) (c) (d): Temperature distribution of cellular flames at Le = 0.5, T_u = 1.5~2.5..... 57

Figure 3.25: Dispersion relation at Le = 0.3 and 0.5, T_u = 1.0~0.6. 62

Figure 3.26: Normalized dispersion relation at Le = 0.3 and 0.5, T_u = 1.0~0.6. 62

Figure 3.27 (a): Evolution of disturbed flame fronts at Le = 0.3, T_u = 1.0. 63

Figure 3.27 (b) (c): Evolution of disturbed flame fronts at Le = 0.3, T_u = 0.8 and 0.6..... 64

Figure 3.28 (a): Evolution of disturbed flame fronts at Le = 0.5, T_u = 1.0. 64

Figure 3.28 (b) (c): Evolution of disturbed flame fronts at Le = 0.5, T_u = 0.8 and 0.6..... 65

Figure 3.29 (a) (b) (c): Temperature distribution of cellular flame fronts at Le = 0.3, T_u = 1.0~0.6..... 66

Figure 3.30 (a) (b) (c): Temperature distribution of cellular flame fronts at Le = 0.5, T_u = 1.0~0.6..... 67

Figure 3.31: Relation between heat loss parameter and burning velocity at Le = 0.3 and 0.5..... 69

Figure 3.32: Dispersion relation at Le = 0.3 and 0.5, T_u = 1.0~0.6 ($A = 4\times10^{-5}$)..... 71

Figure 3.33: Normalized dispersion relation at Le = 0.3 and 0.5, T_u = 1.0~0.6 ($A = 4\times10^{-5}$). 71

Figure 3.34 (a) (b) (c): Evolution of disturbed flame fronts at Le = 0.3, T_u=1.0~0.6 ($A = 4\times10^{-5}$). 73

Figure 3.35 (a) (b) (c): Evolution of disturbed flame fronts at Le = 0.5, T_u=1.0~0.6 ($A = 4\times10^{-5}$). 74

Figure 3.36 (a) (b) (c): Temperature distribution of cellular flame fronts at Le = 0.3, T_u=1.0~0.6 ($A = 4\times10^{-5}$). 75

Figure 3.37 (a) (b) (c): Temperature distribution of cellular flame fronts at Le = 0.5, T_u=1.0~0.6 (A = 4×10^{-5}). 76

Figure 4.1: Distribution of T, ρ, e, p, Y at Le = 0.5 and T_u =1.0. 81

Figure 4.2: Distribution of T, ρ, e, p, Y at Le = 0.5 and T_u =0.8. 81

Figure 4.3: Distribution of T, ρ, e, p, Y at Le = 0.5 and T_u =0.6. 81

Figure 4.4: Evolution of the disturbed flame front at Le = 0.5 and T_u = 1.0 for adiabatic premixed flame. 84

Figure 4.5: Amplitude growth rate of disturbance at Le = 0.5 and T_u = 1.0. 84

Figure 4.6: Dispersion relation at Le = 0.5~1.0 and T_u = 1.0~0.6. 85

Figure 4.7: Normalized dispersion relation at Le = 0.5~1.0 and T_u = 1.0~0.6. 85

Figure 4.8 (a) (b) (c): Evolution of disturbed flame fronts at Le = 0.5 and T_u = 1.0~0.6. 87

Figure 4.9 (a) (b) (c): Evolution of disturbed flame fronts at Le = 0.7 and T_u = 1.0~0.6. 88

Figure 4.10 (a) (b) (c): Evolution of disturbed flame fronts at Le = 1.0 and T_u = 1.0~0.6. 89

Figure 4.11 (a) (b): Temperature distribution of cellular flames at Le = 0.5 and T_u = 1.0 and 0.8. 90

Figure 4.11 (c): Temperature distribution of cellular flames at Le = 0.5 and T_u = 0.6. 91

Figure 4.12 (a) (b): Temperature distribution of cellular flames at Le = 0.7 and T_u = 1.0 and 0.8. 91

Figure 4.12 (c): Temperature distribution of cellular flames at Le = 0.7 and T_u = 0.6. 92

Figure 4.13 (a) (b): Temperature distribution of cellular flames at Le = 1.0 and T_u = 1.0 and 0.8. 92

Figure 4.13 (c): Temperature distribution of cellular flames at Le =1.0 and T_u = 0.6. 93

Figure 4.14: Relation between heat loss parameter and burning velocity at Le = 0.5… 94

Figure 4.15: Relation between heat loss parameter and burning velocity at Le = 0.7… 95

Figure 4.16: Relation between heat loss parameter and burning velocity at Le = 1.0… 95

Figure 4.17: Distribution of T, ρ, e, p, Y at Le = 0.5 and T_u = 1.0 ($A = 4\times10^{-5}$)..... 97

Figure 4.18: Distribution of T, ρ, e, p, Y at Le = 0.5 and T_u = 0.8 ($A = 4\times10^{-5}$)..... 97

Figure 4.19: Distribution of T, ρ, e, p, Y at Le = 0.5 and T_u = 0.6 ($A = 4\times10^{-5}$)..... 97

Figure 4.20: Dispersion relation at Le = 0.5~1.0 and T_u = 1.0~0.6 ($A = 4\times10^{-5}$). 99

Figure 4.21: Normalized dispersion relation at Le = 0.5~1.0 and T_u = 1.0~0.6 ($A = 4\times10^{-5}$). 99

Figure 4.22 (a) (b) (c): Evolution of disturbed flame fronts at Le = 0.5 and T_u = 1.0~0.6 ($A = 4\times10^{-5}$). 101

Figure 4.23 (a) (b) (c): Evolution of disturbed flame fronts at Le = 0.7 and T_u = 1.0~0.6 ($A = 4\times10^{-5}$). 102

Figure 4.24 (a) (b) (c): Evolution of disturbed flame fronts at Le = 1.0 and T_u = 1.0~0.6 ($A = 4\times10^{-5}$). 103

Figure 4.25 (a) (b): Temperature distribution of cellular flame fronts at Le = 0.5, T_u=1.0 and 0.8 ($A = 4\times10^{-5}$). 104

Figure 4.25 (c): Temperature distribution of cellular flame fronts at Le = 0.5, T_u=0.6 ($A = 4\times10^{-5}$). 105

Figure 4.26 (a) (b): Temperature distribution of cellular flame fronts at Le = 0.7, T_u=1.0 and 0.8 ($A = 4\times10^{-5}$). 105

Figure 4.26 (c): Temperature distribution of cellular flame fronts at Le = 0.7, T_u=0.6 ($A = 4\times10^{-5}$). 106

Figure 4.27 (a) (b): Temperature distribution of cellular flame fronts at Le = 1.0, T_u=1.0 and 0.8 ($A = 4\times10^{-5}$). 106

Figure 4.27 (c): Temperature distribution of cellular flame fronts at Le = 1.0, T_u=0.6 (A = 4×10^{-5}). 107

Figure 4.28: Theoretical and numerical results of dispersion relations at Le = 1.0..... 109

List of Symbols

A	non-dimensional radiation-loss parameter of a planar flame, referred to as κ / $\delta^2 T_{u0}^3$
A_{max}	non-dimensional radiation-loss parameter under the quenching condition of a planar flame, referred to as κ / $\delta^2 T_{u0}^3$
a	non-dimensional amplitude of a disturbance, referred to as δ
a_i	non-dimensional initial amplitude of a disturbance, referred to as δ
B	non-dimensional frequency factor of the reaction rate, referred to as S_{u0}/ δ
C_p	specific heat at constant pressure [J/kgK]
c_u	sound velocity of the unburned gas
D	diffusion coefficient [m^2/s]
D_{cell}	non-dimensional cell depth, referred to as δ
E	non-dimensional activation energy of the reaction rate, referred to as RT_{u0}
e	non-dimensional stored energy, referred to as p_u
Le	Lewis number (= α/D)
L_{cf}	non-dimensional ratio of flame length, referred to as δ
M_u	Mach number of the burning velocity of an adiabatic planar flame (=S_u / c_u)
Pr	Prandtl number (=ν / α)
p	non-dimensional pressure, referred to as p_0
p_0	pressure of the unburned gas
Q	non-dimensional heating value, referred to as $C_p T_{u0}$
R	universal gas constant [J/molK]
S_{u0}	burning velocity of an adiabatic planar flame under the room temperature condition [m/s]
S_u	non-dimensional burning velocity of a planar flame, referred to as S_{u0}

S_{cf}	non-dimensional burning velocity of a cellular flame, referred to as S_{u0}
T	non-dimensional temperature, referred to as T_{u0}
T_b	non-dimensional adiabatic flame temperature, referred to as T_{u0}
T_u	non-dimensional temperature of the unburned gas, referred to as T_{u0}
T_{u0}	room temperature [K]
U	non-dimensional inlet flow velocity of the unburned-gas, referred to as S_{u0}
Y	mass fraction of the unburned-gas [-]
Y_u	mass fraction of the unburned-gas in the inlet flow region [-]
W	non-dimensional reaction rate, referred to as δ/S_{u0}
t	non-dimensional time, referred to as δ/S_{u0}
u, v	non-dimensional velocities in x- and y-directions, referred to as S_u
x, y	space coordinate
α	thermal diffusivity [m^2/s]
δ	preheat zone thickness (= α/S_{u0})
κ	thermal conductivity [W/mK]
γ	ratio of two specific heats
β	Zeldovich number
k	non-dimensional wave number of a disturbance, referred to as $1/\delta$
k_c	non-dimensional critical wave number of a disturbance, referred to as $1/\delta$
k_m	non-dimensional marginal wave number of a disturbance, referred to as $1/\delta$
k^*	non-dimensional normalized wave number (k/S_u)
λ	non-dimensional wavelength of a disturbance, referred to as δ
λ_c	non-dimensional critical wavelength of a disturbance, referred to as δ
μ	dynamic viscosity [kg/m.s]
ν	kinematic viscosity [m^2/s]

ρ_0	density of the unburned gas [kg/m^3]
ρ	density of burned and unburned gases [kg/m^3]
ω	growth rate, referred to as S_{u0}/δ
ω^*	normalized growth rate, (ω/S_u^2)

Chapter 1: Overview

1.1 INTRODUCTION

Various forms of energy from combustions of fuels (solid, liquid or gas) and oxidizer (oxygen from air) is used in many different applications in our society, as in domestic needs; cooking and space heating, and in industrial needs; power generation and manufacturing, and in transportation. Energy from combustion is invaluable power for our needs, but many hazardous cases have been occurred due to the explosion and emissions of harmful gases from the combustions of fossil fuels, which cause the losses of human lives and their properties. Emissions from combustion such as carbon monoxide, carbon dioxide (CO_2), nitrogen oxides (NO_x), sulphur dioxide and particulate matter can cause air pollution and climate change. Carbon dioxide emission from fuel combustion in 2012 was approximately 2 times that in 1972 from both industrialized and developing countries. The increase of pollutant emissions leads to cause more intense storms, flood, and sever draught, wildfire, intense heat waves, and an increase of ozone level. In addition, water scarcities caused by natural or man-made scarify the world. [1-5]

The increase of world population demands more energy needs as shown in Fig.1.1 [6] and energy production from the combustion will increase along with the population growth.

The more the energy we need, the more the fuel consumes and the more the harmful gases release. Although we have a large variety of alternate energy sources, such as nuclear, solar, wind, hydroelectric, geothermal and ocean thermal energy conversion, energy obtained from burning of fossil fuels supplies a large fraction for the total world energy needs, approximately 87 percent in 2012. [7] Thus, combustion science needs to allow the increase of energy without increasing emissions, making climate worse,

and wasting fossil fuels. We need better combustion systems to reduce pollutant emissions by maximizing the efficiency with as little fuel as possible. [8] Figure1.2 shows the global emission of CO_2 from combustion of fossil fuels. [3] Carbon dioxide emission increases along with the increase of energy demand and population growth.

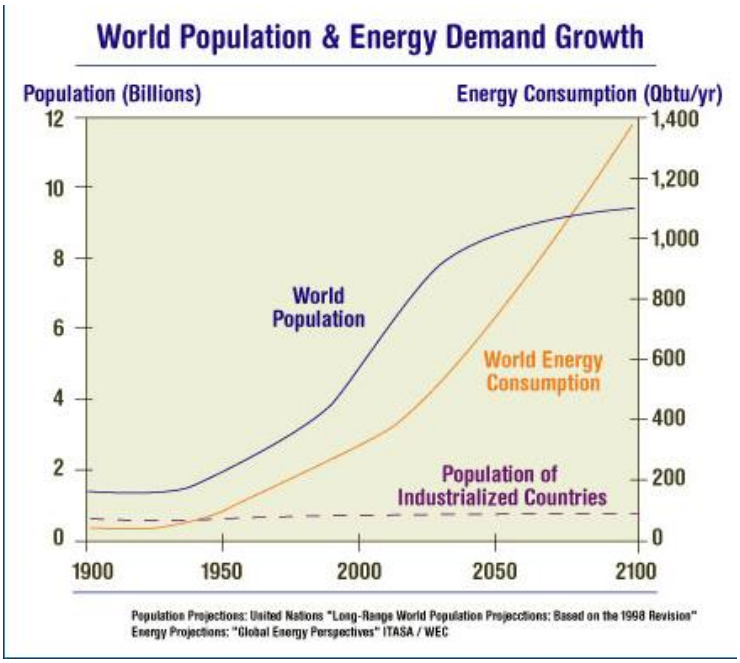

Figure 1.1: World population and energy demand growth. [6]

Source: http://pictorial-guide-to-energy.blogspot.jp/2011/03/world-population-and-energy-demand.html

Some examples for reducing CO_2 include: replacing oil with gas fuel, increasing renewable energy applications and nuclear power generation in power production sectors; increasing efficiency of vehicles in transportation and furnaces or combustors in industrial sectors. Among the various possible ways in increasing efficiency in combustion systems, one type of combustion, known as lean combustion in which deficient amount of fuel (gas, liquid or solid) react with excess amount of air has been used for many decades in energy production and power generation in gas turbines, boilers furnaces and internal combustion

engines. The reduction in hydrocarbon fuels reduces hydrocarbon and carbon monoxide emissions in flue gases. In addition, the decrease of flame temperature reduces the NO_x formation. Because of its advantages, the progress in research of the technology for lean combustion system in various applications is noticeably in combustion science.

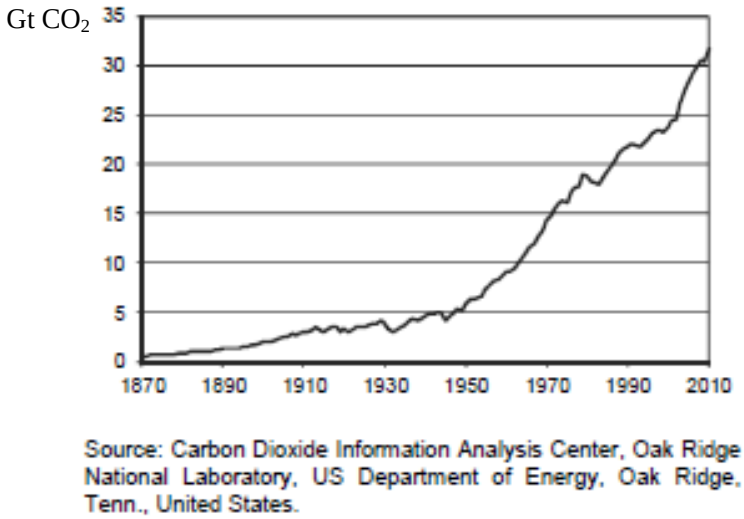

Figure 1.2: CO_2 emission trend from combustion of fossil fuels. [3]

Source:
http://www.iea.org/publications/freepublications/publication/CO2EmissionsFromFuelCombustionHighlights2014.pdf

1.2 BACKGROUND

1.2.1 Instabilities in Premixed Flames

Premixing of fuel and oxidizer prior to reaction in lean combustion, so called lean premixed combustion favors the complete combustion of fuel with excess air. Because of its merit in reduction of CO and NOx, lean premixed combustion is used in a wide range of applications, such as gas turbines, industrial furnaces, boilers and internal combustion engines. Intrinsic instabilities involve in combustion phenomena within the combustion

chamber, and basically, there are three types: hydrodynamic instability (Darrieus-Landau, DL instability), diffusive-thermal instability and body-force instability.

Hydrodynamic instability occurs due to the thermal expansion through the flame surface. It is most essential for the flame instability, since all premixed flames in exothermic reactions are accompanied by thermal expansion. Diffusive-thermal instability mostly occurs when molecular diffusivity of the reactant is larger than the thermal diffusivity, i.e. Lewis number of the deficient reactant is lower than unity ($Le < 1$). The preferential diffusion of mass and heat is essential for diffusive-thermal instability. Body-force instability occurs owing to the effects of buoyancy when the densities of upward and downward propagating fluids are different. [10] Specifically, in the combustion of hydrogen-air (H_2-air) premixture, there is no emission of carbon, but diffusive-thermal instability is dominant because density of hydrogen is smaller than that of air, and it is easy to become unstable. However, body-force instability is hardly occurred due to the large burning velocities of H_2-air premixed flames. To apply H_2-air lean premixed combustion, understanding the mechanism of intrinsic instabilities is important to control the combustion system properly and safely. Especially, diffusive-thermal and hydrodynamic instabilities have mainly influence on H_2-air premixture.

The mechanisms of diffusive-thermal instability are illustrated in Figs. 1.3 (a) and (b). The mechanisms of diffusive-thermal instability are as follows:

- If the Lewis number is less than unity ($Le < 1$), the diffusion of reactants is faster than that of heat. When the flame front is convex toward the unburned gas, the diffused reactants are heated and burn faster, local burning velocity (S) becomes higher than the burning velocity of planar flame front (S_u). Thus, the flame moves further toward the unburned-gas region. When the flame front is convex toward the burned gas, reactants diffuse in a large zone, and the local burning

velocity becomes lower than planar flame velocity. Thus, the flame moves further toward the burned-gas region. In this way, the planar flame becomes unstable and cellular flame forms.

- If the Lewis number is greater than unity ($Le > 1$), as the similar analysis, when the flame front is convex toward the unburned gas, the local burning velocity decreases, and it increases when the region is convex towards the burned gas. Flame surface decreases and flame front is stable. [10-12]

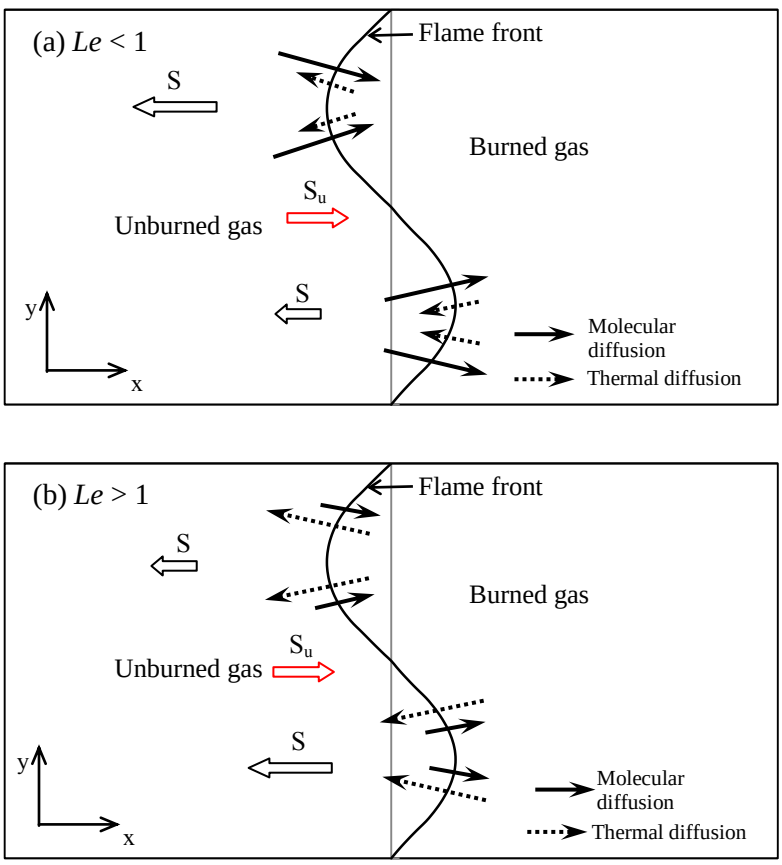

Figure 1.3: Illustration of the mechanism of the diffusive-thermal instability (a) $Le < 1$ and (b) $Le > 1$. [11]

Hydrodynamic (DL) instability is caused by the change in densities through unburned and burned gases because of thermal expansion. The mechanism of DL instability is illustrated in Fig.1.4. [10] When an infinite thin flame is perturbed with a disturbance, noticing that the streamline tube area A is same in both sides far away from flame sheet where disturbance is not exit, the flow velocity normal to the flame sheet (S_b) is large in burned gas region owing to the increase of flame temperature through the thermal expansion if the sheet is convex toward the unburned gas region. The tangential stream lines on the flame in the unburned and burned gas regions continuously diverge and converge as in illustration. Therefore, when the flame sheet is convex toward the unburned-gas region, flow velocity (S) decreases due to the increase of stream tube area. In addition, the negative value of flame displacement favors the decrease in flow velocity and thus flame moves further toward the unburned-gas region. Similarly, when the flame sheet is concave towards the burned-gas region, reduction in stream tube area causes the increase in flow velocity, and positive displacement of the flame displacement favors the flame to move further toward the burned-gas region. This situation causes the unbalance between velocity of a planar flame and local burning velocities, and hence the flame becomes unstable. [10][12]

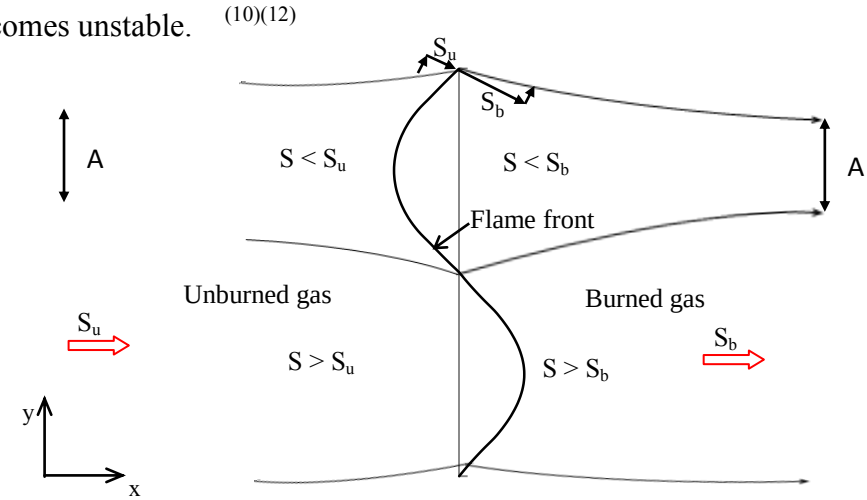

Figure 1.4: Illustration of the mechanism of DL instability.

1.2.2 Heat Loss in Premixed Flames

In practical combustion processes, the available energy from chemical reaction loses in many ways for various reasons. Heat losses from the flame by conduction, convection and radiation are some examples. Temperature in the burned gas region decreases and cannot reach the adiabatic flame temperature due to the heat loss as shown in Fig. 1.5. [14] According to Arrhenius' law, changes in temperature strongly affect the reaction rate, and that decrease of temperature reduces the reaction rate in premixed flames. The flammable limit becomes lower and the flame fronts become unstable. Then, the flame extinguishes when heat loss rate reaches beyond heat production rate. [12][14] Thus, to prevent the extinction of flame in combustion process, the understanding of the effects of heat loss on premixed flame is indispensible.

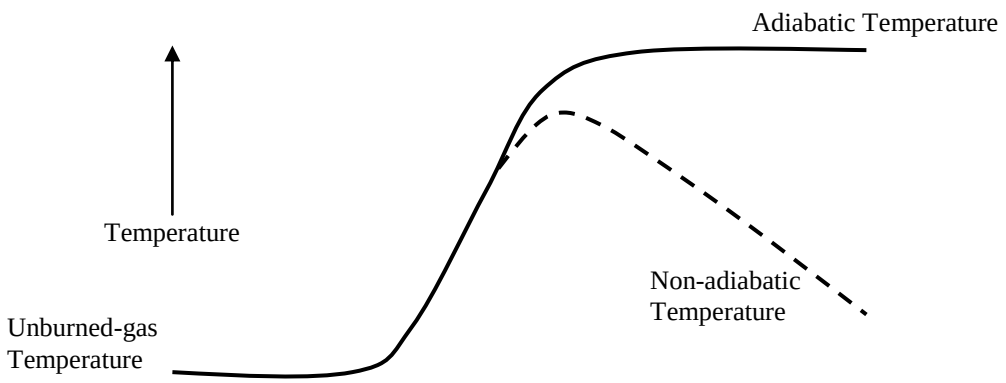

Figure 1.5: Temperature profiles of adiabatic and non-adiabatic premixed flames.

1.3 RELATED WORKS

Although different types of combustion devices have different combustion processes based on the fuels and applications, irreversibility always appears in almost all combustion whatever the flame is premixed or non-premixed. It makes reduction in

available energy (exergy) in many ways including the incomplete combustion and heat losses to the surrounding from the combustion system. If the combustion is not complete, unburned fuel will flue out together with exhaust gases and energy from combustion will decrease. It is essential to increase the exergy, i.e. to reduce the energy loss in combustion processes. One of the effective methods is preheating the combustible mixture by heat transfer from hot burned gases or flue gas, i.e., excess enthalpy combustion, and the another one is preheating the air prior combustion by recirculation of mass together with heat, i.e., high-temperature air combustion. [15-17] The concept of excess enthalpy combustion was introduced by Weinberg [17] and it was extensively studied to the flammable range by heat recirculation. [18][19] Their experimental results show that the mixture having lower limit of lean flammability [18] and ultra lean-mixture [19] were completely burned by the recirculation of heat. There are also several investigations on the fundamentals of excess enthalpy combustion. [20-22]

In high-temperature air combustion, very remarkable phenomena of combustion were observed when the temperature of combustible mixtures was sufficiently high, and the oxygen concentration in mixtures was considerably low. This type of combustion also reduces the NO_x, CO and CO_2 emissions. [23-25] Roman et al. (2005) examined the efficiencies of furnace with gaseous, liquid and solid fuels in the combustion with highly preheated air.[26] Their results prove that high-temperature air combustion is an effective technology for industrial furnaces.

To apply these types of combustion systems in industrial fields, it is indispensible to get the knowledge on flame characteristics including the flammability limit, flame structure, and flame instability. Especially, instability of the flames stands in important role. Thus, the elucidation of the mechanisms of instability is significant in both academicism and industry. Kadowaki (2010) and Kadowaki et al. (2011) performed the

analytical and numerical studies on the intrinsic instabilities in premixed flames with high temperature unburned gas and constant adiabatic flame temperature. [27][28] The results show that the unburned-gas temperature has a great influence on intrinsic instability, i.e., burning velocity and structure of cellular flame fronts.

In practical combustion systems, the instability of premixed flames is strongly affected by heat losses owing to irreversibility. Thus, it is clear that the research on instability of premixed flames with heat loss attracts attention to researchers.

Linear analyses on the instability of non-adiabatic premixed flame, based on the diffusive-thermal model equation with conductive heat loss were performed by Joulin and Clavin, (1979) analytically [29], Soharb and Chao, (1984) [30], and with radiative heat loss by Kagan and Sivashinsky, (1997) numerically. [31] The results show that the flame fronts become more unstable due to effects of heat losses. Moreover, diffusive-thermal and hydrodynamic instabilities were investigated numerically based on the diffusive-thermal model and compressive Navier-Stokes equation to demonstrate the effect of heat loss on unstable behavior of cellular flame fronts. [32-37] There is still lack of information on the intrinsic instability of high-temperature premixed flame with heat loss. Thus, diffusive-thermal instability of high-temperature premixed flames with heat loss was investigated numerically by diffusive-thermal model with constant density approximation under the conditions of constant enthalpy. [38]

However, it still needs to investigate the instability phenomena for low-temperature unburned-gas premixed flames because it is important in finding the source of energy for extremely cold region, especially South Pole of Antarctica where researchers and scientists from various fields are exploring the natural process. [39-41] Most of the energy for research stations and field camps are supplied by the combustion of liquid fuels, and there are some problems in handlings of liquid fuel and in emissions of

pollutant gases and particulate matter from combustion. To reduce the reliance on fossil fuels by using the renewable energy source as a supplementary energy, some researches on wind and solar energy were performed, such as wind-hydrogen energy system [(42)], wind and solar energy with advanced technology. [(43)(44)] Although renewable energy resources are applicable to the effective ways, the payback period of systems depending on the projects takes place many years.[(45)] Thus, it still seriously needs to find the possible ways to solve the problems on energy source.

Choosing the gaseous fuel, such as hydrogen and/or methane, with air for lean premixed combustion is one of the effective ways. This is because that hydrogen and methane keep gaseous state under the conditions of very low temperature (-89.2°C at Antarctica), and reduce the emissions of pollutants comparing with those from the burning of liquid fuels which have been used in research stations. In reality, hydrogen and methane are lighter than air and it is easy to become unstable. Therefore, doing research to obtain the knowledge on the mechanism of hydrogen/methane-air lean premixed flames is of very significance.

Thus, the intrinsic instability of premixed flames not only for high unburned-gas temperature but also for low unburned-gas temperature with the effects of heat loss were studied by numerically with diffusive-thermal model equation to examine the diffusive-thermal instability and Navier-Stokes equation to examine the thermal expansion effect, under the constant temperature jump conditions. [(46)(47)]

1.4 RESEARCH OBJECTIVES

The objectives of this study are:

1. To elucidate numerically the effects of unburned-gas temperature and heat loss on the diffusive-thermal instability of high temperature premixed flames with constant density approximation under the condition of constant temperature jump to obtain the knowledge on burning velocities of planar and cellular flames, characteristics and unstable behavior of the cellular flame fronts for Lewis numbers less than unity.
2. To elucidate numerically the effects of unburned-gas temperature and heat loss on the diffusive-thermal effect and hydrodynamic (thermal expansion) effect of the premixed flames with low unburned-gas temperature under the constant temperature jump condition on the burning velocities of planar and cellular flames, characteristics and unstable behavior of the cellular flame fronts for Lewis numbers equal to and less than unity.

1.5 STRUCTURE OF THE THESIS

This thesis is organized into five chapters.

Chapter 1 consists of introduction on energy demand from combustion and the effects of pollutant emissions; background of the research study including the explanations of the mechanisms of intrinsic instabilities of premixed flames, effect of heat loss; related research works on various investigation of lean premixed combustion including the study of intrinsic stabilities of premixed flames, to improve the efficiency of combustion system and to reduce the pollutant emissions.

Chapter 2 describes the numerical calculation procedures in detail. It consists of theoretical model, assumptions, governing equations and method to elucidate the effects

of unburned-gas temperature and heat loss on intrinsic instabilities of premixed flames.

Chapter 3 presents the numerical results of the elucidations of the effects of unburned-gas temperature and heat loss on the diffusive-thermal instability premixed flames with high- and low-temperature unburned gases, including the burning velocities of planar and cellular flames, dispersion relations, characteristics and unstable behavior of the cellular flame fronts under the adiabatic and non-adiabatic conditions. [46]

Chapter 4 includes the results on the investigation of diffusive-thermal and hydrodynamic instabilities of low temperature unburned-gas premixed flames. The results consist of burning velocities of planar and cellular flames, dispersion relations, characteristics and unstable behavior of the cellular flame fronts under the conditions of adiabatic and non-adiabatic. [47] In addition, the comparison between the theoretical and numerical results of the effect of unburned-gas temperature on hydrodynamic instability of premixed flames at $Le = 1.0$ is included.

Chapter 5 concludes the findings on numerical research calculations and states the future work.

Chapter 2: Research Methodology

2.1 INTRODUCTION

In this research, the diffusive-thermal model equation [48] is used to investigate the diffusive-thermal instability, and compressible Navier-Stokes equation [49] including chemical reaction is applied to study the diffusive-thermal and hydrodynamic instabilities.

2.1.1 General Structure of a Theoretical Model

The essential elements required to create a theoretical model for numerical calculation is illustrated in Fig.2.1 (Kuo, 2005). It describes the relationships between various components of the model.

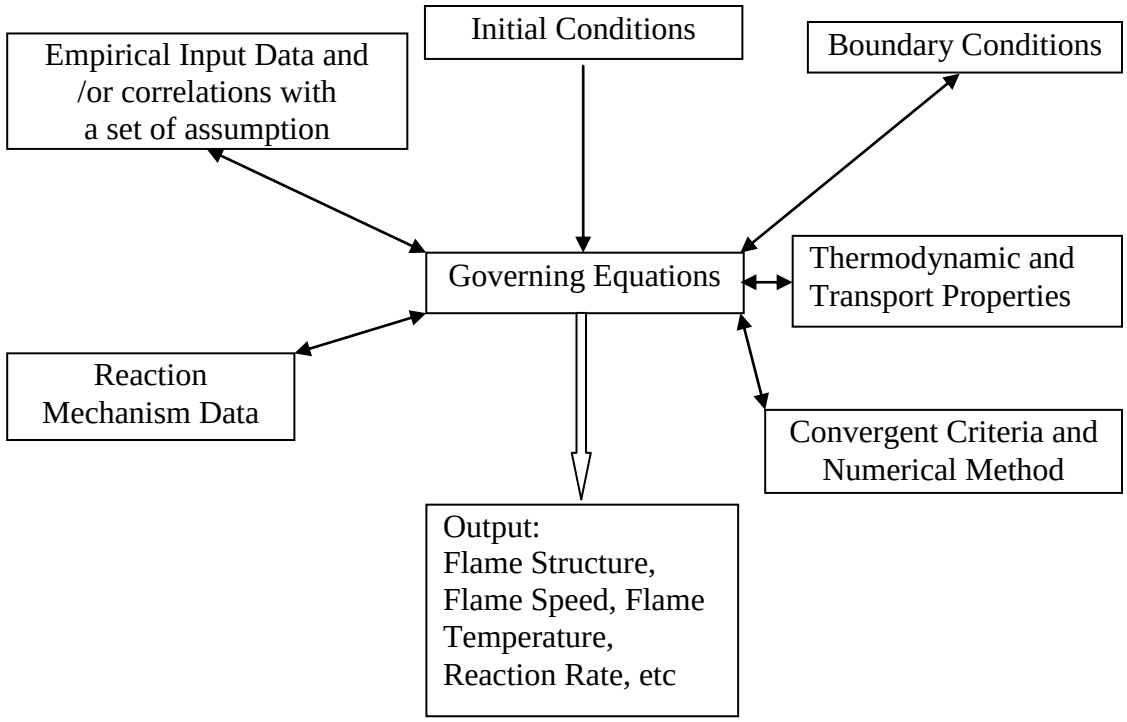

Figure 2.1: General structure of a theoretical model

2.1.2 Assumptions for Governing Equations

In the investigation of intrinsic instabilities excluding the body force instability, single-reactant flames are considered, and the following assumptions are used:

For the diffusive-thermal (D-T) model equation,

(1) the chemical reaction is one-step irreversible exothermic reaction

(2) the reaction rate obeys the Arrhenius law

(3) the unburned and burned gases have the same molecular weights and the same Lewis numbers

(4) the density, specific heat and transport coefficients are constant over the whole region

(5) the effect of thermal expansion is neglected.

For the compressible Navier-Stokes (N-S) equation,

(1) the chemical reaction is a one-step irreversible exothermic reaction

(2) the reaction rate obeys the Arrhenius law

(3) the unburned and burned gases have the same molecular weights and the same Lewis numbers, and the ideal gas equation of state is satisfied

(4) the specific heat and transport coefficients are constant throughout the whole region

(5) the effect of thermal expansion is taken into account

(6) the Soret and Dufour effects, pressure gradient diffusion, bulk viscosity, viscous term in the energy conservation, and acceleration are all neglected.

To study the influence of the heat loss on premixed flames, radiation heat loss is added to the energy conservation.

2.2 GOVERNING EQUATIONS

2.2.1 Diffusive-Thermal Model Equation

The diffusive-thermal model equations, where constant-density approximation is used and thermal expansion effects are disregarded. Using Cartesian coordinates, the direction tangential to the flame front is taken as *y*-direction and with the main flow in the positive *x*-direction. The energy and species conservations for two-dimensional flow based on the diffusive-thermal model are written as follow:

Energy conservation:

$$\rho C_p \frac{\partial \hat{T}}{\partial \hat{t}} + \rho C_p (\widehat{\boldsymbol{U}} \cdot \nabla)\hat{T} - \rho C_p \alpha \nabla^2 \hat{T} = \hat{Q}\widehat{W} \qquad (2-1)$$

Species conservation:

$$\rho \frac{\partial \hat{Y}}{\partial \hat{t}} + \rho (\widehat{\boldsymbol{U}} \cdot \nabla)\hat{Y} - \rho D \nabla^2 \hat{Y} = -\widehat{W} \qquad (2-2)$$

where,

$$\nabla = \begin{pmatrix} \frac{\partial}{\partial \hat{x}} \\ \frac{\partial}{\partial \hat{y}} \end{pmatrix} \qquad (2-3)$$

$$\nabla^2 = \frac{\partial^2}{\partial \hat{x}^2} + \frac{\partial^2}{\partial \hat{y}^2} \qquad (2-4)$$

and the reaction rate in Arrhenius' form is:

$$\widehat{W} = \hat{B}\hat{\rho}\hat{Y} \exp\left(-\frac{\hat{E}}{R\hat{T}}\right) \qquad (2-5)$$

Substituting $(2-5)$ in $(2-1)$ and $(2-2)$, and taking account of the radiation heat flux, the following relations are obtained:

$$\rho C_p \frac{\partial \hat{T}}{\partial \hat{t}} + \rho C_p (\hat{\boldsymbol{U}} \cdot \nabla)\hat{T} - \rho C_p \alpha \nabla^2 \hat{T} = \hat{Q}\hat{B}\hat{\rho}\hat{Y}\exp\left(-\frac{\hat{E}}{R\hat{T}}\right) - \hat{A}(\hat{T}^4 - \hat{T}_{\mathrm{u}}^4) \qquad (2-6)$$

$$\rho \frac{\partial \hat{Y}}{\partial \hat{t}} + \rho (\hat{\boldsymbol{U}} \cdot \nabla)\hat{Y} - \rho D \nabla^2 \hat{Y} = -\hat{B}\hat{\rho}\hat{Y}\exp\left(-\frac{\hat{E}}{R\hat{T}}\right) \qquad (2-7)$$

where the symbol ‘‘ ^’’ denotes dimensional variables.

Since we neglect the change of density across the flame front, there is no more coupling mechanism between the velocity field and the heat release. If the fresh mixture is initially at rest, the velocity of gas is zero everywhere, even though the flame propagates.

This is the typical features of the diffusive-thermal model. The flow rate in the *x*-direction becomes:

$$\mathbf{U} = \begin{pmatrix} U \\ 0 \end{pmatrix} \qquad (2-8)$$

by substituting $(2-8)$ in $(2-6)$and $(2-7)$, then

$$\rho C_p \frac{\partial \hat{T}}{\partial \hat{t}} + \rho C_p \hat{U} \frac{\partial \hat{T}}{\partial \hat{x}} - \rho C_p \alpha \nabla^2 \hat{T} = \hat{Q}\hat{B}\hat{\rho}\hat{Y}\exp\left(-\frac{\hat{E}}{R\hat{T}}\right) - \hat{A}(\hat{T}^4 - \hat{T}_{\mathrm{u}}^4) \qquad (2-9)$$

$$\rho \frac{\partial \hat{Y}}{\partial \hat{t}} + \rho \hat{U} \frac{\partial \hat{Y}}{\partial \hat{x}} - \rho D \nabla^2 \hat{Y} = -\hat{B}\hat{\rho}\hat{Y}\exp\left(-\frac{\hat{E}}{R\hat{T}}\right) \qquad (2-10)$$

2.2.1.1 Non-Dimensionalized Equation

Numerical calculation is accomplished in non-dimensional computational field. The flow variables are non-dimesionalized by the temperature and mass fraction of fuel of unburned-gas, the preheat zone thickness and burning velocity for a standard premixed flame under the adiabatic condition.

$$\hat{t} \to t\frac{\delta}{S_{\mathrm{u}}} \qquad \hat{x} \to x\delta \qquad \hat{T} \to TT_{u0} \qquad \hat{Y} = Y \qquad \hat{T}_u \to T_u T_{u0}$$

$$\hat{Q} \to QC_p T_{u0} \qquad \hat{B} \to \hat{B}\frac{S_{u0}}{\delta} \qquad \hat{E} \to ERT_{u0} \qquad \hat{U} \to US_{u0}$$

The two-dimensional governing equations for unsteady reactive flows are written as follows:

$$\rho C_p \frac{T_{u0}S_{u0}}{\delta}\frac{\partial T}{\partial t} + \rho C_p \frac{T_{u0}S_{u0}}{\delta} U \frac{\partial T}{\partial x} - \rho C_p \alpha \frac{T_{u0}}{\delta^2}\nabla^2 T$$
$$= \rho C_p \frac{T_{u0}S_{u0}}{\delta} QBY\, exp\left(-\frac{E}{T}\right) - \hat{A}T_{u0}^4(T^4 - T_u^4) \qquad (2-11)$$

$$\rho \frac{S_{u0}}{\delta}\frac{\partial Y}{\partial t} + \rho \frac{S_{u0}}{\delta} U \frac{\partial Y}{\partial x} - \rho D \frac{1}{\delta^2}\nabla^2 Y = -\frac{S_{u0}}{\delta}\rho\, BY\, exp\left(-\frac{E}{T}\right) \qquad (2-12)$$

By multiplying $\delta/\rho C_p T_{u0}S_{u0}$with the both sides of $(2-11)$and $\delta/\rho S_{u0}$ with $(2-12)$, the equations become:

$$\frac{\partial T}{\partial t} + U\frac{\partial T}{\partial x} - \frac{\alpha}{S_{u0}\delta}\nabla^2 T = QBY\, exp\left(-\frac{E}{T}\right) - \frac{\hat{A}\delta T_{u0}^3}{\rho C_p S_{u0}}(T^4 - T_u^4) \qquad (2-13)$$

$$\frac{\partial Y}{\partial t} + U\frac{\partial Y}{\partial x} - \frac{D}{S_{u0}\delta}\nabla^2 Y = -\, BY\, exp\left(-\frac{E}{T}\right) \qquad (2-14)$$

The preheat zone thickness, δ is defined as:

$$\delta = \frac{\alpha}{S_{\mathrm{u0}}}$$

and it is substituted in $(2-13)$and $(2-14)$, then

$$\frac{\partial T}{\partial t} + U\frac{\partial T}{\partial x} - \nabla^2 T = QBY\, exp\left(-\frac{E}{T}\right) - \frac{\alpha \hat{A}T_{u0}^3}{\rho C_p S_{u0}^2}(T^4 - T_u^4) \qquad (2-15)$$

$$\frac{\partial Y}{\partial t} + U\frac{\partial Y}{\partial x} - \frac{D}{\alpha}\nabla^2 Y = -\, BY\, exp\left(-\frac{E}{T}\right) \qquad (2-16)$$

by substituting Lewis number: $Le = \alpha/D$ and $\hat{A} \rightarrow A\left(\rho C_p S_{u0}/\alpha T_{u0}^3\right)$ in $(2-15)$ and $(2-16)$, then,

$$\frac{\partial T}{\partial t} + U\frac{\partial T}{\partial x} - \nabla^2 T = QBY\, exp\left(-\frac{E}{T}\right) - A(T^4 - T_u^4) \qquad (2-17)$$

$$\frac{\partial Y}{\partial t} + U\frac{\partial Y}{\partial x} - \frac{1}{Le}\nabla^2 Y = -\,BY\,exp\left(-\frac{E}{T}\right) \qquad (2-18)$$

In addition, the two-dimensional governing equations in non-dimensional form are written as:

$$\frac{\partial T}{\partial t} + U\frac{\partial T}{\partial x} - \left(\frac{\partial^2 T}{\partial x^2} + \frac{\partial^2 T}{\partial y^2}\right) = QBY\,exp\left(-\frac{E}{T}\right) - A(T^4 - T_u^4) \qquad (2-19)$$

$$\frac{\partial Y}{\partial t} + U\frac{\partial Y}{\partial x} - \frac{1}{Le}\left(\frac{\partial^2 Y}{\partial x^2} + \frac{\partial^2 Y}{\partial y^2}\right) = -\,BY\,exp\left(-\frac{E}{T}\right) \qquad (2-20)$$

The conservation equations in the vector form are written as:

$$\frac{\partial \mathbf{U}}{\partial t} + \frac{\partial \mathbf{F}}{\partial x} + \frac{\partial \mathbf{G}}{\partial y} = \mathbf{S} \qquad (2-21)$$

where, **U**, **F**, **G** and **S** are vectors, given by

$$\mathbf{U} = \begin{pmatrix} T \\ Y \end{pmatrix}$$

$$\mathbf{F} = \begin{pmatrix} UT - \dfrac{\partial T}{\partial x} \\ UY - \dfrac{1}{Le}\dfrac{\partial Y}{\partial x} \end{pmatrix}$$

$$\mathbf{G} = \begin{pmatrix} -\dfrac{\partial T}{\partial y} \\ -\dfrac{1}{Le}\dfrac{\partial Y}{\partial y} \end{pmatrix}$$

$$\mathbf{S} = \begin{pmatrix} QBY\,exp\left(-\dfrac{E}{T}\right) - A(T^4 - T_u^4) \\ -\,BY\,exp\left(-\dfrac{E}{T}\right) \end{pmatrix}$$

where, T and Y are variables.

2.2.1.2 Boundary Conditions

The boundary conditions in the *x*-direction are provided by free-flow conditions (linear interpolation). Free-flow conditions at the boundary are:

$$\frac{\partial T}{\partial x} = 0\,, \qquad \frac{\partial Y}{\partial x} = 0 \tag{2 – 22}$$

For upstream flow,

$$\mathbf{U}_{i,j} = \frac{\left(4\mathbf{U}_{2,j} - \mathbf{U}_{3,j}\right)}{3} \tag{2 – 23}$$

For downstream flow,

$$\mathbf{U}_{imax,j} = \frac{\left(4\mathbf{U}_{\mathrm{imax}-1,j} - \mathbf{U}_{\mathrm{imax}-2,j}\right)}{3} \tag{2 – 24}$$

The boundary conditions in the *y*-direction are provided by the periodic condition:

$$\mathbf{U}_{i,jmax+1} = \mathbf{U}_{i,2} \tag{2 – 25}$$

$$\mathbf{U}_{i,1} = \mathbf{U}_{i,jmax} \tag{2 – 26}$$

2.2.2 Compressible Navier-Stokes Equation

The governing equations with the assumptions taken for compressible Navier-Stokes equation are written as follows:

Mass conservation:

$$\frac{\partial}{\partial \hat{t}}\hat{\rho} + \frac{\partial}{\partial \hat{x}}\hat{\rho}\hat{u} + \frac{\partial}{\partial \hat{y}}\hat{\rho}\hat{v} = 0 \tag{2 – 27}$$

Momentum conservation (*x*-direction):

$$\frac{\partial}{\partial \hat{t}}\hat{\rho}\hat{u} + \frac{\partial}{\partial \hat{x}}\left\{\hat{\rho}\hat{u}^2 + \hat{p} - \mu\left(\frac{4}{3}\frac{\partial \hat{u}}{\partial \hat{x}} - \frac{2}{3}\frac{\partial \hat{v}}{\partial \hat{y}}\right)\right\} + \frac{\partial}{\partial \hat{y}}\left\{\hat{\rho}\hat{u}\hat{v} - \mu\left(\frac{\partial \hat{v}}{\partial \hat{x}} + \frac{\partial \hat{u}}{\partial \hat{y}}\right)\right\} = 0 \tag{2 – 28}$$

Momentum conservation (*y*-direction):

$$\frac{\partial}{\partial \hat{t}}\hat{\rho}\hat{v} + \frac{\partial}{\partial \hat{x}}\left\{\hat{\rho}\hat{u}\hat{v} - \mu\left(\frac{\partial \hat{v}}{\partial \hat{x}} + \frac{\partial \hat{u}}{\partial \hat{y}}\right)\right\} + \frac{\partial}{\partial \hat{y}}\left\{\hat{\rho}\hat{v}^2 + \hat{p} - \mu\left(\frac{4}{3}\frac{\partial \hat{v}}{\partial \hat{y}} - \frac{2}{3}\frac{\partial \hat{u}}{\partial \hat{x}}\right)\right\} = 0 \tag{2 – 29}$$

Energy conservation:

$$\frac{\partial}{\partial \hat{t}}\hat{e} + \frac{\partial}{\partial \hat{x}}\left\{(\hat{e}+\hat{p})\hat{u} - \kappa\frac{\partial \hat{T}}{\partial \hat{x}}\right\} + \frac{\partial}{\partial \hat{y}}\left\{(\hat{e}+\hat{p})\hat{v} - \kappa\frac{\partial \hat{T}}{\partial \hat{y}}\right\} = \hat{Q}\widehat{W} - \hat{A}\left(\hat{T}^4 - \hat{T}_{\mathrm{u}}^4\right) \quad (2-30)$$

Species conservation:

$$\frac{\partial}{\partial \hat{t}}\hat{\rho}\hat{Y} + \frac{\partial}{\partial \hat{x}}\left(\hat{\rho}\hat{Y}\hat{u} - \hat{\rho}D\frac{\partial \hat{Y}}{\partial \hat{x}}\right) + \frac{\partial}{\partial \hat{y}}\left(\hat{\rho}\hat{Y}\hat{v} - \hat{\rho}D\frac{\partial \hat{Y}}{\partial \hat{y}}\right) = -\widehat{W} \quad (2-31)$$

State equation:

$$\hat{p} = \hat{\rho}\frac{R}{M}\hat{T} \quad (2-32)$$

where the symbol " ˆ " denotes dimensional variables.

The storage energy is defined as,

$$\hat{e} = \frac{\hat{p}}{\gamma - 1} + \frac{1}{2}\hat{\rho}(\hat{u}^2 + \hat{v}^2) \quad (2-33)$$

and the reaction rate is

$$\widehat{W} = \hat{B}\hat{\rho}\hat{Y}\exp\left(-\frac{\hat{E}}{R\hat{T}}\right) \quad (2-34)$$

2.2.2.1 Non-Dimensionalized Equations

The flow variables are non-dimensionalized by the preheat zone thickness, burning velocity, pressure and temperature of the unburned gas for numerical computation.

$$\hat{x} \to x\delta \qquad \hat{y} \to y\delta \qquad \hat{\rho} \to \rho\rho_0 \qquad \hat{u} \to uS_{u0} \qquad \hat{T} = TT_{\mathrm{u}0}$$

$$\hat{v} \to vS_{u0} \qquad \hat{p} \to pp_0 \qquad \hat{e} \to ep_o \qquad \hat{T}_{\mathrm{u}} \to T_u T_{u0} \qquad \hat{Y} \to Y$$

$$\hat{Q} \to QC_pT_{uo} \qquad \hat{B} \to B\frac{S_{u0}}{\delta} \qquad \hat{t} \to t\frac{\delta}{S_{u0}} \qquad \hat{E} \to ERT_{u0} \qquad \hat{A} \to A\frac{\rho_0 C_p S_{u0}^2}{\alpha T_{u0}^3}$$

By simplifying the equations $(2-27)$ to $(2-31)$, non-dimensionalized equations for two dimensional unsteady reactive flows are obtained as follows:

Equation $(2-27)$ becomes,

$$\left(\frac{\rho_0 S_{u0}}{\delta}\right)\frac{\partial}{\partial t}\rho + \left(\frac{\rho_0 S_{u0}}{\delta}\right)\frac{\partial}{\partial x}\rho u + \left(\frac{\rho_0 S_{u0}}{\delta}\right)\frac{\partial}{\partial y}\rho v = 0 \qquad (2-27)'$$

Multiply by $\delta/\rho_0 S_{u0}$ to both sides of equation $(2-27)'$,

$$\frac{\partial}{\partial t}\rho + \frac{\partial}{\partial x}\rho u + \frac{\partial}{\partial y}\rho v = 0 \qquad (2-35)$$

Equation $(2-28)$becomes,

$$\left(\frac{\rho_0 S_{u0}^2}{\delta}\right)\frac{\partial}{\partial t}\rho u + \left(\frac{\rho_0 S_{u0}^2}{\delta}\right)\frac{\partial}{\partial x}\left\{\rho u^2 + \frac{pp_0}{\rho_0 S_{u0}^2} - \frac{\mu}{\delta\rho_0 S_{u0}}\left(\frac{4}{3}\frac{\partial u}{\partial x} - \frac{2}{3}\frac{\partial v}{\partial y}\right)\right\}$$
$$+\left(\frac{\rho_0 S_{u0}^2}{\delta}\right)\frac{\partial}{\partial y}\left\{\rho uv - \frac{\mu}{\delta\rho_0 S_{u0}}\left(\frac{\partial v}{\partial x} + \frac{\partial u}{\partial y}\right)\right\} = 0 \qquad (2-28)'$$

Simplifying the equation $(2-28)'$, Momentum equation in *x*-direction becomes

$$\frac{\partial}{\partial t}\rho u + \frac{\partial}{\partial x}\left\{\rho u^2 + \frac{p}{\gamma M_u^2} - \Pr\left(\frac{4}{3}\frac{\partial u}{\partial x} - \frac{2}{3}\frac{\partial v}{\partial y}\right)\right\}$$
$$+\frac{\partial}{\partial y}\left\{\rho uv - \Pr\left(\frac{\partial v}{\partial x} + \frac{\partial u}{\partial y}\right)\right\} = 0 \qquad (2-36)$$

Equation $(2-29)$becomes,

$$\left(\frac{\rho_0 S_{u0}^2}{\delta}\right)\frac{\partial}{\partial t}\rho v + \left(\frac{\rho_0 S_{u0}^2}{\delta}\right)\frac{\partial}{\partial x}\left\{\rho uv - \frac{\mu}{\delta\rho_0 S_{u0}}\left(\frac{\partial v}{\partial x} + \frac{\partial u}{\partial y}\right)\right\}$$
$$+\left(\frac{\rho_0 S_{u0}^2}{\delta}\right)\frac{\partial}{\partial y}\left\{\rho v^2 + \frac{pp_0}{\rho_0 S_{u0}^2} - \frac{\mu}{\delta\rho_0 S_{u0}}\left(\frac{4}{3}\frac{\partial v}{\partial y} - \frac{2}{3}\frac{\partial u}{\partial x}\right)\right\} = 0 \qquad (2-29)'$$

After simplifying $(2-29)'$, Momentum equation in *y*-direction becomes,

$$\frac{\partial}{\partial t}\rho v + \frac{\partial}{\partial x}\left\{\rho uv - \Pr\left(\frac{\partial v}{\partial x} + \frac{\partial u}{\partial y}\right)\right\}$$
$$+\frac{\partial}{\partial y}\left\{\rho v^2 + \frac{p}{\gamma M_u^2} - \Pr\left(\frac{4}{3}\frac{\partial v}{\partial y} - \frac{2}{3}\frac{\partial v}{\partial y}\right)\right\} = 0 \qquad (2-37)$$

Equation $(2-30)$becomes,

$$\left(\frac{p_0 S_{u0}}{\delta}\right)\frac{\partial}{\partial t}e+\left(\frac{p_0 S_{u0}}{\delta}\right)\frac{\partial}{\partial x}\left\{(e+p)u-\left(\frac{\kappa T_{u0}}{\delta p_0 S_{u0}}\right)\frac{\partial T}{\partial x}\right\}$$

$$+\left(\frac{p_0 S_{u0}}{\delta}\right)\frac{\partial}{\partial y}\left\{(e+p)v-\left(\frac{\kappa T_{u0}}{\delta p_0 S_{u0}}\right)\frac{\partial T}{\partial y}\right\}$$

$$=\left(\frac{p_0 S_{u0}}{\delta}\right)\left(\frac{\delta}{p_0 S_{u0}}\right)\left(\frac{\rho_0 C_p S_{u0} T_{u0}}{\delta}\right)(Q\mathrm{W})$$

$$-\left(\frac{p_0 S_{u0}}{\delta}\right)\left(\frac{\delta}{p_0 S_{u0}}\right)\left(\frac{\rho_0 C_p T_{u0}}{p_0}\right)\left(\frac{p_0}{\rho_0 C_p T_{u0}}\right)A\frac{\rho_0 C_p S_{u0}^2}{\alpha T_{u0}^3}T_{u0}^4(T^4-T_{\mathrm{u}}^4) \qquad (2-30)'$$

Simplifying the equation $(2-30)'$, Energy conservation equation becomes

$$\frac{\partial}{\partial t}e+\frac{\partial}{\partial x}\left\{(e+p)u-\frac{\gamma}{\gamma-1}\frac{\partial T}{\partial x}\right\}+\frac{\partial}{\partial y}\left\{(e+p)v-\frac{\gamma}{\gamma-1}\frac{\partial T}{\partial y}\right\}$$

$$=\frac{\gamma}{\gamma-1}QW-A(T^4-T_{\mathrm{u}}^4) \qquad (2-38)$$

Equation $(2-31)$becomes,

$$\left(\frac{\rho_0 S_{u0}}{\delta}\right)\frac{\partial}{\partial t}\rho Y+\left(\frac{\rho_0 S_{u0}}{\delta}\right)\frac{\partial}{\partial x}\left(\rho Y u-\frac{\rho D}{\delta S_{u0}}\frac{\partial \mathrm{Y}}{\partial x}\right)+\left(\frac{\rho_0 S_{u0}}{\delta}\right)\frac{\partial}{\partial y}\left(\rho Y v-\frac{\rho D}{\delta S_{u0}}\frac{\partial \mathrm{Y}}{\partial y}\right)$$

$$=-\left(\frac{\rho_0 S_{u0}}{\delta}\right)\ W \qquad (2-31)'$$

Simplifying the equation $(2-31)'$, Energy conservation equation becomes

$$\frac{\partial}{\partial t}\rho Y+\frac{\partial}{\partial x}\left(\rho Y u-\frac{1}{Le}\frac{\partial \mathrm{Y}}{\partial x}\right)+\frac{\partial}{\partial y}\left(\rho Y v-\frac{1}{Le}\frac{\partial \mathrm{Y}}{\partial y}\right)=-W \qquad (2-39)$$

where

$$W=\ B\rho Y\exp\left(-\frac{E}{T}\right)$$

$$C_u=\sqrt{\gamma\frac{p_0}{\rho_0}} \qquad M_u=\frac{S_{u0}}{C_u} \qquad \nu\equiv\frac{\mu}{\hat{\rho}} \qquad \alpha=\frac{\kappa}{\hat{\rho}C_p} \qquad \mathrm{P_r}=\frac{\nu}{\alpha} \qquad \delta=\frac{\kappa}{\rho_0 S_{u0}C_p}$$

$$\frac{pp_0}{\rho_0 S_{u0}^2} = \frac{pC_u^2}{S_{u0}^2\gamma} = \frac{p}{\gamma M_u^2} \qquad \frac{\mu}{\delta\rho_0 S_{u0}} = \frac{\rho_0 S_{u0} C_p}{\kappa}\frac{\mu}{\rho_0 S_{u0}} = C_p\frac{\mu}{\kappa} = C_p\frac{\hat{\rho}\nu}{\hat{\rho}C_p\alpha} = \frac{\nu}{\alpha} = \mathrm{P_r}$$

$$C_p = \frac{\gamma}{\gamma - 1}R \qquad p_0 = \rho_0 R T_0$$

$$\frac{\kappa T_{u0}}{\delta p_0 S_{u0}} = \frac{C_p\rho_0 S_{u0}}{\kappa}\frac{\kappa T_{u0}}{p_0 S_{u0}} = \frac{C_p\rho_0 T_{u0}}{p_0} = \frac{\gamma}{\gamma-1}R\frac{\rho_0 T_{u0}}{p_0} = \frac{\gamma}{\gamma-1}\frac{p_0}{p_0} = \frac{\gamma}{\gamma-1}$$

$$\alpha = \frac{\kappa}{\hat{\rho}C_p} \qquad \mathrm{Le} = \frac{\alpha}{D}$$

$$\frac{\hat{\rho}D}{\delta\rho_0 S_{u0}} = \frac{C_p\rho_0 S_{u0}}{\kappa}\frac{\hat{\rho}D}{\rho_0 S_{u0}} = \frac{C_p\hat{\rho}D}{\kappa} = \frac{C_p\hat{\rho}D}{\alpha\hat{\rho}C_p} = \frac{D}{\alpha} = \frac{1}{Le}$$

The non-dimensionalized conservation equations in vector form are written as:

$$\frac{\partial\mathbf{U}}{\partial t} + \frac{\partial\mathbf{F}}{\partial x} + \frac{\partial\mathbf{G}}{\partial y} = \mathbf{S} \qquad (2-40)$$

where

$$\mathbf{U} = \begin{pmatrix} \rho \\ \rho u \\ \rho v \\ e \\ \rho Y \end{pmatrix}$$

$$\mathbf{F} = \begin{pmatrix} \rho u \\ \rho u^2 + \dfrac{p}{\gamma M_u^2} - \mathrm{Pr}\left(\dfrac{4}{3}\dfrac{\partial u}{\partial x} - \dfrac{2}{3}\dfrac{\partial v}{\partial y}\right) \\ \rho uv - \mathrm{Pr}\left(\dfrac{\partial v}{\partial x} + \dfrac{\partial u}{\partial y}\right) \\ (e+p)u - \dfrac{\gamma}{\gamma-1}\dfrac{\partial T}{\partial x} \\ \rho Yu - \dfrac{1}{Le}\dfrac{\partial \mathrm{Y}}{\partial x} \end{pmatrix}$$

$$\mathbf{G} = \begin{pmatrix} \rho v \\ \rho u v - \Pr\left(\frac{\partial v}{\partial x} + \frac{\partial u}{\partial y}\right) \\ \rho v^2 + \frac{p}{\gamma M_u^2} - \Pr\left(\frac{4}{3}\frac{\partial v}{\partial y} - \frac{2}{3}\frac{\partial v}{\partial y}\right) \\ (e+p)v - \frac{\gamma}{\gamma - 1}\frac{\partial T}{\partial y} \\ \rho Y v - \frac{1}{Le}\frac{\partial \mathrm{Y}}{\partial y} \end{pmatrix}$$

$$\mathbf{S} = \begin{pmatrix} 0 \\ 0 \\ 0 \\ \frac{\gamma}{\gamma - 1} Q B \rho Y \exp\left(-\frac{E}{T}\right) - A(T^4 - T_{\mathrm{u}}^4) \\ -B\rho Y \exp\left(-\frac{E}{T}\right) \end{pmatrix}$$

State equation becomes

$$p = \rho T \qquad (2-41)$$

2.2.2.2 Boundary Conditions

The boundary conditions in the *x*-direction are provided by the free flow conditions.

$$\frac{\partial Z}{\partial \mathrm{x}} = 0, \qquad \text{where } Z = \rho, \rho u, e, \rho Y$$

For the upstream flow,

$$Z_{1,j} = \frac{(4Z_{2,j} - Z_{3,j})}{3} \qquad (2-42)$$

For the downstream flow,

$$Z_{imax,j} = \frac{(4Z_{iamx-1,j} - Z_{iamx-2,j})}{3} \qquad (2-43)$$

The periodic boundary conditions in the *y*-direction are:

$$Z_{i,jmax+1} = Z_{i,2} \tag{2-44}$$

$$Z_{i,jmax+1} = Z_{i,jmax} \tag{2-45}$$

2.2.3 Numerical Method

The governing equations are numerically solved by the explicit MacCormack scheme [49], which has second order accuracy in both time and space. In this scheme, forward differences are used for all spatial derivatives in the predictor step while backward differences are used in the corrector steps. The forward and backward differencing can be alternated between predictor and corrector steps. For

$$\frac{\partial \mathbf{U}}{\partial t} + \frac{\partial \mathbf{F}}{\partial x} + \frac{\partial \mathbf{G}}{\partial y} = \mathbf{S}$$

the algorithm is as follows:

Predictor_1

$$\Delta \mathbf{U}_{i,j}^{\overline{n+1}} = -\Delta t \frac{\mathbf{F}_{i+1,j}^{n} - \mathbf{F}_{i,j}^{n}}{\Delta x} - \Delta t \frac{\mathbf{G}_{i,j}^{n} - \mathbf{G}_{i,j-1}^{n}}{\Delta y} + \Delta t \mathbf{S}_{i,j}^{n} \tag{2-46}$$

$$\mathbf{U}_{i,j}^{\overline{n+1}} = \mathbf{U}_{i,j}^{n} + \Delta \mathbf{U}_{i,j}^{\overline{n+1}} \tag{2-47}$$

Corrector_1

$$\Delta \mathbf{U}_{i,j}^{n+1} = \frac{1}{2}\left(-\Delta \mathbf{U}_{i,j}^{\overline{n+1}} - \Delta t \frac{\mathbf{F}_{i,j}^{\overline{n+1}} - \mathbf{F}_{i-1,j}^{\overline{n+1}}}{\Delta x} - \Delta t \frac{\mathbf{G}_{i,j+1}^{\overline{n+1}} - \mathbf{G}_{i,j}^{\overline{n+1}}}{\Delta y} + \Delta t \mathbf{S}_{i,j}^{\overline{n+1}}\right) \tag{2-48}$$

$$\Delta \mathbf{U}_{i,j}^{n+1} = \mathbf{U}_{i,j}^{\overline{n+1}} + \Delta \mathbf{U}_{i,j}^{n+1} \tag{2-49}$$

Predictor_2

$$\Delta\mathbf{U}_{i,j}^{\overline{n+2}} = -\Delta t\frac{\mathbf{F}_{i,j}^{n+1} - \mathbf{F}_{i-1,j}^{n+1}}{\Delta x} - \Delta t\frac{\mathbf{G}_{i,j+1}^{n+1} - \mathbf{G}_{i,j}^{n+1}}{\Delta y} + \Delta t\mathbf{S}_{i,j}^{n+1} \qquad (2-50)$$

$$\mathbf{U}_{i,j}^{\overline{n+2}} = \mathbf{U}_{i,j}^{n+1} + \Delta\mathbf{U}_{i,j}^{\overline{n+2}} \qquad (2-51)$$

Corrector_2

$$\Delta\mathbf{U}_{i,j}^{n+2} = \frac{1}{2}\left(-\Delta\mathbf{U}_{i,j}^{\overline{n+2}} - \Delta t\frac{\mathbf{F}_{i+1,j}^{\overline{n+2}} - \mathbf{F}_{i,j}^{\overline{n+2}}}{\Delta x} - \Delta t\frac{\mathbf{G}_{i,j}^{\overline{n+2}} - \mathbf{G}_{i,j-1}^{\overline{n+2}}}{\Delta y} + \Delta t\mathbf{S}_{i,j}^{\overline{n+2}}\right) \qquad (2-52)$$

$$\mathbf{U}_{i,j}^{n+2} = \mathbf{U}_{i,j}^{\overline{n+2}} + \Delta\mathbf{U}_{i,j}^{n+2} \qquad (2-53)$$

where $x = i \cdot \Delta x$ and $t = n \cdot \Delta t$

The *x*-derivative terms in F are differenced in the opposite directions to that used for $\partial\mathbf{F}/\partial x$, while the *y*-derivative terms are approximated with the central differences. Likewise, the *y*-derivative terms in G are differenced in the opposite direction to that used for $\partial\mathbf{G}/\partial y$, while the cross-derivative terms in F are approximated with central differences.

2.2.4 Calculation Domain

The calculation domain in Cartesian coordinate for all numerical calculations is shown in Fig.2.2. The unburned gas flows in from the left with the burning velocity of a steady, planar flame and burned gas flows out to the right. The domain in the *x*-direction is 200 times of preheat zone thickness for D-T model and 400 times for N-S model. For both models, the domain in the *y*-direction is set to one wavelength; grid size in *x*-direction is uniformly set to 0.1 and that in *y*-direction is $\lambda/64$; time step interval is set to1×10^{-4}. The calculation domain is resolved by 2000×65 and 4000×65 for D-T and N-S model, respectively. Non-dimensional calculation time, *t* ranges from 50 to 200.

All the numerical calculations are performed by IBM Power 780 at Nagaoka University of Technology.

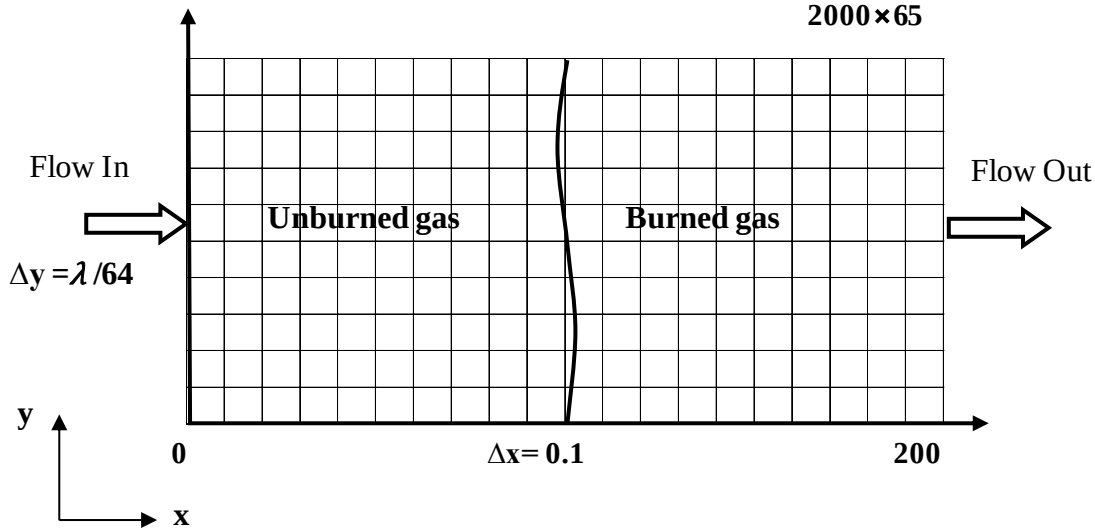

Figure 2.2: Calculation domain and coordinate system.

2.2.5 Characteristics of Dimensionless Parameter

The physical parameters are given to simulate a standard premixture with the adiabatic flame temperature of 2086 K at atmospheric pressure and room temperature. The non-dimensional adiabatic flame temperature for a standard premixed flame is set to 7.0, which is general for hydrogen and/or methane-air premixed flames. The non-dimensional parameter used in all numerical calculations are Q = 6.0, E = 70 and Le = 0.3, 0.5, 0.7 and 1.0. The value of Q is obtained from the difference in temperature between unburned and burned gases, and the non-dimensional activation energy is correlated with the activation energy of 173kJ/mol. The inlet flow velocity is set to the burning velocity of a planar flame. The frequency factor is obtained under the conditions that the calculated burning velocity of an adiabatic planar flame is equal to the set value. The unburned-gas temperature is set to 0.6, 0.8, 1.0, 1.5, 2.0 and 2.5 (-94.2°C, -34.6°C,

25°C, 174°C, 323°C and 472°C). Y_u is set to 1.0. Because of the constant temperature jump condition, the burned-gas temperatures are 6.6, 6.8, 7.0, 7.5 and 8.5.The burning velocity is sufficiently small compared with the sound velocity which means the Mach number, M_u is sufficiently low and it is set to1×10^{-2}. Prandtl number, Pr is set to 1.0 and the ratio of two specific heats, $\gamma = 1.4$.

2.2.6 Initial Conditions

The initial conditions for the temperature distribution and mass fraction of one-dimensional (1D) stationary flame are:

$$T = \begin{cases} T_u + (T_b - T_u)exp(x - x_0) & at\ x \leq x_0 \\ T_b & at\ x \geq x_0 \end{cases} \qquad (2-54)$$

$$Y = \begin{cases} \{Y_u - \exp\{Le(x - x_0)\} & at\ x \leq x_0 \\ 0 & at\ x \geq x_0 \end{cases} \qquad (2-55)$$

The initial conditions for two dimensional (2D) numerical calculations in D-T model are provided by the steady, planar flame solutions under the adiabatic condition: mass fraction (Y) and temperature (T) distribution as in Fig.2.3.

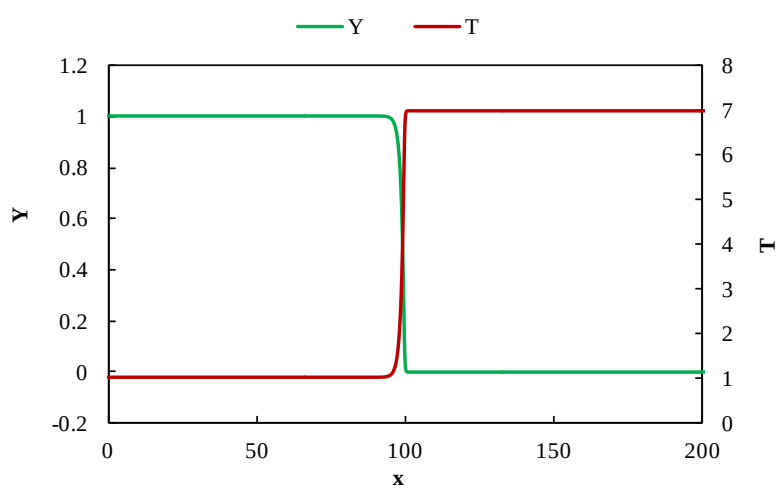

Figure 2.3: Distribution of Y and T in a stationary planar flame, D-T model.

The initial conditions for 2D numerical calculations in N-S model are provided by the steady, planar flame solutions under the adiabatic condition: density (ρ), energy (e), pressure (p), mass fraction (Y) and temperature distribution (T) as in Fig.2.4.

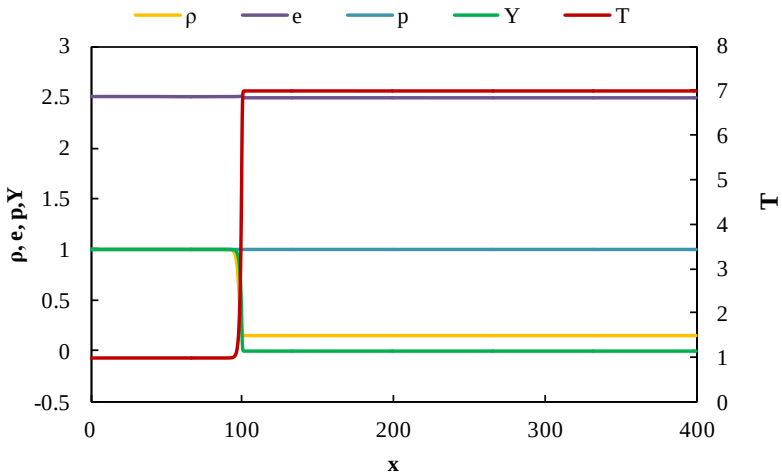

Figure 2.4: Distribution of ρ, e, p, Y and T in a stationary planar flame, N-S model.

In both D-T and N-S models, a sinusoidal disturbance is superimposed on a stationary planar flame. The displacement of the flame front in the x-direction a_i (sin $2\pi y / \lambda$) is shown in Fig.2.5. The value of a_i is 0.1 for the calculation of dispersion relation and 1.0 for cellular flame.

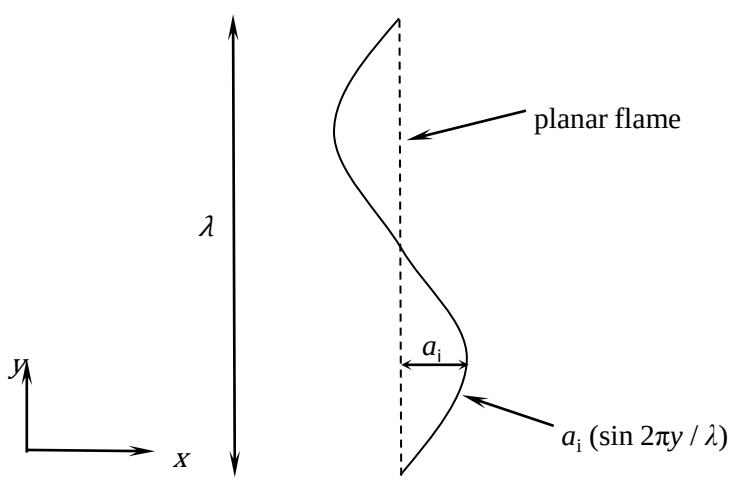

Figure 2.5: Disturbance on a stationary planar flame.

Chapter 3: Diffusive-Thermal Instability of Premixed Flames

3.1 INTRODUCTION

Diffusive-thermal instability of premixed flames is studied not only with high-temperature unburned gas but also with low-temperature unburned gas under the adiabatic and non-adiabatic conditions. Diffusive-thermal model equation with constant density approximation [48] is used to perform the numerical calculations of two-dimensional unsteady reactive flows under the conditions of constant temperature jump, where thermal expansion effect is neglected. The adiabatic flame temperature, T_b is set to 7.0 which is general for premixed flames of hydrogen-air or methane-air. Lewis number, Le is set to 0.3 and 0.5, where preferential diffusion of mass and heat is strong and diffusive-thermal instability is dominant. For constant temperature jump condition, Y_u is set to 1.0, and the following relation is obtained:

$$T_b - T_u = Q \qquad \text{..... (3.1)}$$

The inlet flow velocity, $U = S_u$. The frequency factors B for different Lewis numbers were calculated under the conditions that the calculated burning velocity of an adiabatic planar flame was equal to the set value, $S_u = 1.0$. Table 3.1 shows the frequency factors for $Le = 0.3$ and 0.5.

Table 3.1: Frequency factors for $Le = 0.3$ and 0.5.

T_u	Y_u	S_u	Le	B
1.0	1.0	1.0	0.3	2948478
1.0	1.0	1.0	0.5	1843867

3.2 NUMERICAL RESULTS FOR HIGH TEMPERATURE UNBURNED-GAS PREMIXED FLAMES

Numerical calculations for high temperature unburned-gas premixed flames are performed to investigate the effects of unburned-gas temperature and radiative heat loss on diffusive-thermal instability, especially on the burning velocities of stationary planar flame and cellular flames, dispersion relations, characteristics and formation of cellular flame fronts.

3.2.1 Effect of Unburned-Gas Temperature

To study the effect of unburned-gas temperature, the effect of radiation heat loss is neglected. The radiation heat loss parameter A is set to zero. Thus, the term $A\ (T^4 - T_u^4)$ becomes zero.

3.2.1.1 Numerical results for adiabatic stationary planar flame

One dimensional numerical calculations are performed for unburned-gas temperature, T_u = 1.0, 1.5, 2.0 and 2.5 to obtain the burning velocity of a stationary planar flame and initial conditions of temperature and mass fraction at Le = 0.3 and 0.5 without heat loss. Table 3.2 shows the burning velocity of a stationary planar flame. Because of the increase of temperature of the unburned gas, burning velocity increases. This is because reaction rate in Arrhenius' form strongly depends on temperature, i.e. exp ($-E/RT$). When the temperature increases, the reaction becomes faster and burning velocity increases. The burning velocity at Le = 0.5 is slightly lower than that at Le = 0.3. This is due to the decrease of the diffusive-thermal effect. The distributions of temperature, mass fraction and reaction rate depend on the unburned-gas temperature at Le = 0.3 and 0.5 are shown in Figs. 3.1, 3.2 and 3.3, respectively.

Table 3.2: Burning velocity of adiabatic planar flame at *Le* = 0.3 and 0.5.

T_u	T_b	Y_u	S_u	
			Le =0.3	*Le* =0.5
1.0	7.0	1.0	1.000	1.000
1.5	7.5	1.0	1.629	1.623
2.0	8.0	1.0	2.532	2.513
2.5	8.5	1.0	3.796	3.745

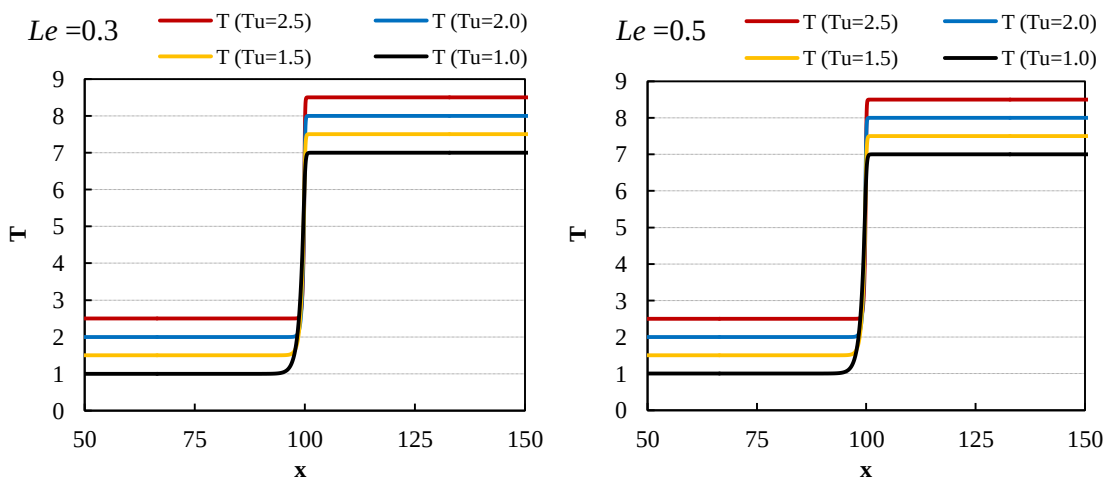

Figure 3.1: Distribution of temperature at *Le* = 0.3 and 0.5.

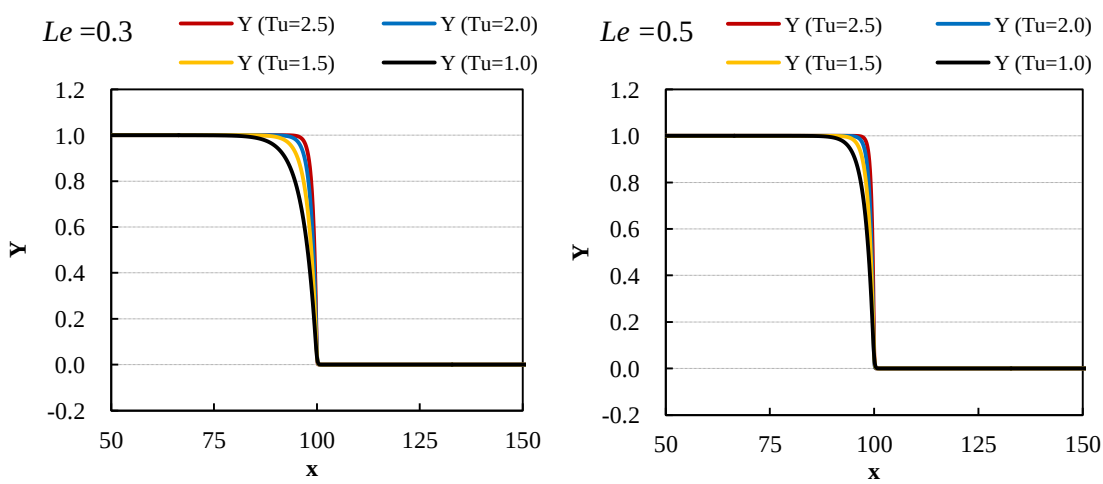

Figure 3.2: Distribution of mass fraction at *Le* = 0.3 and 0.5.

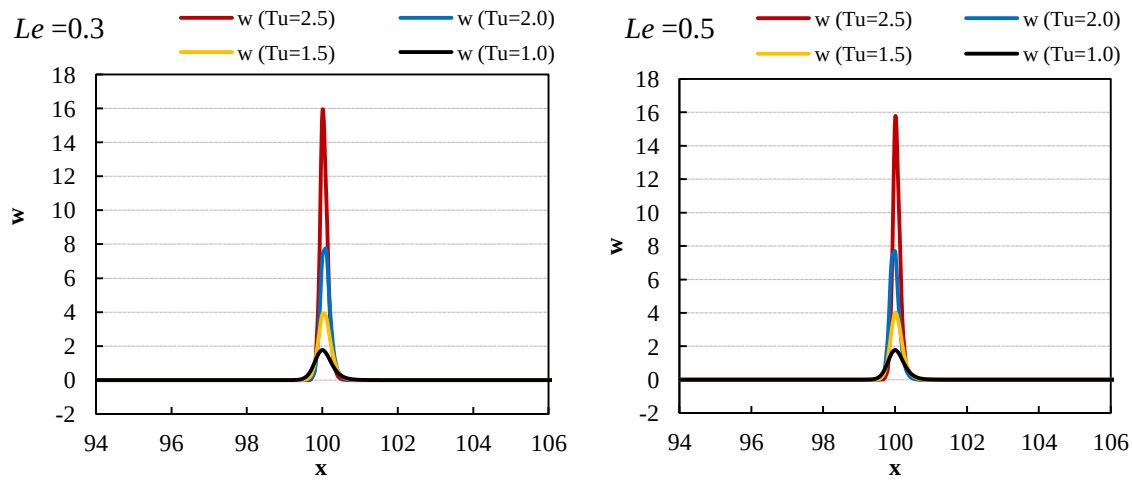

Figure 3.3: Reaction rate at Le = 0.3 and 0.5.

3.2.1.2 Dispersion relations

The numerical calculation for dispersion relation, i.e. the relation between the growth rate ω and wave number k, is performed with initial conditions from one dimensional calculation to study the diffusive-thermal instability on premixed flame. To obtain the dispersion relation, a sufficiently small disturbance, i.e., initial amplitude, a_i = 0.1 is superimposed on a stationary planar flame. The displacement of the flame front in the x-direction due to the superimposed disturbance is a_i {sin $(2\pi y/\lambda)$}. The flame surface is defined as the region where the reaction rate takes a maximum value. The unburned gas flows into the left with the burning velocity of a stationary planar flame and flows out from the right. The sinusoidal flame front is growing with time and moving to the upstream in the x-direction indicating the increase of burning velocity. The evolution of the disturbed flame front at Le = 0.5 and T_u = 1.0 with the wavelength of 17.4 is shown in Fig.3.4.

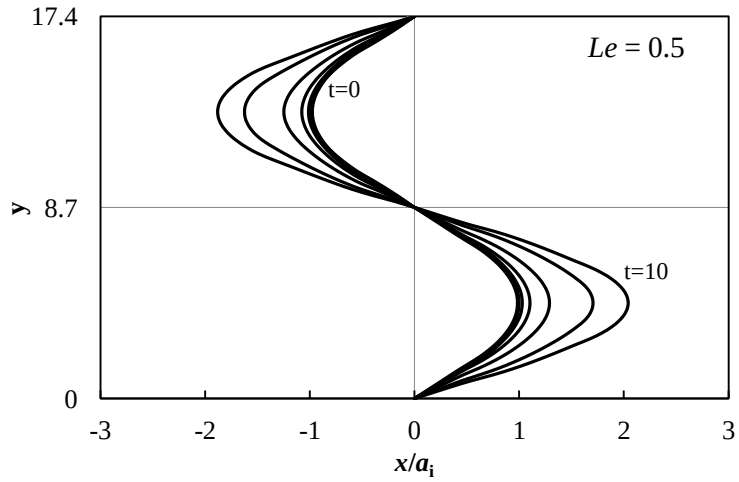

Figure 3.4: Evolution of disturbed flame front at $Le = 0.5$, $T_u = 1.0$.

The amplitude growth rate in each time at $Le = 0.5$ and $T_u = 1.0$ is shown in Fig.3.5. The ordinate is the natural logarithm of the ratio of the amplitude of a disturbance to the initial amplitude. The abscissa is the non-directional time. The amplitude growth rate increases linearly with time, and thus, the amplitude of the disturbance grows exponentially with time $\{a \sim a_i \exp(\omega t)\}$. The amplitude growth rate is defined as:

$$\omega = \frac{\mathrm{d}}{\mathrm{d}t}\ln(a/a_i) \qquad \dots\dots\dots\dots\dots (3.2)$$

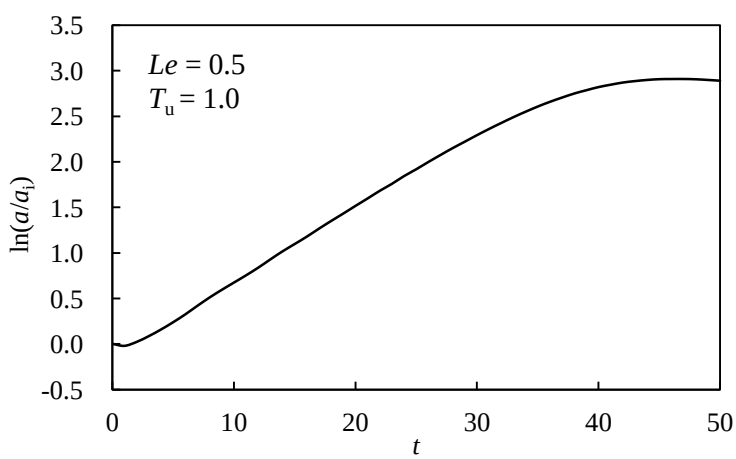

Figure 3.5: Amplitude growth rate of disturbance at $Le = 0.5$, $T_u = 1.0$.

This behavior of a disturbance, growing exponentially with time, is consistent with the prediction of linear analysis. This type of evolution of a disturbance appears only when the amplitude is sufficiently small. When the disturbance grows to some degrees, the growth rate gradually decreases and eventually drops to zero, which is due to the non-linearity brought about by the finite amplitude of disturbance.

By varying the wave number, k (= $2\pi/\lambda$), the dispersion relation is obtained. The dispersion relations at Le = 0.3 and T_u = 1.0 to 2.5 are described in Fig. 3.6. The growth rate slows down to zero when the wave number approaches to zero. Conversely, the growth rate approaches to a maximum value when the wave number becomes larger. When the wave number further increases, the growth rate decreases monotonically and there is a marginal wave number which separates the unstable and stable range.

When the wave number is larger than a marginal value, the growth rate becomes negative. When the unburned-gas temperature becomes higher, the growth rate increases, and the unstable range becomes widen. This is mainly due to the increase of the burning velocity of a planar flame.

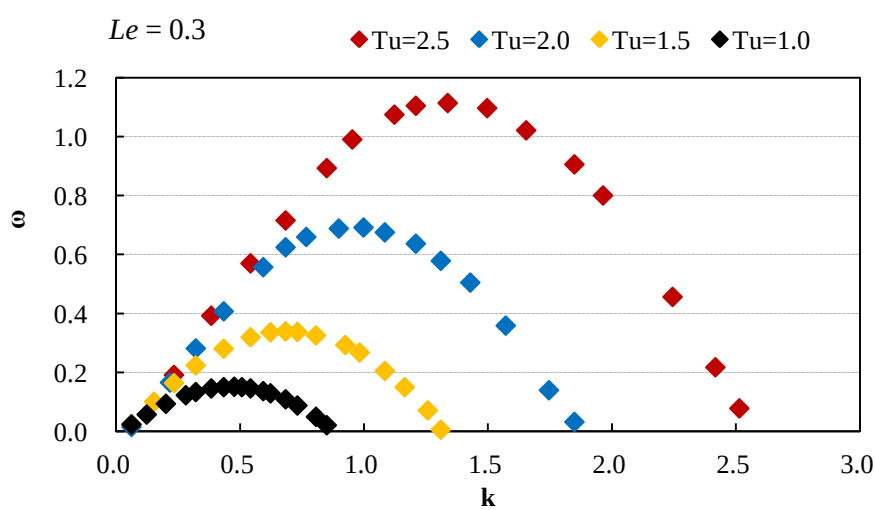

Figure 3.6: Dispersion relations at Le = 0.3 and T_u = 1.0~2.5.

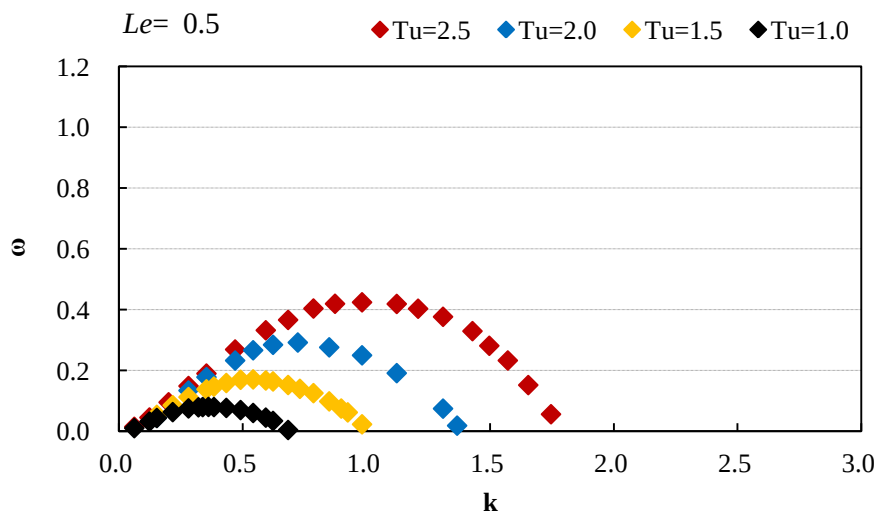

Figure 3.7: Dispersion relations at Le = 0.5 and T_u = 1.0~2.5.

Figure 3.7 shows the dispersion relation at Le = 0.5 and T_u = 1.0 to 2.5. When the Lewis number increases or approaches to unity, diffusive-thermal instability becomes weaker. Thus, the burning velocity of a planar flame is low, and then the growth rate decreases and unstable range narrows compared with those at Le = 0.3. The marginal wave number k_m and critical wave number k_c decrease.

The critical wavelengths λ_c (= $2\pi/k_c$), which are closely related to the spacing between cells of cellular flames induce by the intrinsic instability [50] at Le = 0.3 and 0.5 and T_u = 1.0 to 2.5 are tabulated in Table 3.3.

Table 3.3: Critical wavelengths at Le = 0.3 and 0.5, T_u = 1.0~2.5.

T_u	T_b	Y_u	λ_c	
			Le =0.3	Le =0.5
1.0	7.0	1.0	13.3	16.4
1.5	7.5	1.0	9.2	11.6
2.0	8.0	1.0	6.3	8.7
2.5	8.5	1.0	4.7	6.4

To study the intensity of the instability, we normalized the growth rate and wave number by burning velocity of a planar flame which strongly affects on growth rate. Normalized growth rate and wave number are defined as $\omega^* = \omega/S_u^2$ and $k^* = k/S_u$. Figures 3.8 and 3.9 show the normalized dispersion relations at Le = 0.3 and 0.5 for T_u = 1.0 to 2.5. The normalized growth rate decreases and unstable range narrows when unburned-gas temperature increases. For the Lewis numbers less than unity, we consider Zeldovich number which is closely related to the diffusive-thermal instability to elucidate the effects of unburned-gas temperature. Zeldovich number is defined as:

$$\beta = \frac{T_b - T_u}{T_b^2} E \qquad \dots\dots\dots\dots\dots (3.3)$$

Zeldovich numbers for T_u = 1.0 to 2.5 are listed in Table 3.4. At Le < 1, the instability intensity becomes stronger as the Zeldovich number enlarges (Sivashinsky, 1983). [52] The higher unburned-gas temperature causes the reduction of Zeldovich numbers, so that the instability becomes weaker as the unburned-gas temperature becomes higher.

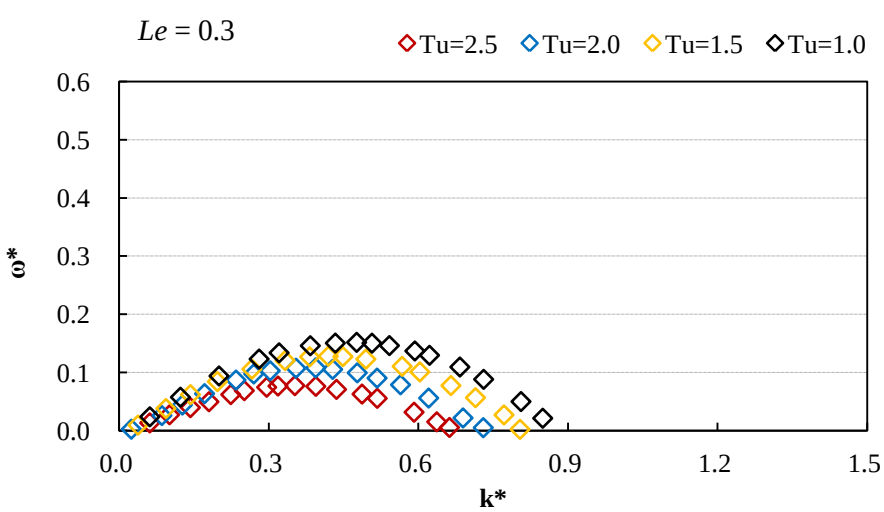

Figure 3.8: Normalized dispersion relations at Le = 0.3 and T_u = 1.0~2.5.

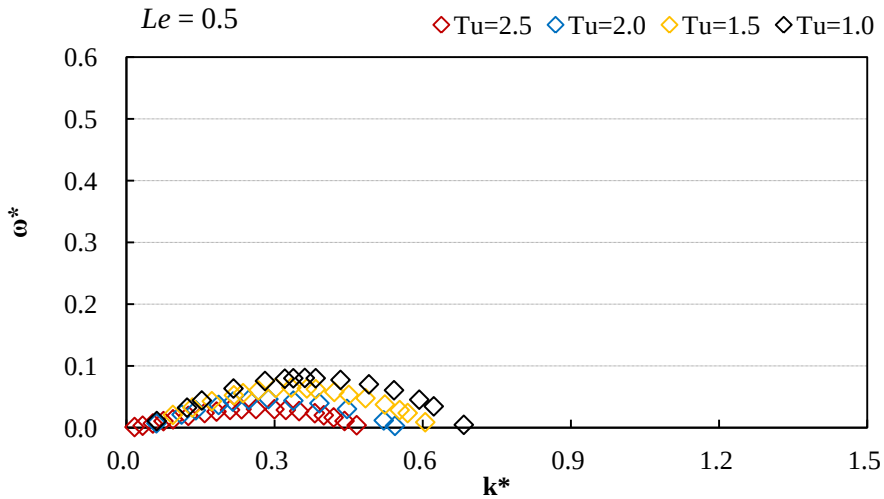

Figure 3.9: Normalized dispersion relations at Le = 0.5 and T_u = 1.0~2.5.

Table 3.4: Zeldovich numbers for T_u = 1.0~2.5.

T_u	T_b	β
1.0	7.0	8.57
1.5	7.5	7.47
2.0	8.0	6.56
2.5	8.5	5.81

3.2.1.2 Formation of cellular flame fronts

To study the formation of cellular flame fronts, the critical wavelength is superimposed as the disturbance wavelength on the planar flame, and the initial amplitude for this calculation is set to a_i = 1.0. The inlet velocity is set to the burning velocity of a planar flame. The flame front is defined as the site where the reaction rate takes the maximum value. The superimposed disturbance evolves and then cellular flame fronts form owing to the diffusive-thermal instability. Figures 3.10 (a) (b) (c) and (d) show the evolution of disturbed flame fronts for T_u = 1.0 to 2.5 at Le = 0.3. After forming the

cellular shape, the flame moves to the upstream. This indicates that the burning velocity of the cellular flame is increased along with the increase of flame surface area.

In addition, the cell depth of the cellular flame front, D_{cell} decreases when unburned gas temperature increases. Here D_{cell} is defined as the distance between the convex and concave flame fronts. This suggests that higher unburned gas temperature reduces D_{cell} and thus suppress the flame instability. Furthermore, higher unburned-gas temperature shortens the length ratio of the cell, L_{cf}. L_{cf} is defined as the ratio of length of the cell in the y-direction to the critical wavelength. Then D_{cell} is normalized by λ_c, and D_{cell}/λ_c decreases when unburned-gas temperature increases. The results show that the diffusive-thermal effect becomes weaker when unburned-gas temperature becomes higher. This is mainly because of the decrease of Zeldovich number.

The temperature distributions of cellular flames at $Le = 0.3$ and $T_u = 1.0$~2.5 are illustrated in Figs.3.11 (a) (b) (c) and (d) at non-dimensional time $t = 60$. The overshoot of the temperature forms at convex flame fronts toward the upstream owing to the diffusive-thermal instability at $Le < 1.0$. This overshoot of the temperature causes the unstable behavior of the cellular flame fronts. [51] The unstable behavior of the cellular flame at $T_u = 2.5$ is weaker than that of $T_u = 1.0$.

Characteristics of cellular flames at $Le = 0.5$ are also examined. The evolution of disturbed flame fronts at $Le = 0.5$ are shown in Figs.3.12 (a) (b) (c) and (d) for $T_u = 1.0$~2.5. Figures 3.13 (a) (b) (c) and (d) show the temperature distribution of the cellular flame fronts at $Le = 0.5$ at $t = 60$. D_{cell}, L_{cf} and D_{cell}/λ_c at $Le = 0.3$ and 0.5 are listed in Table 3.5. Compared with the cellular flames at $Le = 0.3$, the unstable behavior are weak, flame fronts are smooth, D_{cell}, L_{cf} and D_{cell}/λ_c are small at $Le = 0.5$. In addition, the overshoot of the temperature becomes smaller. This is because the intensity of diffusive-thermal instability becomes milder when Lewis number becomes larger.

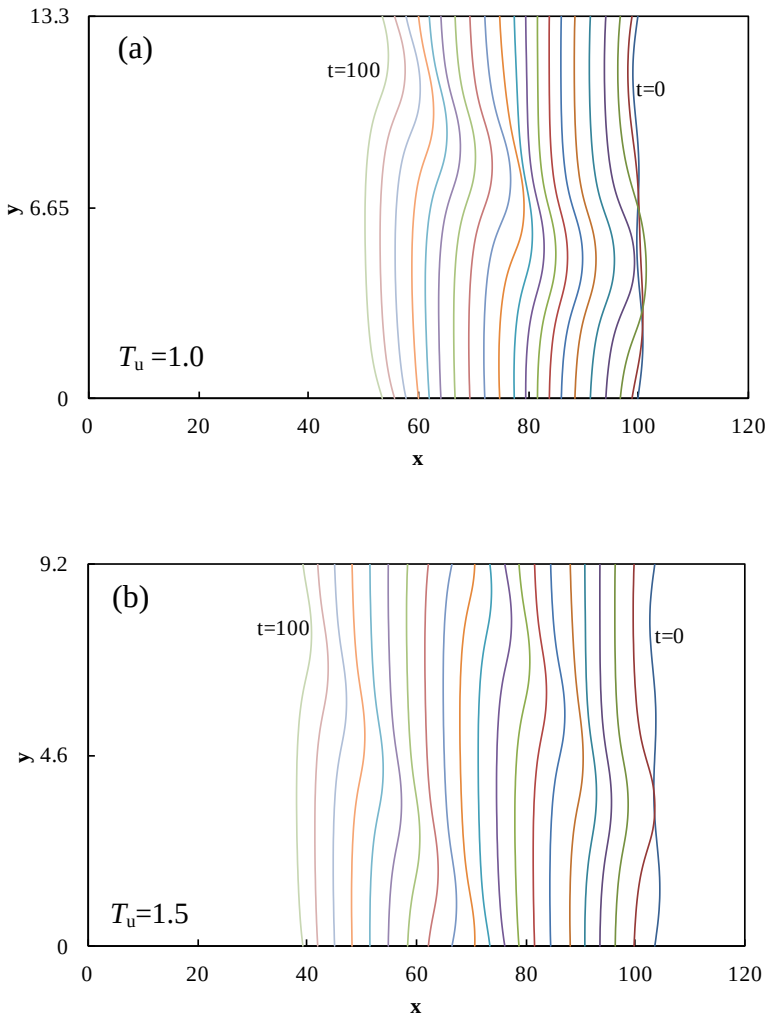

Figure 3.10(a) (b): Evolution of disturbed flame fronts at Le = 0.3, T_u = 1.0 and 1.5.

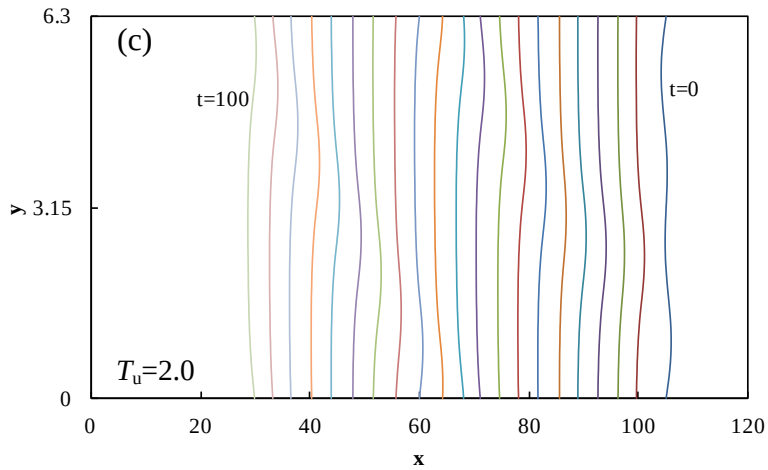

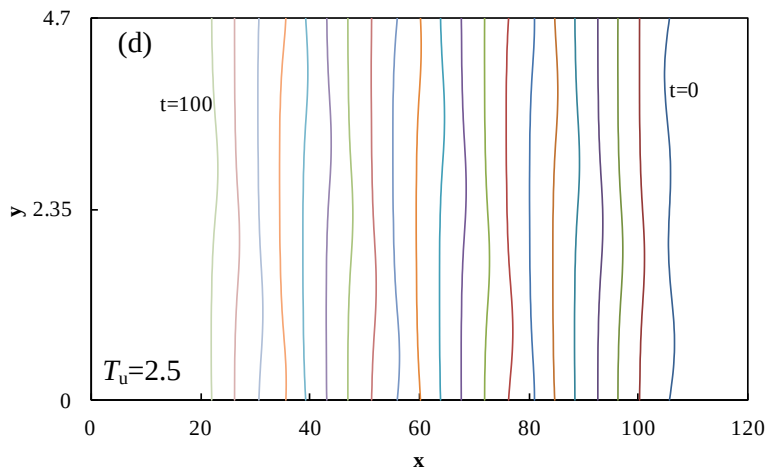

Figure 3.10(c) (d): Evolution of disturbed flame fronts at Le = 0.3, T_u=2.0 and 2.5.

Table 3.5: D_{cell}, L_{cf} and D_{cell}/λ_c of cellular flames at Le = 0.3 and 0.5.

T_u	D_{cell}		L_{cf}		D_{cell}/λ_c	
	Le = 0.3	Le = 0.5	Le = 0.3	Le = 0.5	Le = 0.3	Le = 0.5
1.0	4.0183	3.0311	1.2613	1.1143	0.3021	0.1848
1.5	2.5268	1.8219	1.2210	1.0894	0.2747	0.1571
2.0	1.5060	1.1990	1.1760	1.0735	0.2390	0.1378
2.5	0.9757	0.7610	1.1435	1.0613	0.2076	0.1189

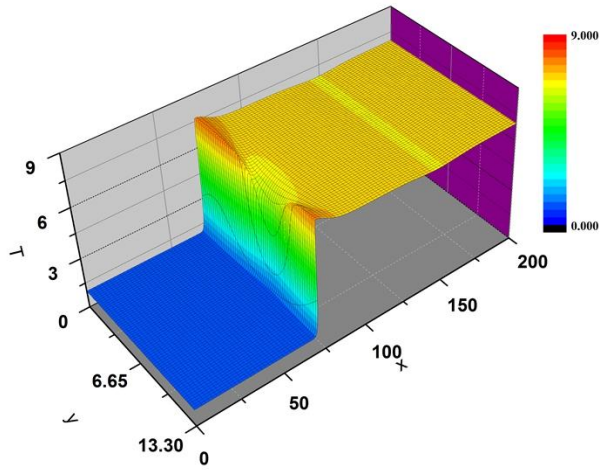

(a) T_u **= 1.0**

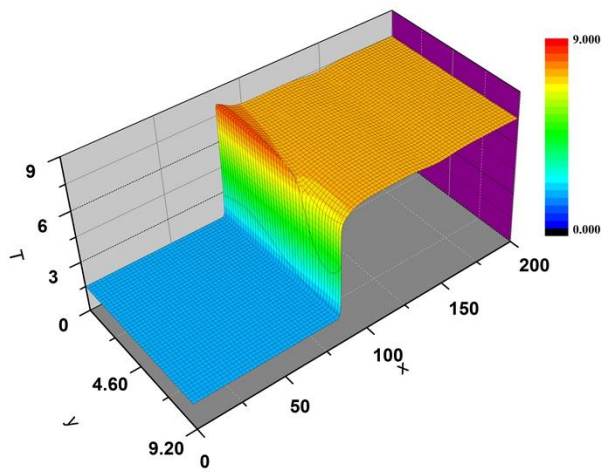

(b) T_u **= 1.5**

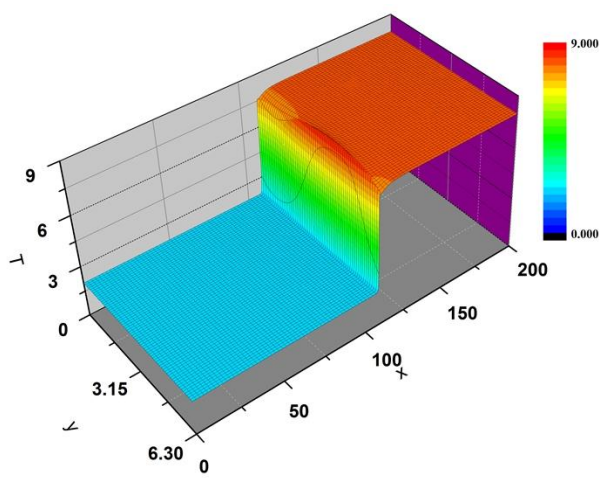

(c) T_u **= 2.0**

Figure 3.11 (a) (b) (c): Temperature distribution of cellular flame fronts at Le = 0.3 and T_u =1.0~2.0.

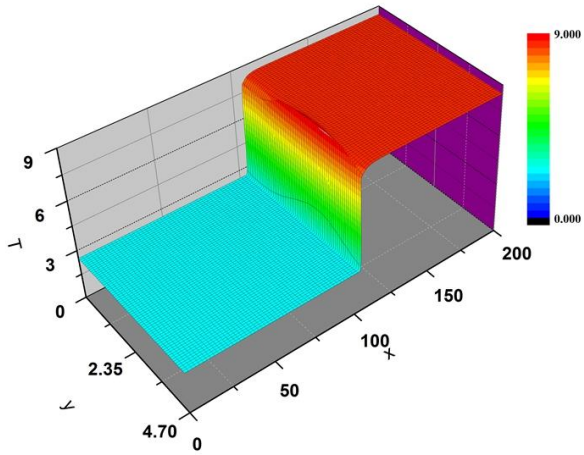

(d) T_u = 2.5

Figure 3.11 (d): Temperature distribution of cellular flame fronts at Le = 0.3 and T_u =2.5.

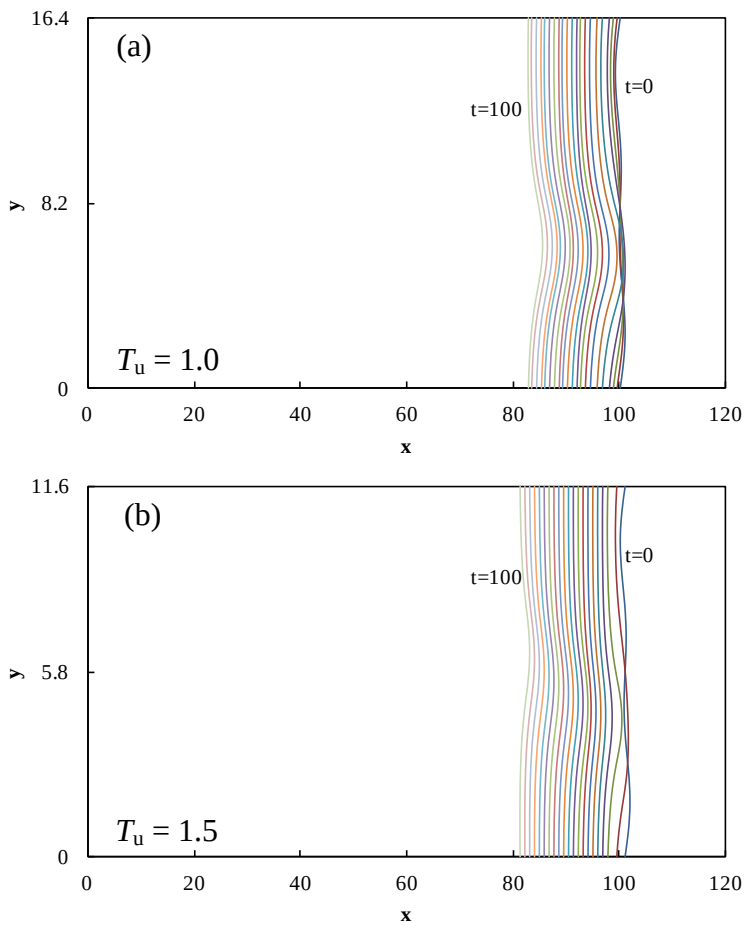

Figure 3.12 (a) (b): Evolution of disturbed flame fronts at Le = 0.5, T_u=1.0 and 1.5.

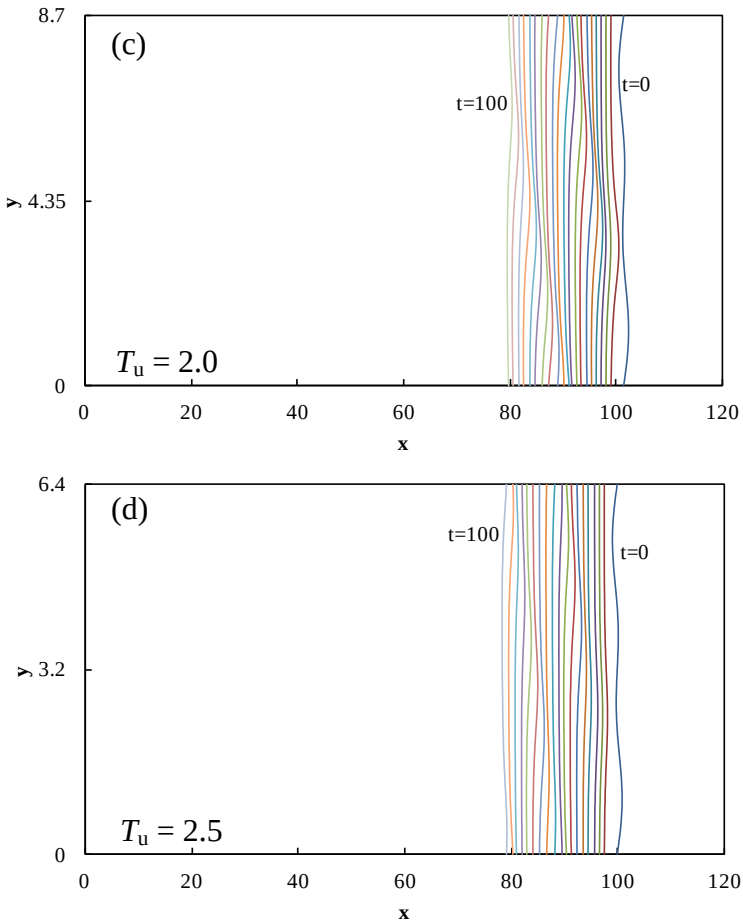

Figure 3.12 (c) (d): Evolution of disturbed flame fronts at Le = 0.5, T_u=2.0 and 2.5.

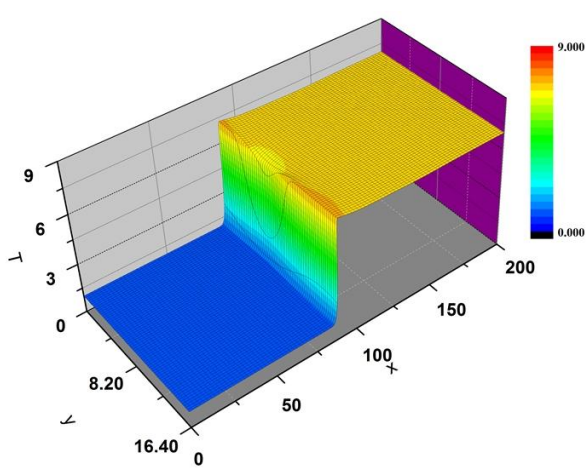

(a) T_u = 1.0

Figure 3.13 (a): Temperature distribution of cellular flame fronts at Le = 0.5 and T_u =1.0.

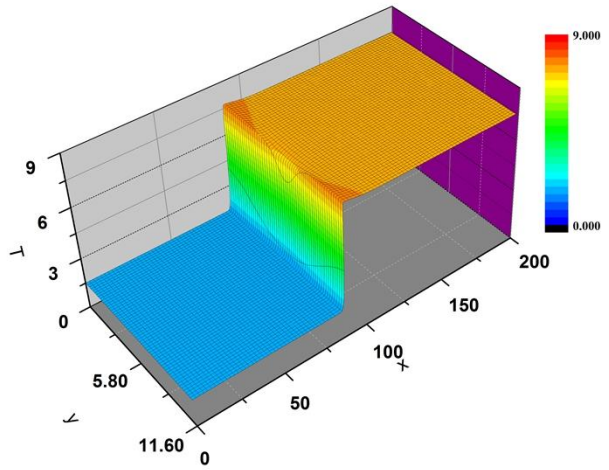

(b) T_u = 1.5

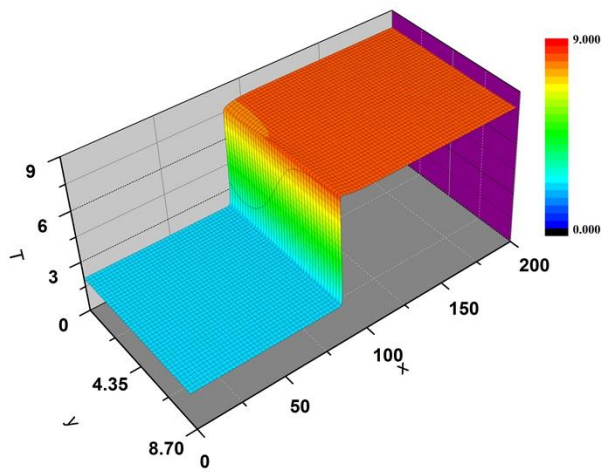

(c) T_u = 2.0

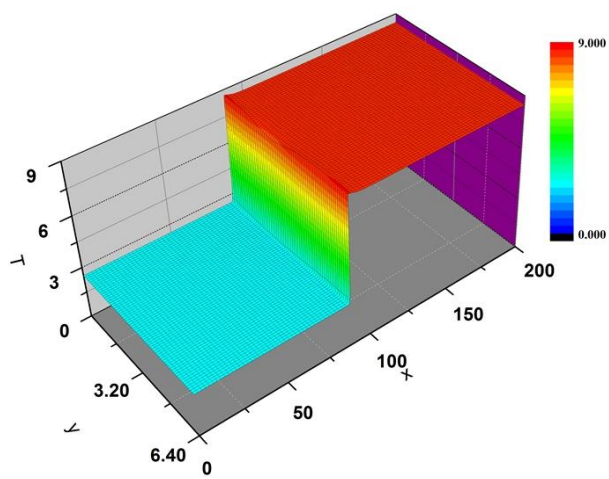

(d) T_u = 2.5

Figure 3.13 (b) (c) (d): Temperature distribution of cellular flame fronts at Le = 0.5 and T_u =1.5~2.5.

3.2.1.4 Burning velocities of cellular flame

The effect of unburned-gas temperature on the burning velocity of cellular flame is elucidated. The burning velocity of cellular flame S_{cf} increases due to the increase of the burning velocity of a planar flame as the unburned-gas temperature becomes higher. It is calculated by the following procedure. The reaction rate is integrated throughout the simulation domain, and the integrated value is normalized by that of a planar flame. The normalized value is consistent with the non-dimensional burning velocity of a cellular flame. When the Lewis number increases, S_{cf} decreases because of the lowness of the diffusive-thermal effect. Burning velocities of cellular flames are normalized by those of planar flames. Normalized burning velocity decreases slightly when the unburned-gas temperature increases. This is because of the reduction of Zeldovich number. Table 3.6 shows the burning velocities of cellular flames and normalized values at Le = 0.3 and 0.5, T_u = 1.0~2.5.

Table 3.6: Burning velocities of cellular flames and normalized values at Le = 0.3 and 0.5.

T_u	Le = 0.3		Le = 0.5	
	S_{cf}	S_{cf}/S_u	S_{cf}	S_{cf}/S_u
1.0	1.532	1.532	1.198	1.198
1.5	2.299	1.411	1.838	1.132
2.0	3.331	1.316	2.760	1.098
2.5	4.694	1.236	4.018	1.073

3.2.2 Effect of Heat Loss

As the combustion processes are strongly affected by heat loss owing to the irreversibility, we study the effect of raidative heat loss on the diffusive-thermal instability of premixed flames.

3.2.2.1 Numerical results for non-adiabatic planar flame

Figures 3.14 and 3.15 show the relation between the heat loss parameter A and burning velocity of non-adiabatic planar flame at Le = 0.3 and 0.5, and T_u = 1.0~2.5. The burning velocities of non-adiabatic flames are smaller than those of adiabatic flames because of the decrease in flame temperature in downstream owing to the effect of heat loss. If the heat loss parameter is larger than maximum value A_{max}, the flame will extinguish. The maximum heat loss parameter at Le = 0.3 and 0.5 for T_u = 1.0~2.5 are tabulated in Table 3.7.

The burning velocities of planar flames at $A = 1\times10^{-4}$ and A_{max} at Le = 0.3 and 0.5 depend on the unburned-gas temperature are listed in Table 3.8.

The temperature distribution, mass fraction and reaction rate at $A = 1\times10^{-4}$, Le = 0.3 and 0.5, and T_u = 1.0~2.5 are shown in Figs. 3.16, 3.17and 3.18.

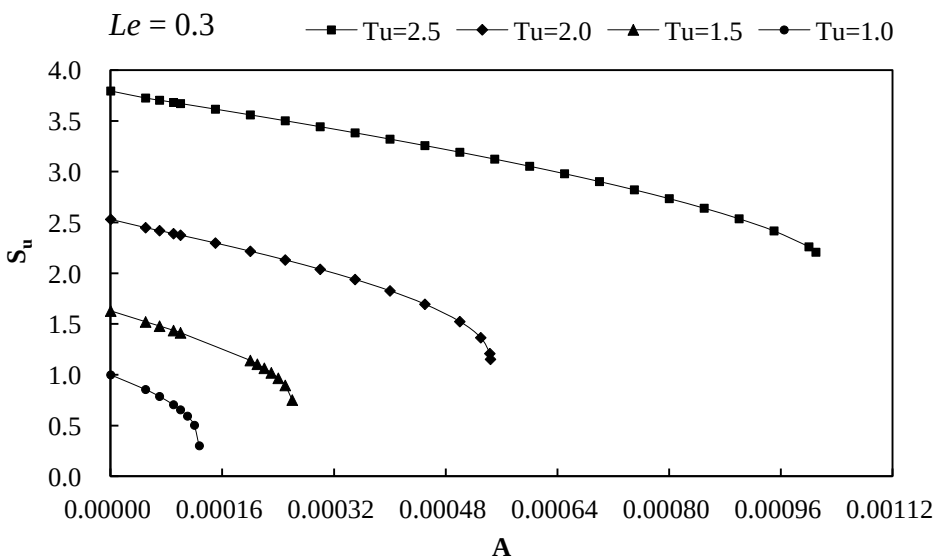

Figure 3.14: Relation between heat loss parameter and burning velocity at Le = 0.3.

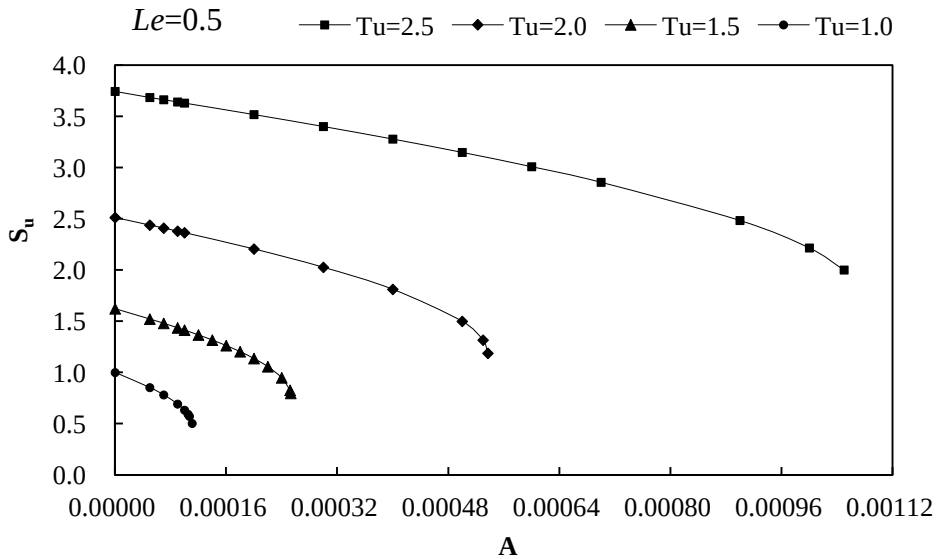

Figure 3.15: Relation between heat loss parameter and burning velocity at *Le* = 0.5.

Table 3.7: Maximum heat loss parameter at *Le* = 0.3 and 0.5.

T_u	A_{max}	
	Le =0.3	*Le* =0.5
1.0	1.27×10^{-4}	1.11×10^{-4}
1.5	2.60×10^{-4}	2.53×10^{-4}
2.0	5.44×10^{-4}	5.37×10^{-4}
2.5	1.01×10^{-3}	1.05×10^{-3}

Table 3.8: Burning velocities of non-adiabatic planar flames at *Le* = 0.3 and 0.5, $A = 1\times10^{-4}$.

T_u	S_u			
	Le =0.3		*Le* =0.5	
	$A = 1\times10^{-4}$	A_{max}	$A = 1\times10^{-4}$	A_{max}
1.0	0.6562	0.3018	0.6326	0.5035
1.5	1.4144	0.7525	1.4142	0.7969
2.0	2.3756	1.1534	2.3647	1.1878
2.5	3.6724	2.2083	3.6308	2.0013

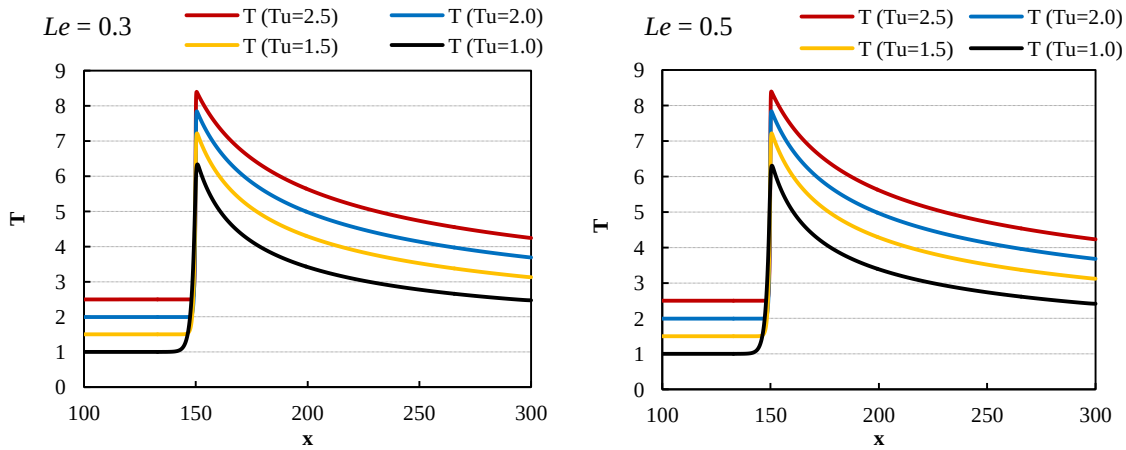

Figure 3.16: Distribution of temperature at $Le = 0.3$ and 0.5 ($A = 1\times10^{-4}$).

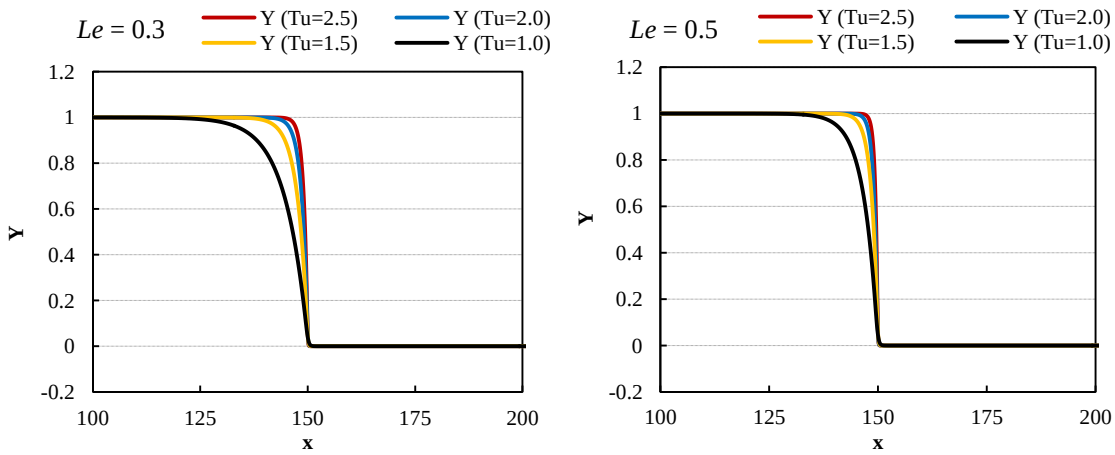

Figure 3.17: Distribution of mass fraction at $Le = 0.3$ and 0.5 ($A = 1\times10^{-4}$).

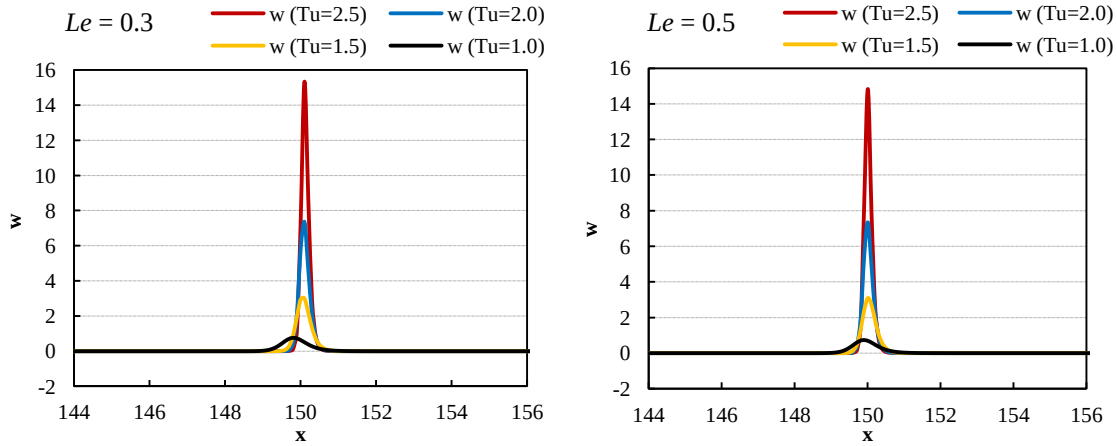

Figure 3.18: Reaction rate at $Le = 0.3$ and 0.5 ($A = 1\times10^{-4}$).

3.2.2.2 Dispersion relations

Dispersion relation and normalized dispersion relation at $A = 1\times10^{-4}$, $Le = 0.3$, and $T_u = 1.0\sim2.5$ are shown in Figs. 3.19 (a) and (b). The growth rate increases as the unburned-gas temperature increases. When it is normalized by the burning velocity of a planar flame, we get the qualitatively same result as in adiabatic flame. In quantitatively, the growth rate of non-adiabatic flames are small compared with the adiabatic flame because of the decrease of burning velocity of planar flame owing to the effect of heat loss. Although the growth rate at $T_u = 2.5$, $Le = 0.3$ in non-adiabatic flame is almost same as that in adiabatic flame, the normalized growth rate is high in non-adiabatic premixed flame. This indicates that the heat loss has a pronounced influence on the premixed flames. Figures 3.20 (a) and (b) show the dispersion relation and normalized one at $Le = 0.5$ and $T_u = 1.0\sim2.5$. The critical wavelengths at both Lewis numbers for $A = 1\times10^{-4}$ are large compared with the adiabatic flames and are listed in Table.3.9.

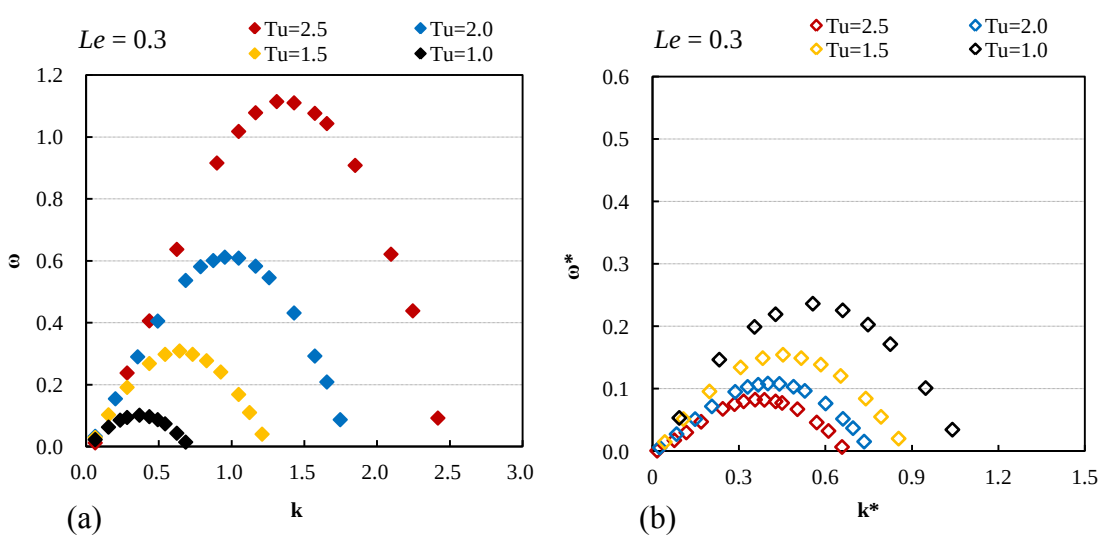

Figure 3.19: Dispersion relation (a) and normalized dispersion relation (b) at $Le = 0.3$ and $T_u = 1.0\sim2.5$ ($A = 1\times10^{-4}$).

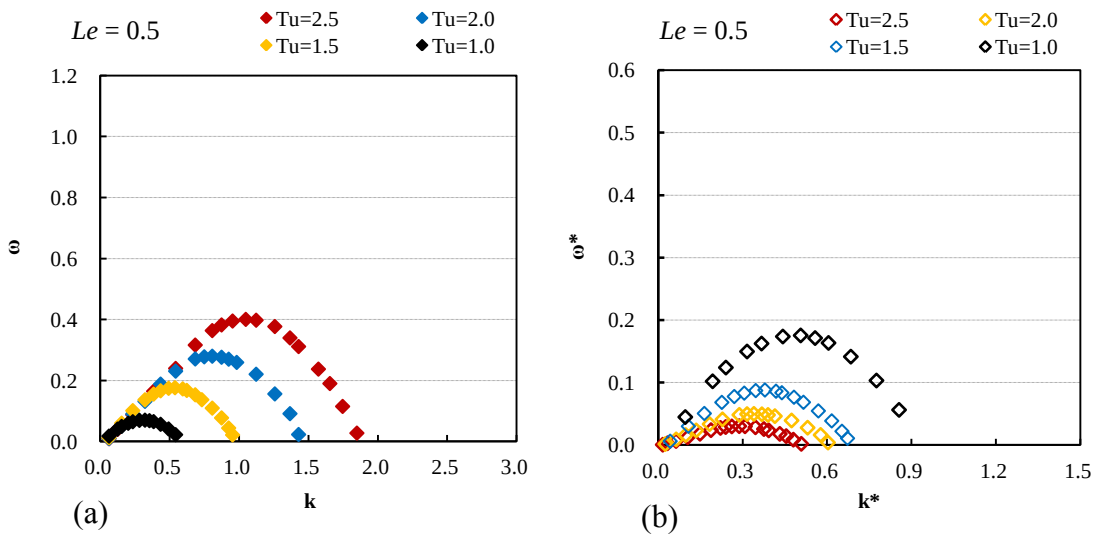

Figure 3.20: Dispersion relation (a) and normalized dispersion relation (b) at $Le = 0.5$ and $T_u = 1.0$~2.5 ($A = 1\times10^{-4}$).

Table 3.9: Critical wavelengths at $Le = 0.3$ and 0.5 ($A = 1\times10^{-4}$).

T_u	T_b	Y_u	λ_c	
			Le =0.3	Le =0.5
1.0	7.0	1.0	17.2	19.6
1.5	7.5	1.0	9.8	11.7
2.0	8.0	1.0	6.6	9.1
2.5	8.5	1.0	4.8	6.6

3.2.2.3 Formation of cellular flame fronts

Cellular flame forms owing to the diffusive-thermal effect. Because of the effects of heat loss, burning velocities of cellular flames decreases compared with the adiabatic cellular flames. Figures 3.21 (a) (b) (c) and (d) show the evolution of the disturbed flame fronts at $Le = 0.3$ and $T_u = 1.0$~2.5. The distance between the convex and concave flame fronts, i.e., D_{cell} becomes larger, and L_{cf} which is the ratio of the length of cell in y-direction to the critical wavelength, increases due to the effect of heat loss. It shows that unstable behavior of the cellular flame is strong in non-adiabatic premixed flames. The

evolutions of the disturbed flame fronts at Le = 0.5 and T_u = 1.0~2.5 are shown in Figs. 3.22 (a) (b) (c) and (d). The unstable behavior of the flame fronts becomes weaker when the Lewis number becomes larger. Temperature distributions of the cellular flames at Le = 0.3 and 0.5, and T_u = 1.0~2.5 (t = 60) are shown in Figs. 3.23 (a) (b) (c) (d) and 3.24 (a) (b) (c) (d). Flame temperature decreases in downstream, and the overshoot of the temperature becomes larger because of the heat loss effect. Table 3.10 describes D_{cell}, L_{cf} and D_{cell}/λ_c at Le = 0.3 and 0.5, and T_u = 1.0~2.5.

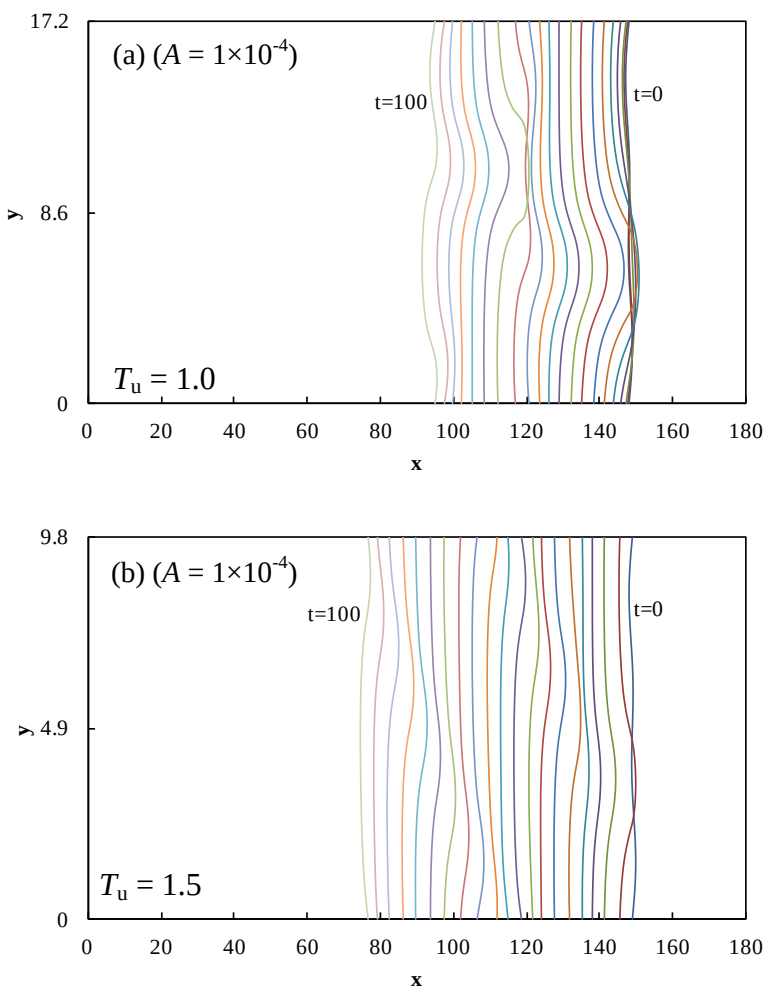

Figure 3.21 (a) (b): Evolution of disturbed flame fronts at Le = 0.3, T_u = 1.0 and 1.5.

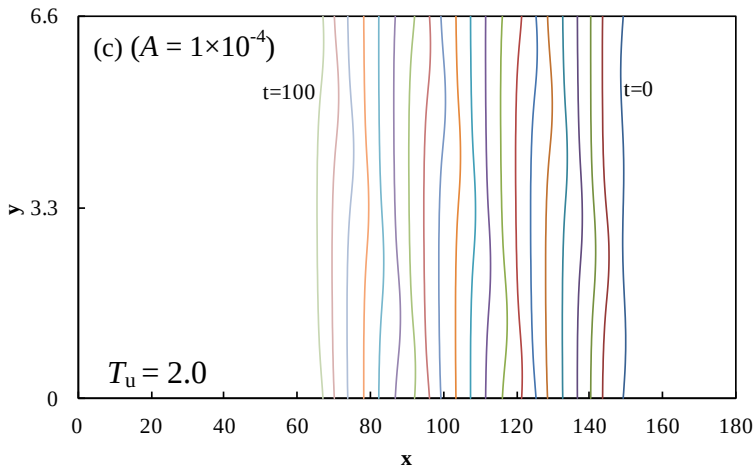

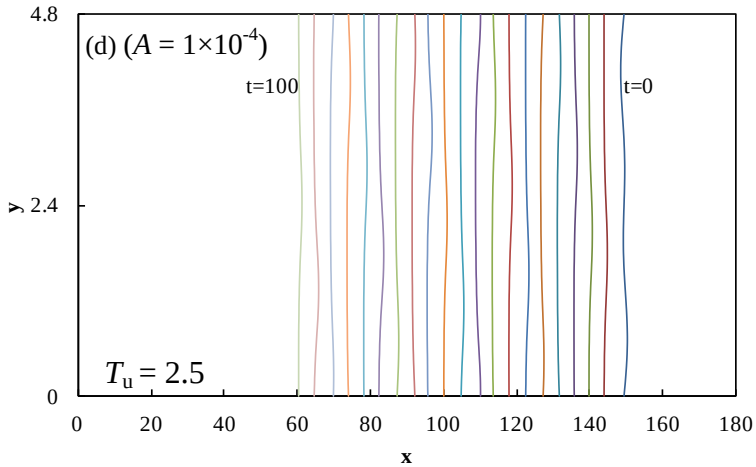

Figure 3.21 (c) (d): Evolution of disturbed flame fronts at Le = 0.3, T_u = 2.0 and 2.5.

Table 3.10: D_{cell}, L_{cf} and D_{cell}/λ_c at Le = 0.3 and 0.5, and T_u = 1.0~2.5 (A = 1×10^{-4}).

T_u	D_{cell}		L_{cf}		D_{cell}/λ_c	
	Le = 0.3	Le = 0.5	Le = 0.3	Le = 0.5	Le = 0.3	Le = 0.5
1.0	5.3690	4.3842	1.3218	1.1666	0.3122	0.2237
1.5	2.8678	2.1394	1.2476	1.1121	0.2926	0.1829
2.0	1.6576	1.3622	1.1906	1.0832	0.2512	0.1494
2.5	1.0252	0.7978	1.1496	1.0624	0.2136	0.1209

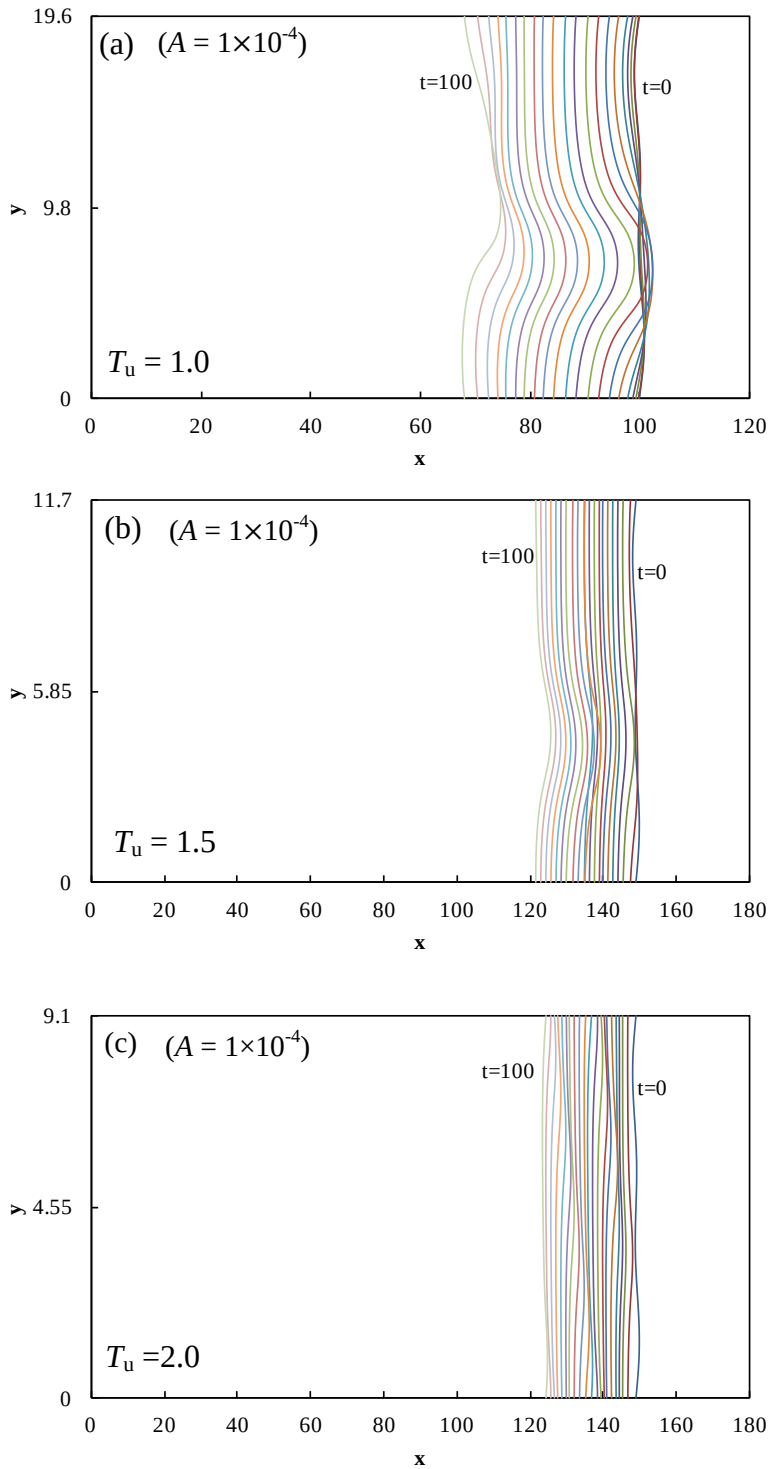

Figure 3.22 (a) (b) (c): Evolution of disturbed flame fronts at Le = 0.5, T_u = 1.0~2.0.

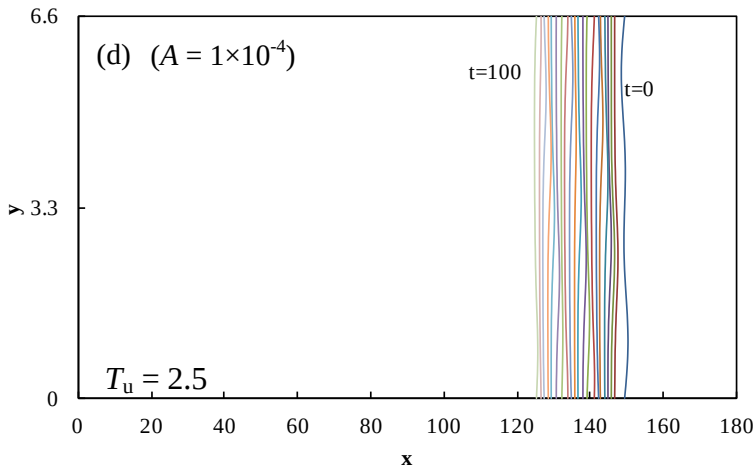

Figure 3.22 (d): Evolution of disturbed flame fronts at Le = 0.5, T_u = 2.5.

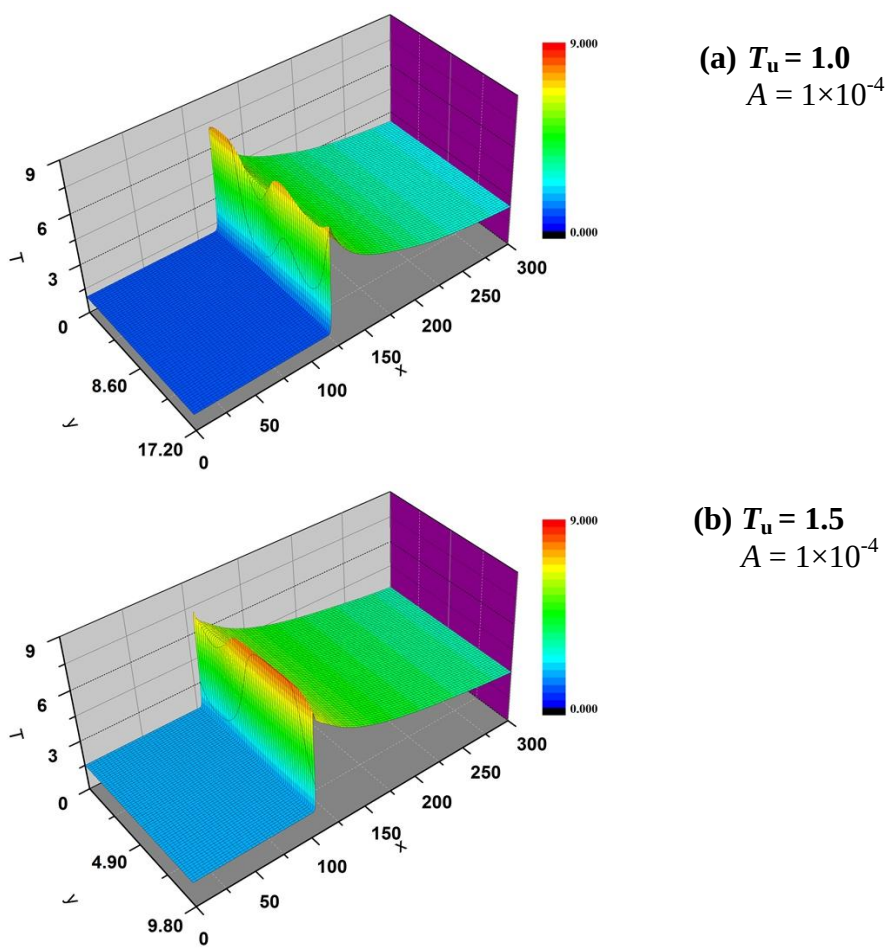

Figure 3.23 (a) (b): Temperature distribution of cellular flames at Le = 0.3, T_u = 1.0, 1.5.

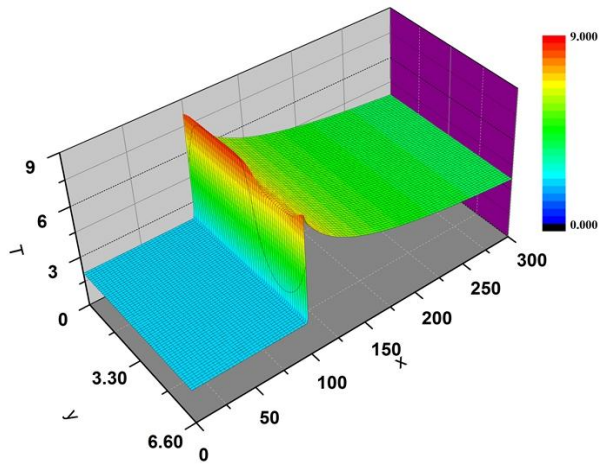

(c) $\boldsymbol{T_u = 2.0}$
$A = 1\times10^{-4}$

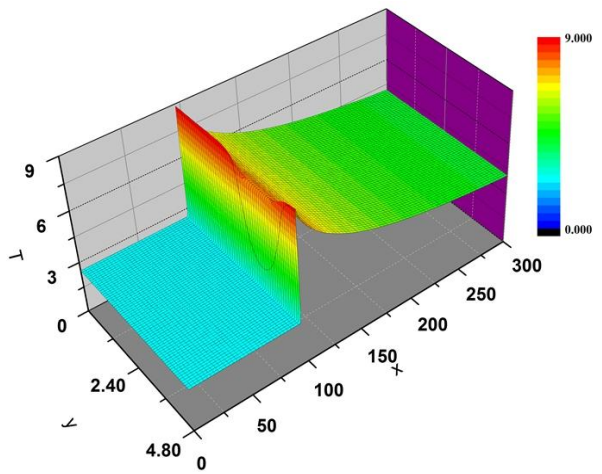

(d) $\boldsymbol{T_u = 2.5}$
$A = 1\times10^{-4}$

Figure 3.23 (c) (d): Temperature distribution of cellular flames at $Le = 0.3$, $T_u = 2.0, 2.5$.

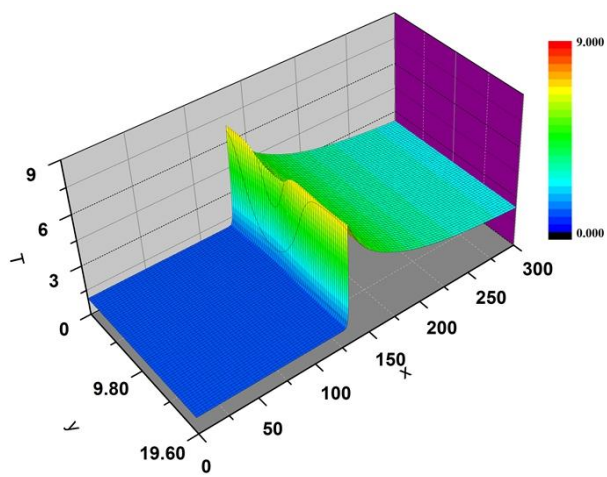

(a) $\boldsymbol{T_u = 1.0}$
$A = 1\times10^{-4}$

Figure 3.24 (a): Temperature distribution of cellular flames at $Le = 0.5$, $T_u = 1.0$.

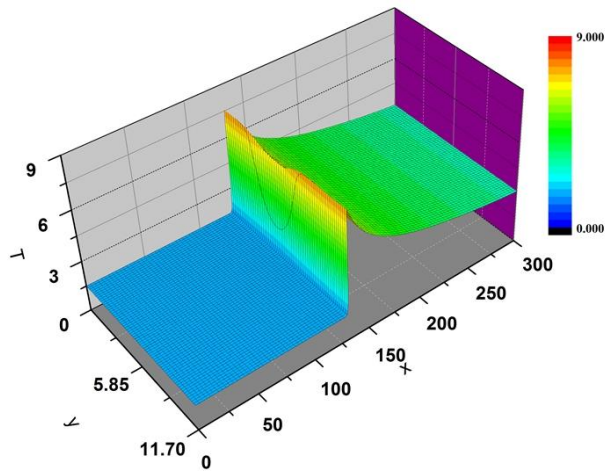

(b) $\boldsymbol{T_u = 1.5}$
$A = 1\times10^{-4}$

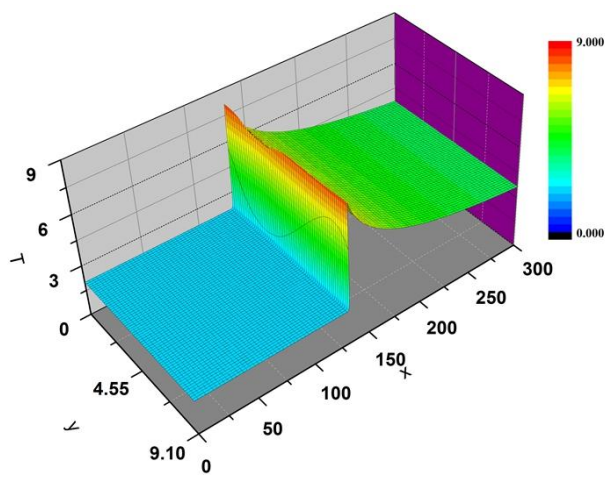

(c) $\boldsymbol{T_u = 2.0}$
$A = 1\times10^{-4}$

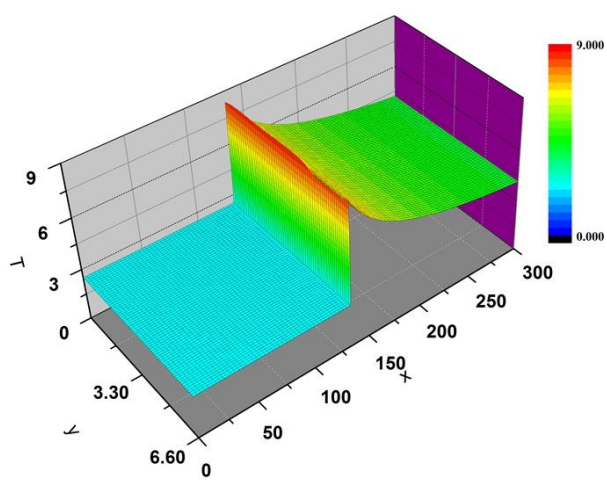

(d) $\boldsymbol{T_u = 2.5}$
$A = 1\times10^{-4}$

Figure 3.24 (b) (c) (d): Temperature distribution of cellular flames at $Le = 0.5$, $T_u = 1.5\sim2.5$.

3.2.2.4 Burning velocities of non-adiabatic cellular flames

The burning velocity of cellular flame, S_{cf} decreases because of the decrease of flame temperature due to the effect of heat loss. Burning velocities of the cellular flames and normalized values at Le = 0.3 and 0.5, and T_u = 1.0~2.5 are tabulated in Table.3.11. Compared with the adiabatic cellular flames, S_{cf} decreases due to the reduction of flame temperature and S_{cf}/S_u increases due to the effect of heat loss. This indicates that heat loss has a pronounced influence on diffusive-thermal instability of premixed flames at Lewis numbers less than unity.

Table 3.11: Burning velocities of cellular flames and normalized values at Le =0.3 and 0.5 ($A = 1\times10^{-4}$).

T_u	Le = 0.3		Le = 0.5	
	S_{cf}	S_{cf}/S_u	S_{cf}	S_{cf}/S_u
1.0	1.198	1.826	0.889	1.405
1.5	2.177	1.539	1.696	1.199
2.0	3.251	1.368	2.656	1.123
2.5	4.619	1.258	3.929	1.082

3.3 NUMERICAL RESULTS FOR LOW TEMPERATURE UNBURNED-GAS PREMIXED FLAMES

Numerical calculations for low temperature unburned-gas premixed flames are performed to investigate the effects of unburned-gas temperature and heat loss on the diffusive-thermal instability of premixed flames. The characteristic of the flames such as burning velocities of planar and cellular flames, dispersion relation, unstable behavior and structure of cellular flames are examined.

3.3.1 Effect of Unburned-Gas Temperature

The effect of unburned-gas temperature on low temperature unburned-gas premixed flame is investigated without taking into account the heat loss. The unburned-gas temperature is set to 1.0, 0.8 and 0.6 (25°C, -34.6°C, -94.2°C), Lewis number is set to 0.3 and 0.5.

3.3.1.1 Numerical results for adiabatic stationary planar flame

One dimensional numerical calculations are performed for T_u = 1.0, 0.8 and 0.6 to obtain the burning velocity of a stationary planar flame and initial conditions of temperature and mass fraction at Le = 0.3 and 0.5 without heat loss. Table 3.12 is the list of burning velocity of a stationary planar flame. Burning velocity of a planar flame decreases as the unburned-gas temperature becomes lower. This is because reaction rate in Arrhenius' form strongly depends on temperature, i.e. exp $(-E/RT)$. When the unburned-gas temperature decreases, the reaction becomes slower and burning velocity decreases. The burning velocity at Le = 0.5 is slightly lower than that at Le = 0.3 because of the decrease of the diffusive-thermal effect.

Table 3.12: Burning velocity of a planar flame for Le = 0.3 and 0.5, T_u = 1.0~0.6.

T_u	T_b	Y_u	S_u	
			Le = 0.3	Le = 0.5
1.0	7.0	1.0	1.0000	1.0000
0.8	6.8	1.0	0.8123	0.8110
0.6	6.6	1.0	0.6553	0.6509

3.3.1.2 Dispersion relations

The numerical calculation for dispersion relation, i.e. the relation between the growth rate ω and wave number k, is performed with initial conditions from one dimensional calculation to study the diffusive-thermal instability on premixed flame.

To obtain the dispersion relation, a sufficiently small disturbance, a_i = 0.1 is superimposed on a stationary planar flame. The displacement of the flame front in the x-direction due to the superimposed disturbance is a_i {sin ($2\pi y/\lambda$)}. The flame surface is defined as the region where the reaction rate takes a maximum value. The unburned gas flows into the left with the burning velocity of a stationary planar flame and flows out from the right. The sinusoidal flame front is growing with time and moving to the upstream in the x-direction indicating the increase of burning velocity. By varying the wave number, k (= $2\pi/\lambda$), the dispersion relation is obtained. The dispersion relations at Le = 0.3and 0.5 and T_u = 1.0 to 0.6 are shown in Fig. 3.25.

As the unburned-gas temperature becomes lower, the growth rate decreases and the unstable range narrows. This is mainly due to the decrease of the burning velocity of a planar flame. When the Lewis number increases or approaches to unity, diffusive-thermal instability becomes weaker. Thus, the growth rate at Le = 0.5 is low and unstable range is narrow. The marginal wave number k_m and critical wave number k_c decrease. The critical wavelengths λ_c (= $2\pi/k_c$), which are closely related to the spacing between cells of cellular flames induce by the intrinsic instability [50] at Le = 0.3

and 0.5 and T_u = 1.0 to 0.6 are tabulated in Table 3.13. The critical wavelength increases as the unburned-gas temperature becomes lower.

Table 3.13: Critical wavelengths at Le = 0.3 and 0.5.

T_u	T_b	Y_u	λ_c	
			Le =0.3	Le =0.5
1.0	7.0	1.0	13.3	16.4
0.8	6.8	1.0	16.6	19.3
0.6	6.6	1.0	19.6	22.4

As the burning velocity strongly affects the dispersion relation, it depends drastically on the unburned-gas temperature. Thus, growth rate and unstable range are normalized by the burning velocity of a planar flame to investigate the characteristics of the diffusive-thermal instability. Figure 3.26 shows the normalized dispersion relation at Le = 0.3 and 0.5. The normalized growth rate increases as the unburned-gas temperature decreases. To elucidate the effects of unburned-gas temperature, Zeldovich number (β) which is closely related to the diffusive-thermal instability, is considered. When the Lewis numbers is less than unity, the instability intensity becomes stronger as the Zeldovich number enlarges (Sivashinsky, 1983). The values of β at T_u = 1.0, 0.8 and 0.6 are 8.57, 9.08 and 9.64, respectively. The low unburned-gas temperature causes the increase of β since

$$\beta = \frac{T_b - T_u}{T_b^2} E$$

Thus the intensity of diffusive-thermal instability becomes stronger.

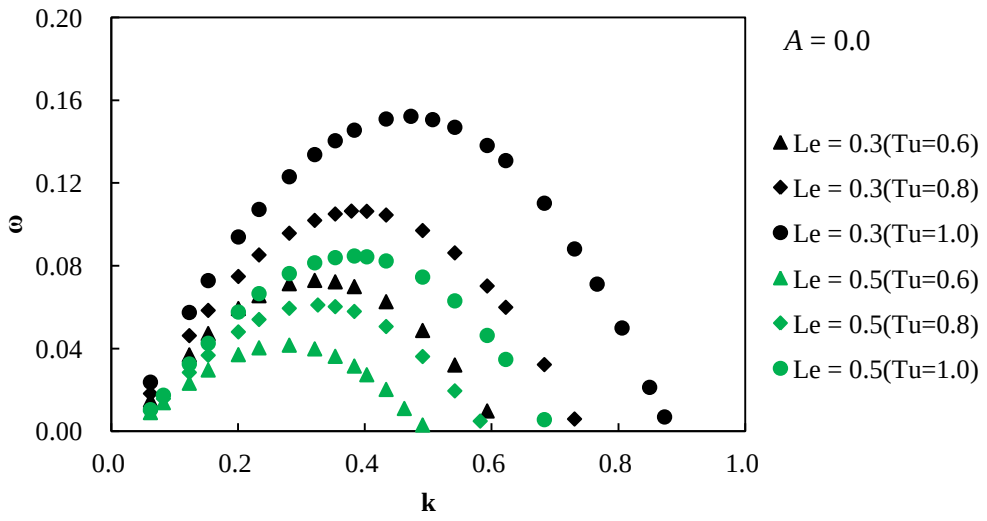

Figure 3.25: Dispersion relation at Le = 0.3 and 0.5, T_u = 1.0~0.6.

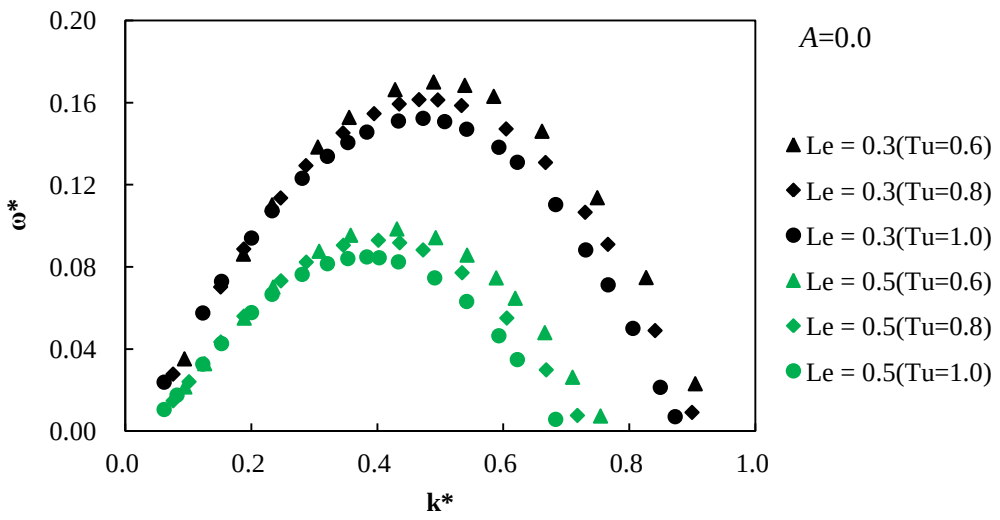

Figure 3.26: Normalized dispersion relation at Le = 0.3 and 0.5, T_u = 1.0~0.6.

3.3.1.3 Formation of cellular flame fronts

Cellular flames induced by the diffusive-thermal instability are investigated. To obtain the cellular flame, a disturbance with the critical wavelength is superimposed, where a_i = 1.0. Figures 3.27(a) (b) (c) and 3.28 (a) (b) (c) show the evolution of disturbed flame fronts at Le = 0.3 and 0.5, and T_u = 1.0 and 0.6. The flame front is defined as the

place where the reaction rate takes the maximum value. The superimposed disturbance evolves owing to the diffusive-thermal instability, and then cellular flame forms and moves upstream. The cell depth increases when the unburned-gas temperature becomes lower. This is because of the strength of intensity of diffusive-thermal instability. D_{cell}, D_{cell}/λ_c and L_{cf} are listed in Table 3.14. Here, L_{cf} is defined as the ratio of the length of cell in the y-direction to the critical wavelength. The increase of L_{cf} shows that the cell size becomes larger as the unburned-gas temperature becomes lower.

Table 3.14: D_{cell}, L_{cf} and D_{cell}/λ_c at Le = 0.3 and 0.5, and T_u = 1.0~0.6.

T_u	D_{cell}		L_{cf}		D_{cell}/λ_c	
	Le = 0.3	Le = 0.5	Le = 0.3	Le = 0.5	Le = 0.3	Le = 0.5
1.0	4.0183	3.0311	1.2613	1.1143	0.3021	0.1848
0.8	5.0353	3.6608	1.2697	1.1206	0.3033	0.1891
0.6	5.9715	4.2377	1.2722	1.1225	0.3047	0.1892

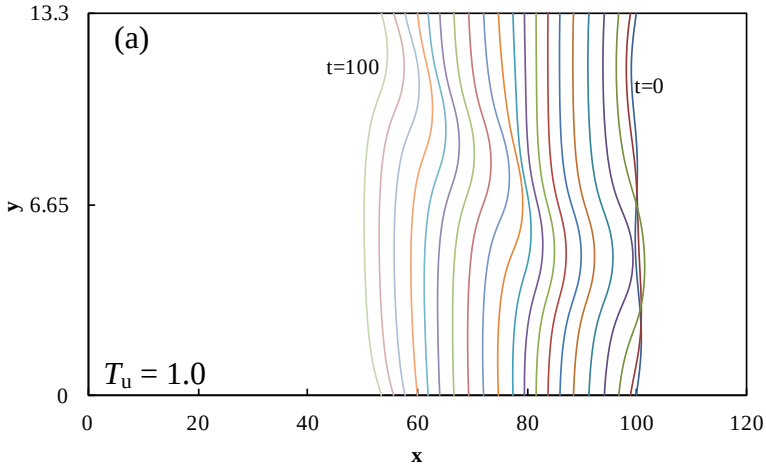

Figure 3.27 (a): Evolution of disturbed flame fronts at Le = 0.3, T_u = 1.0.

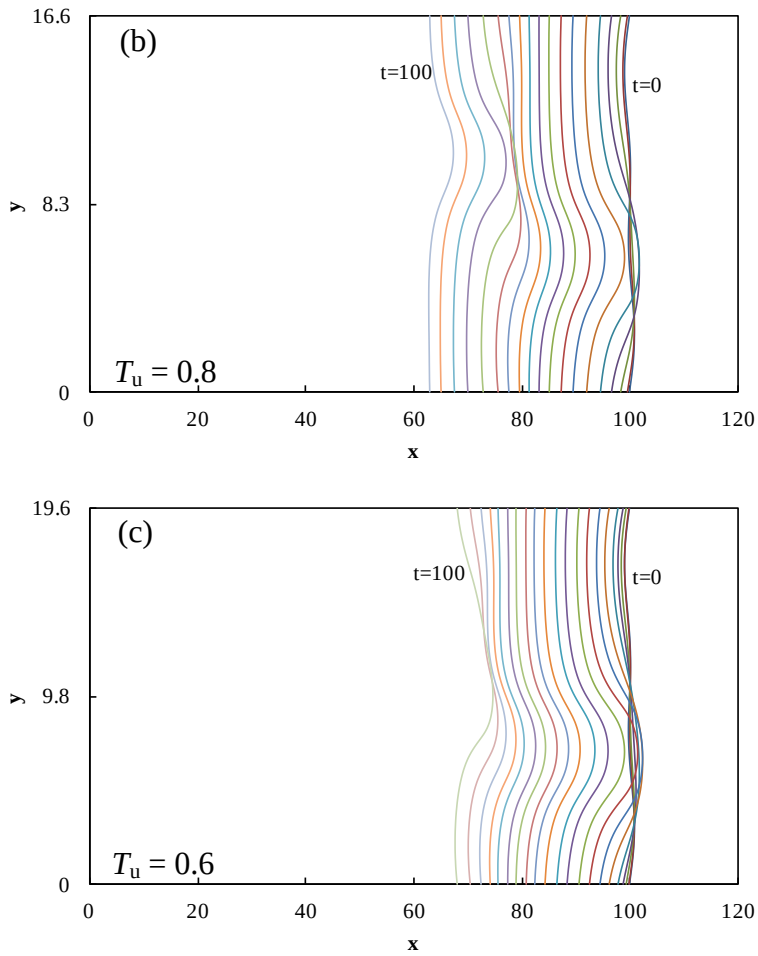

Figure 3.27 (b) (c): Evolution of disturbed flame fronts at Le = 0.3, T_u = 0.8 and 0.6.

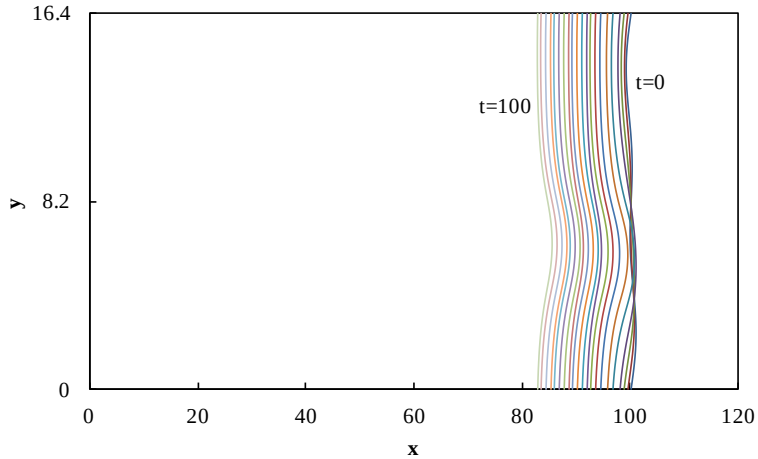

Figure 3.28 (a): Evolution of disturbed flame fronts at Le = 0.5, T_u = 1.0.

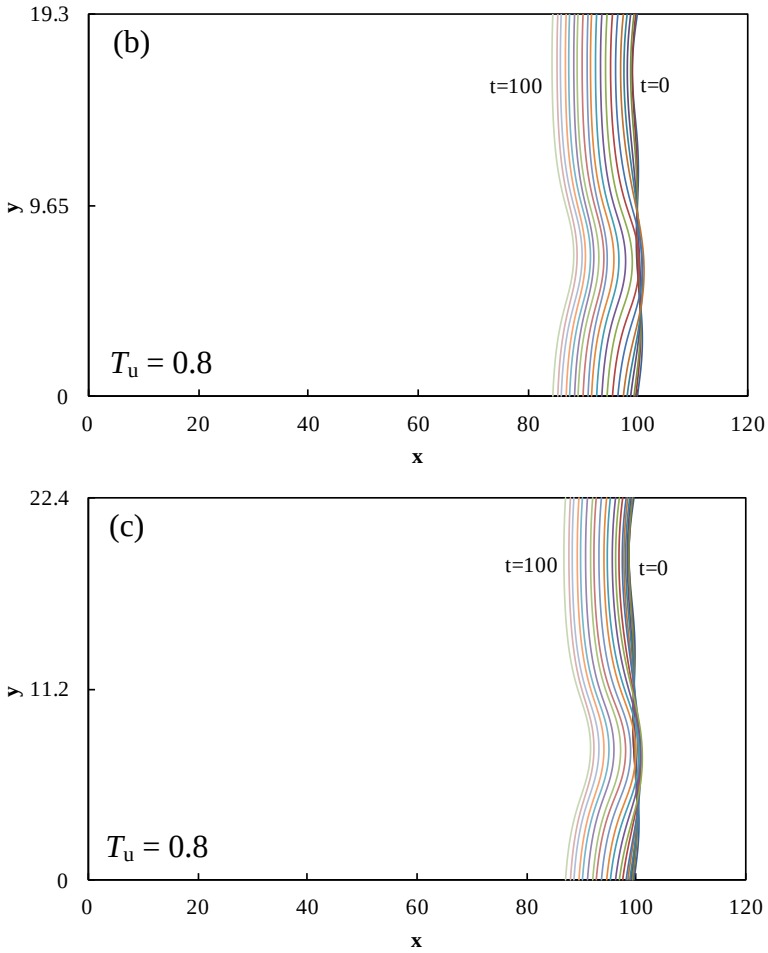

Figure 3.28 (b) (c): Evolution of disturbed flame fronts at Le = 0.5, T_u = 0.8 and 0.6.

Temperature distributions of cellular flames for T_u = 0.8 and 0.6 at Le = 0.3 and 0.5 are shown in Figs 3.29 (a) (b) (c), and 3.30 (a) (b) (c) (t = 60). The overshoot of the temperature is found at convex flame fronts toward the upstream. This is due to the diffusive-thermal effects, and this overshoot of the temperature causes the unstable behavior of the cellular flame fronts. [51] The overshoot portion becomes larger as the unburned-gas temperature becomes lower. This is because of the increase in strength of the intensity of diffusive-thermal instability.

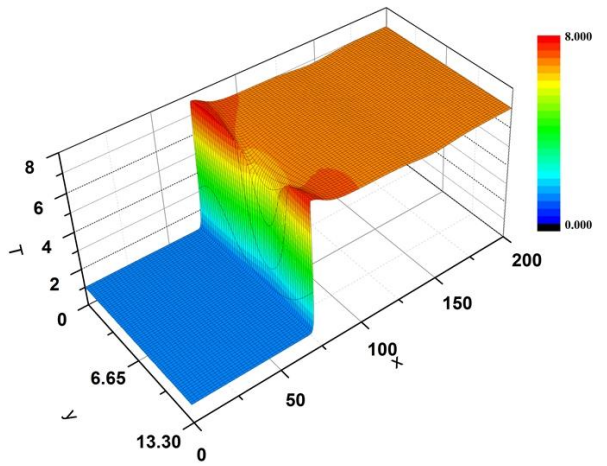

(a) T_u **= 1.0**

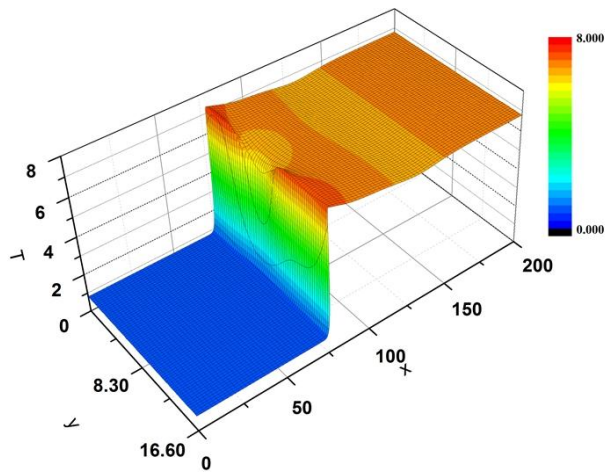

(b) T_u **= 0.8**

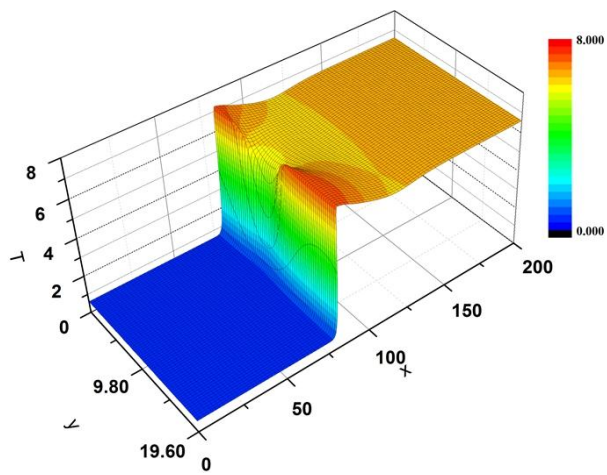

(c) T_u **= 0.6**

Figure 3.29 (a) (b) (c): Temperature distribution of cellular flame fronts at Le = 0.3, T_u = 1.0~0.6.

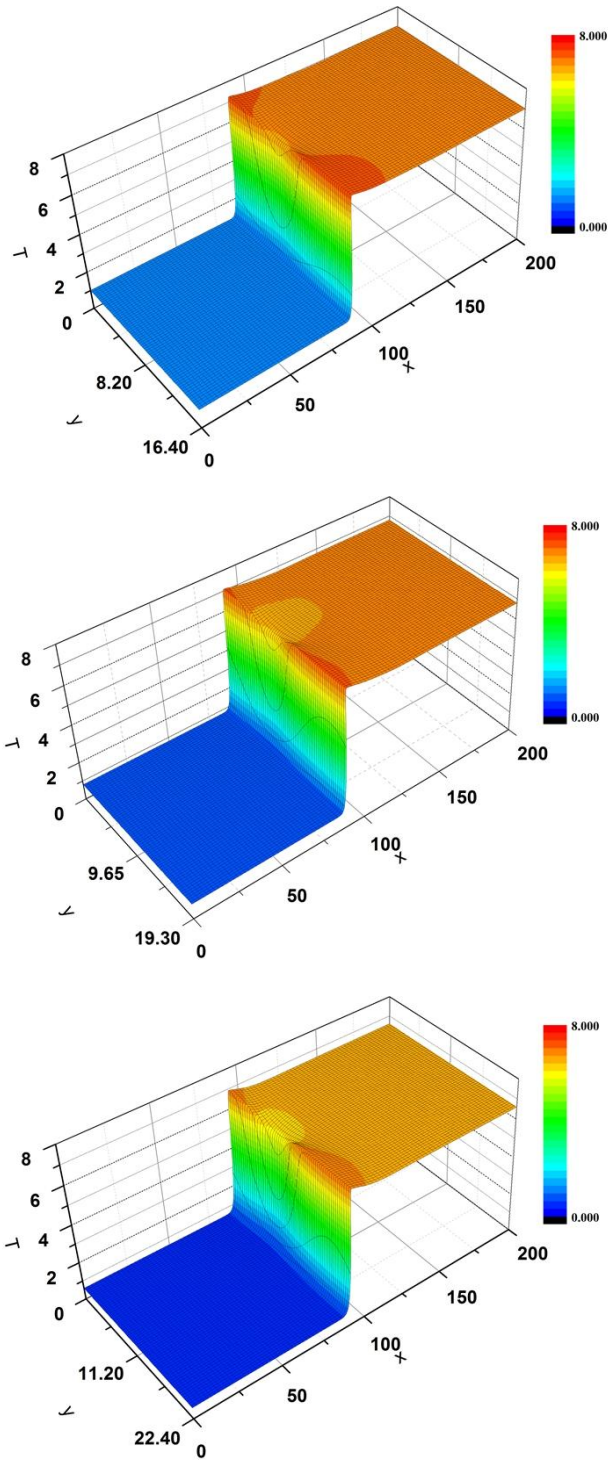

(a) T_u **= 1.0**

(b) T_u **= 0.8**

(c) T_u **= 0.6**

Figure 3.30 (a) (b) (c): Temperature distribution of cellular flame fronts at Le = 0.5, T_u = 1.0~0.6.

3.3.1.4 Burning velocities of cellular flames

The effect of unburned-gas temperature on the burning velocity of cellular flame is elucidated. The burning velocity of cellular flame S_{cf} decreases as the unburned-gas temperature becomes lower. It is calculated by the following procedure. The reaction rate is integrated throughout the simulation domain, and the integrated value is normalized by that of a planar flame. The normalized value is consistent with the non-dimensional burning velocity of a cellular flame. When the Lewis number increases, S_{cf} decreases because of the lowness of the diffusive-thermal effect. Burning velocities of cellular flames are normalized by those of planar flames. Normalized burning velocity increases slightly when unburned-gas temperature decreases. This is because of the enlargement of Zeldovich numbers. Table 3.15 shows the burning velocities of cellular flames and normalized values at Le = 0.3 and 0.5, T_u = 1.0~0.6.

Table 3.15: Burning velocities of cellular flames and normalized values at Le =0.3 and 0.5.

T_u	Le = 0.3		Le = 0.5	
	S_{cf}	S_{cf}/S_u	S_{cf}	S_{cf}/S_u
1.0	1.532	1.532	1.198	1.198
0.8	1.261	1.552	0.980	1.208
0.6	1.028	1.568	0.792	1.217

3.3.2 Effect of Heat Loss

As the combustion processes are strongly affected by heat loss owing to the irreversibility, we study the effect of radiative heat loss on the diffusive-thermal instability of low temperature unburned-gas premixed flames.

3.3.2.1 Numerical results for non-adiabatic stationary planar flame

Figure 3.31 shows the relation between the heat loss parameter and burning velocity of non-adiabatic planar flame at Le = 0.3 and 0.5, and T_u = 1.0~0.6. The burning velocities of non-adiabatic flames are smaller than those of adiabatic flames because of the decrease in flame temperature in downstream owing to the effect of heat loss. If the heat loss parameter is larger than maximum value A_{max}, the flame will extinguish. Burning velocities of planar flames depend on A are listed in Table 3.16 (a) (b) (c) and 3.17 (a) (b) (c) for Le = 0.3 and 0.5, respectively.

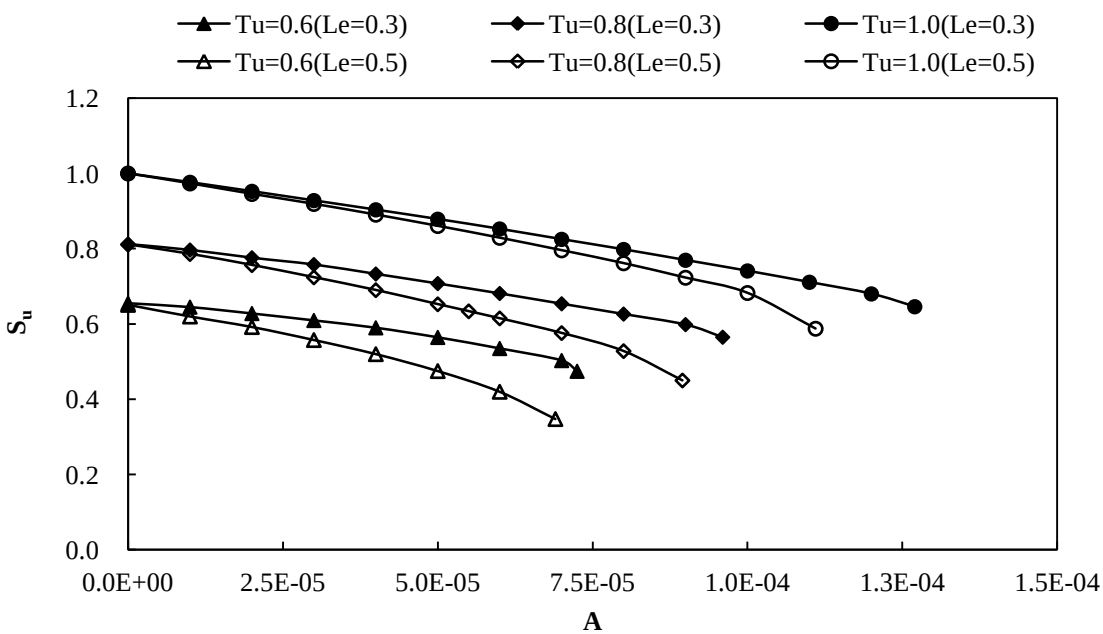

Figure 3.31: Relation between heat loss parameter and burning velocity at Le = 0.3 and 0.5.

Table 3.16: Burning velocities of planar flames depend on A at $Le = 0.3$.

A	S_u		
	$T_u = 1.0$	$T_u = 0.8$	$T_u = 0.6$
0	1.0000	0.8123	0.6553
0.00002	0.9525	0.7760	0.6280
0.00004	0.9035	0.7330	0.5900
0.0000725	-	-	0.4745
0.000096	-	0.5650	-
0.000127	0.6460	-	-

Table 3.17: Burning velocities of planar flames depend on A at $Le = 0.5$.

A	S_u		
	$T_u = 1.0$	$T_u = 0.8$	$T_u = 0.6$
0	1.0000	0.8109	0.6509
0.00002	0.9455	0.7565	0.5920
0.00004	0.8905	0.6900	0.5200
0.000069	-	-	0.3475
0.0000895	-	0.4500	-
0.000111	0.5875	-	-

3.3.2.2 Dispersion relations

Dispersion relation and normalized dispersion relation at $A = 4\times10^{-5}$, $Le = 0.3$ and 0.5, and $T_u = 1.0$~0.6 are shown in Figs. 3.32 and 3.33. The growth rate decreases due to the heat loss effect compared with the adiabatic premixed flames. Normalized growth rate increases when heat loss parameter increases. This indicates that the heat loss has a pronounced influence on the premixed flames at $Le < 1.0$. The critical wave number also decreases. The growth rate becomes lower and the unstable range becomes narrow when Lewis number becomes larger. This is the lowness of diffusive-thermal instability. The normalized growth rate increases and normalized unstable range widens as the unburned-

gas temperature decreases. This is because of the enlargement of Zeldovich number and effect of heat loss, and thus the intensity of diffusive-thermal instability is strong compared with adiabatic premixed flames. The critical wavelengths at $Le = 0.3$ and 0.5 for $A = 4\times10^{-4}$ are listed in Table.3.18.

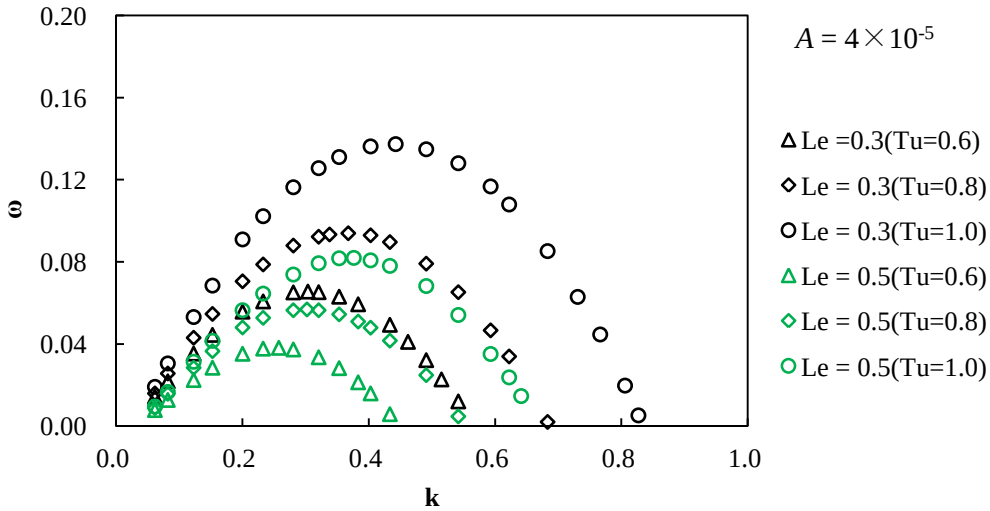

Figure 3.32: Dispersion relation at $Le = 0.3$ and 0.5, $T_u = 1.0\sim0.6$ ($A = 4\times10^{-5}$).

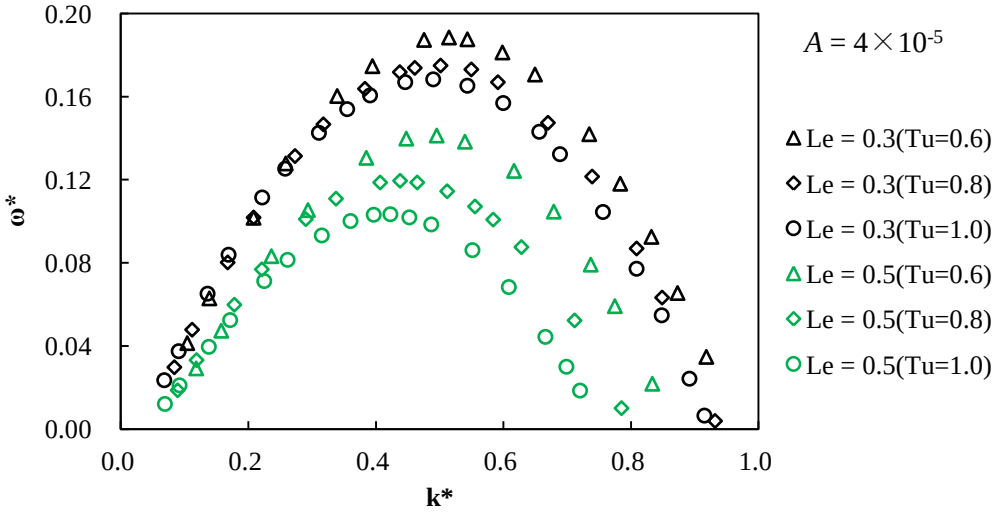

Figure 3.33: Normalized dispersion relation at $Le = 0.3$ and 0.5, $T_u = 1.0\sim0.6$ ($A = 4\times10^{-5}$).

Table 3.18: Critical wavelengths at Le = 0.3 and 0.5 ($A = 4\times10^{-5}$).

T_u	T_b	Y_u	λ_c	
			Le =0.3	Le =0.5
1.0	7.0	1.0	14.2	16.7
0.8	6.8	1.0	17.1	20.8
0.6	6.6	1.0	20.7	24.4

3.3.2.3 Formation of cellular flame fronts

Cellular flame forms owing to the diffusive-thermal effect. To obtain the cellular flame, a disturbance with the critical wavelength is superimposed, where a_i = 1.0. Because of the effects of heat loss, burning velocities of cellular flames decreases compared with the adiabatic cellular flames. Figures 3.34 (a) (b) and (c) show the evolution of the disturbed flame fronts at Le = 0.3 and T_u = 1.0~0.6, $A = 4\times10^{-5}$. The distance between the convex and concave flame fronts, i.e., D_{cell} becomes larger, D_{cell}/λ_c and L_{cf} increases due to the heat loss effect. It shows that unstable behavior of the cellular flame is strong in non-adiabatic premixed flames.

The evolutions of the disturbed flames at Le = 0.5 are shown in Figs. 3.35 (a) (b) and (c), $A = 4\times10^{-5}$. The unstable behavior of the flame fronts becomes weaker when Lewis number becomes larger. Temperature distributions of the non-adiabatic cellular flames at Le = 0.3, T_u = 1.0~0.6 (t = 60) are shown in Figs. 3.36 (a) (b) and (c). Flame temperature decreases in downstream, and the overshoot of the temperature becomes larger because of the heat loss effect. Figures 3.37 (a) (b) and(c) show the temperature distribution of cellular flames at Le = 0.5 and T_u = 1.0~0.6 (t = 60), $A = 4\times10^{-5}$. Table 3.19 describes D_{cell}, L_{cf} and D_{cell}/λ_c at Le = 0.3 and 0.5, and T_u = 1.0~0.6.

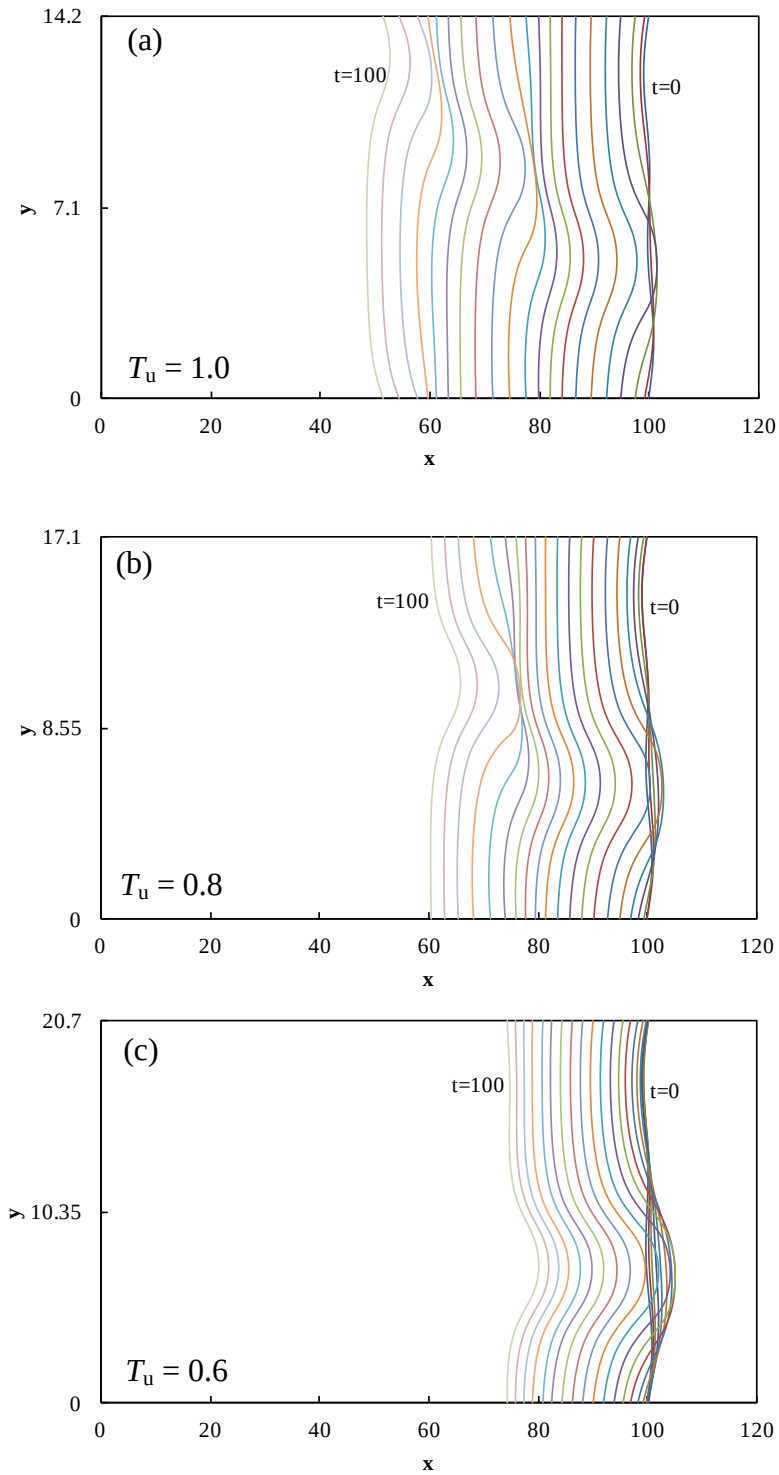

Figure 3.34 (a) (b) (c): Evolution of disturbed flame fronts at Le = 0.3, T_u=1.0~0.6 (A = 4×10^{-5}).

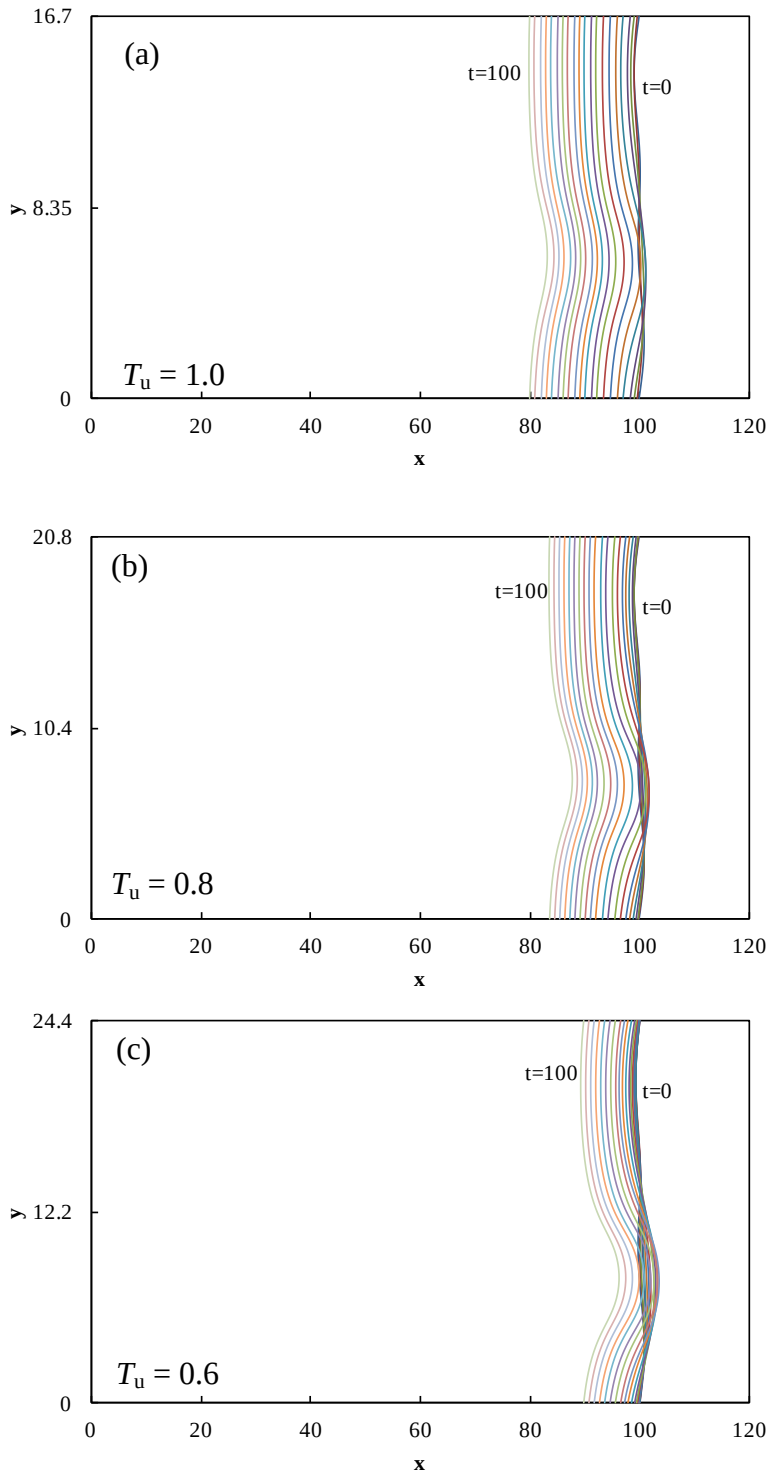

Figure 3.35 (a) (b) (c): Evolution of disturbed flame fronts at Le = 0.5, T_u=1.0~0.6 (A = 4×10^{-5}).

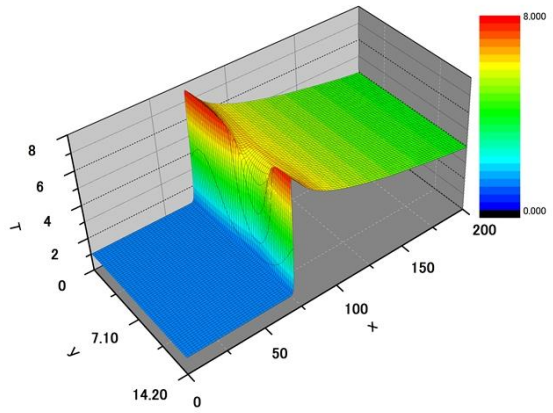

(a) T_u = 1.0

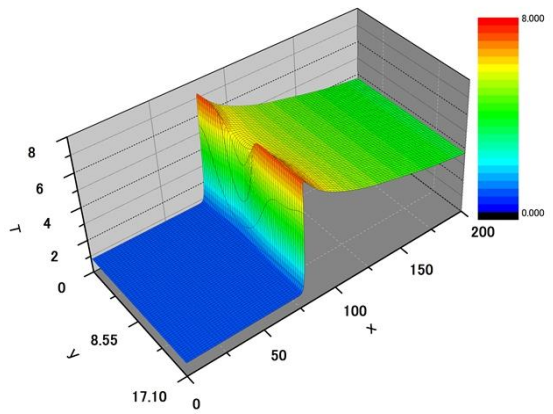

(b) T_u = 0.8

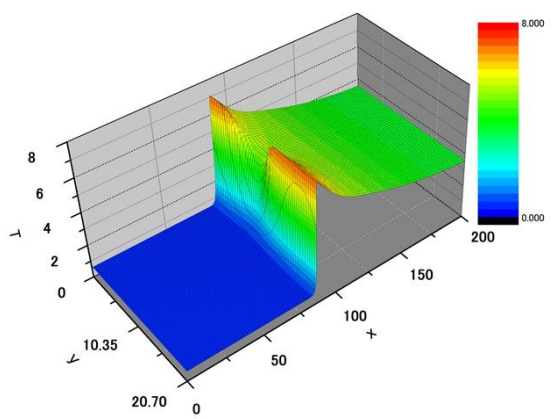

(c) T_u = 0.6

Figure 3.36 (a) (b) (c): Temperature distribution of cellular flame fronts at Le = 0.3, T_u=1.0~0.6 ($A = 4\times10^{-5}$).

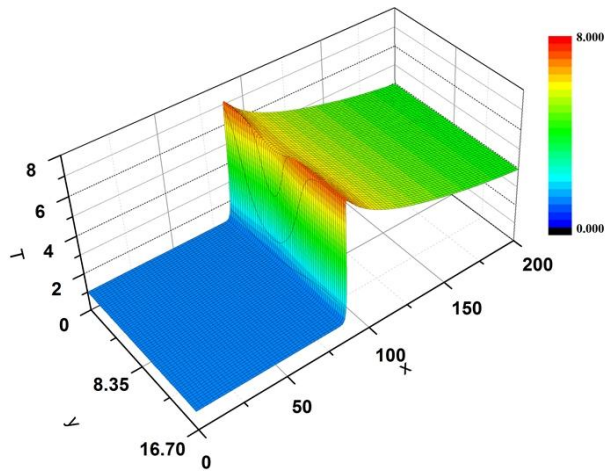

(a) T_u = 1.0

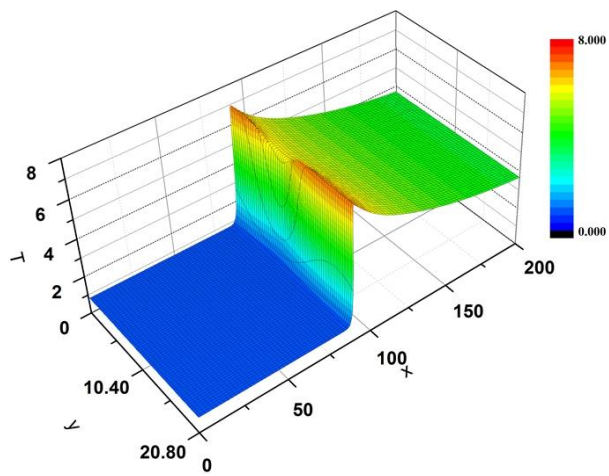

(b)T_u = 0.8

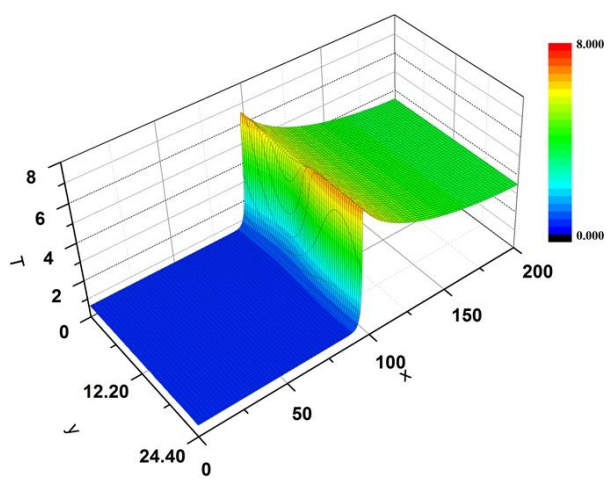

(c) T_u = 0.6

Figure 3.37 (a) (b) (c): Temperature distribution of cellular flame fronts at Le = 0.5, T_u=1.0~0.6 (A = 4×10^{-5}).

Table 3.19: D_{cell}, L_{cf} and D_{cell}/λ_c at Le = 0.3 and 0.5, and T_u = 1.0~0.6 ($A = 4\times10^{-5}$).

T_u	D_{cell}		L_{cf}		D_{cell}/λ_c	
	Le = 0.3	Le = 0.5	Le = 0.3	Le = 0.5	Le = 0.3	Le = 0.5
1.0	4.4688	3.395	1.2855	1.133	0.3147	0.2033
0.8	5.5878	4.342	1.3077	1.144	0.3268	0.2087
0.6	6.8478	5.148	1.3206	1.153	0.3308	0.2110

3.3.2.4 Burning velocities of non-adiabatic cellular flames

The burning velocity of cellular flame S_{cf} decreases because of the decrease of flame temperature due to the effect of heat loss. Burning velocities of cellular flames and normalized values at Le = 0.3 and 0.5 for T_u = 1.0~0.6 are tabulated in Table.3.20. Compared with adiabatic cellular flames, S_{cf} decreases due to the reduction of flame temperature and S_{cf}/S_u increases due to the effect of heat loss. This indicates that heat loss has a pronounced influence on diffusive-thermal instability of premixed flames at Lewis numbers less than unity.

Table 3.20: Burning velocities of cellular flames and normalized values at Le = 0.3 and 0.5, and T_u = 1.0~0.6 ($A = 4\times10^{-5}$).

T_u	T_b	Y_u	Le = 0.3		Le = 0.5	
			S_{cf}	S_{cf}/S_u	S_{cf}	S_{cf}/S_u
1.0	7.0	1.0	1.413	1.564	1.094	1.229
0.8	6.8	1.0	1.164	1.588	0.860	1.246
0.6	6.6	1.0	0.944	1.600	0.661	1.271

3.4 CONCLUDING REMARKS

The effects of unburned-gas temperature and radiative heat loss on the diffusive-thermal instability of high and low temperature unburned-gas premixed flames are studied based on the diffusive-thermal model equation where thermal expansion effect is neglected. The obtained results are as follows:

When the Lewis number is less than unity, as the unburned-gas temperature increases (decreases), the burning velocity of a planar flame increases (decreases); the growth rate increases (decreases) and the normalized growth rate decreases (increases); λ_c, D_{cell}, L_{cf} and D_{cell}/λ_c decrease (increase); the burning velocity of cellular flame increases (decreases) and the normalized burning velocity decreases (increases).

When the heat loss parameter becomes larger, the burning velocity of a planar flame becomes lower; the growth rate decreases and the normalized growth rate increases; the burning velocity of cellular flame decreases and the normalized burning velocity increases.

The overshoot of the temperature at $Le = 0.5$ is small compared with that at $Le = 0.3$, and the unstable behavior of the cellular flame is weak.

Chapter 4: Diffusive-Thermal and Hydrodynamic Instabilities of Premixed Flames

4.1 INTRODUCTION

The effects of unburned-gas temperature and radiative heat loss on diffusive-thermal and hydrodynamic instabilities are studied for low temperature unburned-gas premixed flames under the adiabatic and non-adiabatic conditions. Unsteady reactive flow based on the compressible Navier-Stokes equation including chemical reaction and radiative heat loss is calculated numerically to investigate not only the diffusive-thermal instability but also the hydrodynamic one. [47] The adiabatic flame temperature, T_b is set to 7.0 which is general for premixed flames of hydrogen-air or methane-air. Lewis number, Le is set to 0.5, 0.7 and 1.0, where the effect of preferential diffusion of mass and heat, and effect of thermal expansion occur. For constant temperature jump condition, Y_u is set to 1.0. Unburned-gas temperature, T_u is set to 1.0, 0.8 and 0.6. The ideal gas equation of state is satisfied and pressure is assumed as a constant for all calculations.

4.2 NUMERICAL RESULTS FOR LOW TEMPERATURE UNBURNED-GAS PREMIXED FLAMES

To study the effects of unburned-gas temperature and heat loss on the intrinsic instability of premixed flames, one- and two-dimensional numerical calculations are performed. The characteristics of the premixed flames, such as burning velocity, dispersion relations, unstable behavior and formation of cellular flame fronts are investigated.

4.2.1 Effect of Unburned-Gas Temperature

To study the effect of unburned-gas temperature, radiative heat loss is neglected, i.e. A = 0. T_u is set to 1.0, 0.8 and 0.6, and then T_b becomes 7.0, 6.8 and 6.6, respectively. Le is set to 0.5, 0.7 and 1.0.

4.2.1.1 Numerical results for adiabatic stationary planar flame

One-dimensional numerical calculations are performed for unburned-gas temperature, T_u = 1.0, 0.8 and 0.6 to obtain the burning velocity of a stationary planar flame and initial conditions for two-dimensional calculations, at Le = 0.5, 0.7 and 1.0 without taking into account the heat loss. Table 4.1 shows the burning velocity of a stationary planar flame at Le = 0.5~1.0 depending on the unburned-gas temperature. Burning velocity of a planar flame decreases when the unburned-gas temperature decreases. This is because reaction rate in Arrhenius' form strongly depends on temperature, i.e. exp (-E/RT). Burning velocity of a planar flame slightly decreases when the Lewis number increases at T_u = 0.8 and 0.6. The distributions of density, energy, pressure, temperature and mass fraction, ρ, e, p, T, Y at Le = 0.5 and T_u = 1.0~0.6 are shown in Figs. 4.1, 4.2 and 4.3.

Table 4.1: Burning velocity of adiabatic planar flame at Le = 0.5~1.0.

T_u	T_b	Y_u	S_u		
			Le = 0.5	Le = 0.7	Le = 1.0
1.0	7.0	1.0	1.000	1.000	1.000
0.8	6.8	1.0	0.667	0.656	0.651
0.6	6.6	1.0	0.425	0.401	0.397

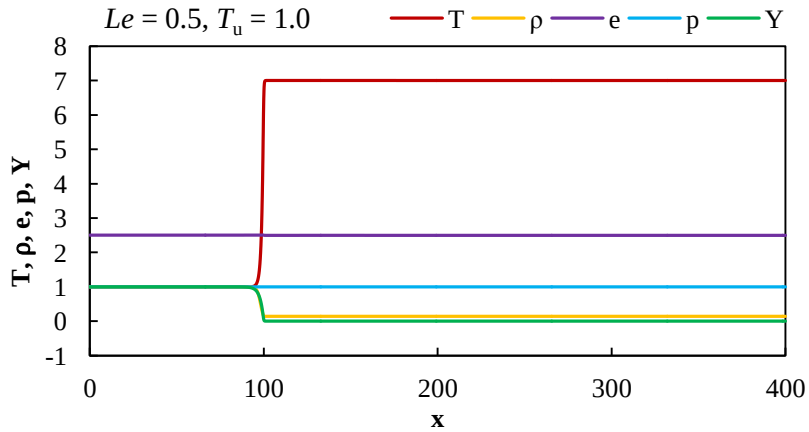

Figure 4.1: Distribution of T, ρ, e, p, Y at $Le = 0.5$ and $T_u = 1.0$.

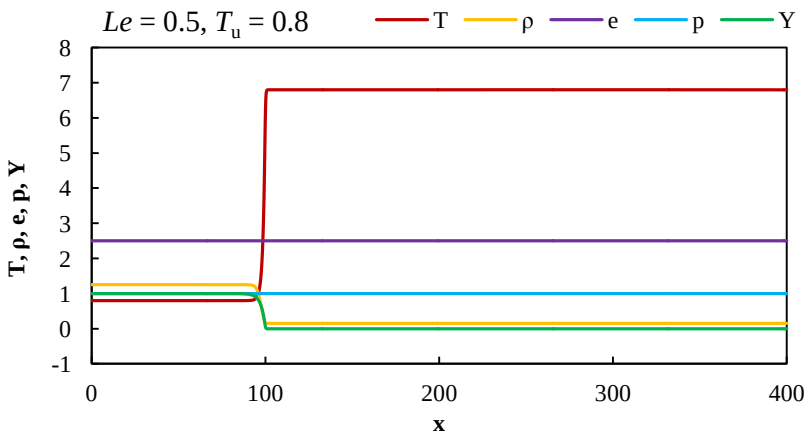

Figure 4.2: Distribution of T, ρ, e, p, Y at $Le = 0.5$ and $T_u = 0.8$.

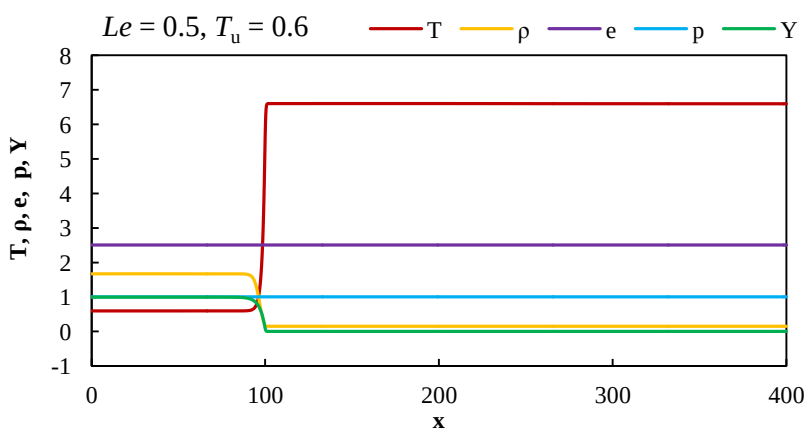

Figure 4.3: Distribution of T, ρ, e, p, Y at $Le = 0.5$ and $T_u = 0.6$.

4.2.1.2 Dispersion relations

For the numerical calculations of dispersion relation, initial conditions are provided by the solutions from one dimensional calculation. A sinusoidal disturbance is superimposed on a planar flame. The displacement of the flame front in the x-direction due to the superimposed disturbance is a_i {sin $(2\pi y/\lambda)$}. The initial amplitude a_i is set to 0.1. Flame surface is the site where the reaction takes a maximum value. The unburned gas flows into the left with the burning velocity of a stationary planar flame and flows out from the right. The sinusoidal flame front is growing with time. This shows the flame is unstable due to intrinsic instabilities. The evolution of the disturbed flame front along with time at Le = 0.5 and T_u = 1.0 with the wavelength of 11.7 is shown in Fig.4.4. The abscissa is normalized by the initial amplitude.

The amplitude growth rate in each time at Le = 0.5 and T_u = 1.0 is shown in Fig.4.5. The ordinate is the natural logarithm of the ratio of the amplitude of a disturbance to the initial amplitude. The abscissa is the non-dimensional time. The amplitude growth rate increases linearly with time, and thus, the amplitude of the disturbance grows exponentially with time $\{a \sim a_i \exp(\omega t)\}$.

By varying the wave number, k (= $2\pi/\lambda$), the dispersion relation is obtained. The growth rate slows down to zero when the wave number approaches to zero. Similarly, the growth rate approaches to a maximum value when the wave number becomes larger. When the wave number further increases, the growth rate decreases monotonically and there is a marginal wave number which separates the unstable and stable range. When the wave number is larger than a marginal value, the growth rate becomes negative.

The dispersion relations at Le = 0.5~1.0 depending on the unburned-gas temperature are described in Fig. 4.6. The growth rate decreases and unstable range narrows as the decrease of burning velocity of planar flame, and the former increases and

the latter widens when Lewis number becomes lower, which is due to the strength of diffusive-thermal effect at $Le < 1$. The linearly most unstable wave number corresponding to the maximum growth rate is obtained, and which is referred as the critical wave number, k_c. The critical wavelength λ_c (= $2\pi/k_c$) becomes longer. The obtained critical wavelengths are listed in Table.4.2.

The burning velocity affects the dispersion relation, and it depends drastically on the unburned-gas temperature. Thus, to study the characteristics of the intrinsic instability, the growth rate and wave number are normalized by the burning velocity of a planar flame. Figure 4.7 shows the normalized dispersion relation. The normalized growth rate increases as the unburned-gas temperature becomes lower. When the Lewis number is unity, the flame is affected only by thermal expansion which causes the hydrodynamic instability. For Lewis numbers less than unity, we consider Zeldovich number which is closely related to the diffusive-thermal instability to elucidate the effects of unburned-gas temperature. At $Le < 1$, the instability intensity becomes stronger as the Zeldovich number enlarges (Sivashinsky, 1983). [52] The values of Zeldovich number, β for unburned-gas temperature 0.6 to 1.0 are listed in Table 4.3. The low unburned-gas temperature causes the enlargement of Zeldovich numbers, so that the instability becomes stronger as the unburned-gas temperature becomes lower. In addition, thermal expansion effect raises the strength of instability.

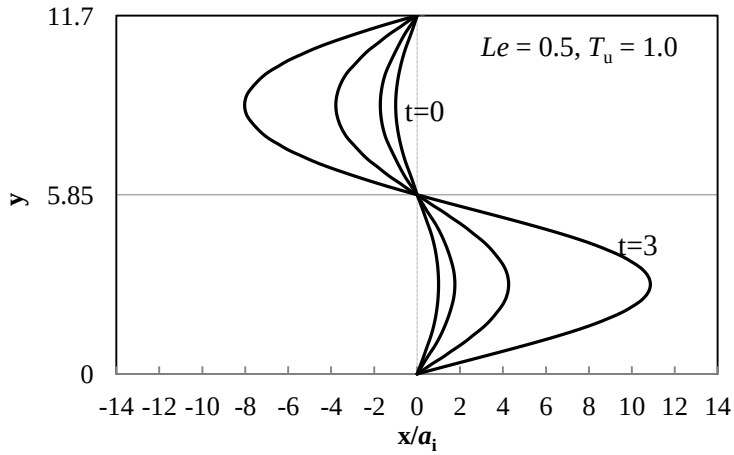

Figure 4.4: Evolution of the disturbed flame front at Le = 0.5 and T_u = 1.0 for adiabatic premixed flame.

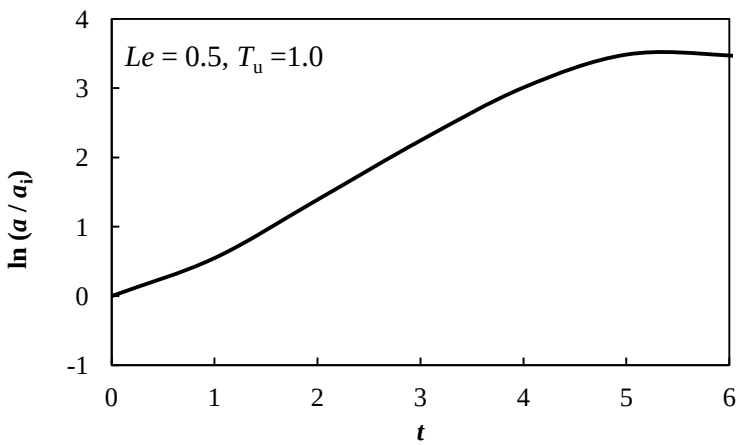

Figure 4.5: Amplitude growth rate of disturbance at Le = 0.5 and T_u = 1.0.

Table 4.2: Critical wavelengths at Le = 0.5~1.0.

T_u	T_b	Y_u	λ_c		
			Le = 0.5	Le = 0.7	Le =1.0
1.0	7.0	1.0	11.7	14.9	34.0
0.8	6.8	1.0	13.6	17.2	38.4
0.6	6.6	1.0	15.8	20.1	42.8

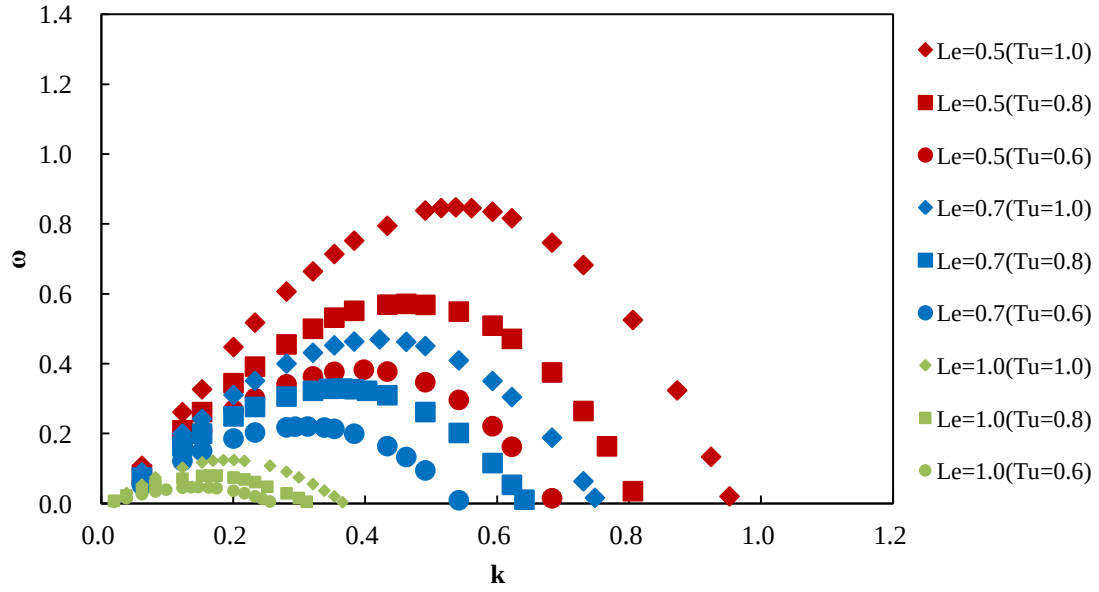

Figure 4.6: Dispersion relation at Le = 0.5~1.0 and T_u = 1.0~0.6.

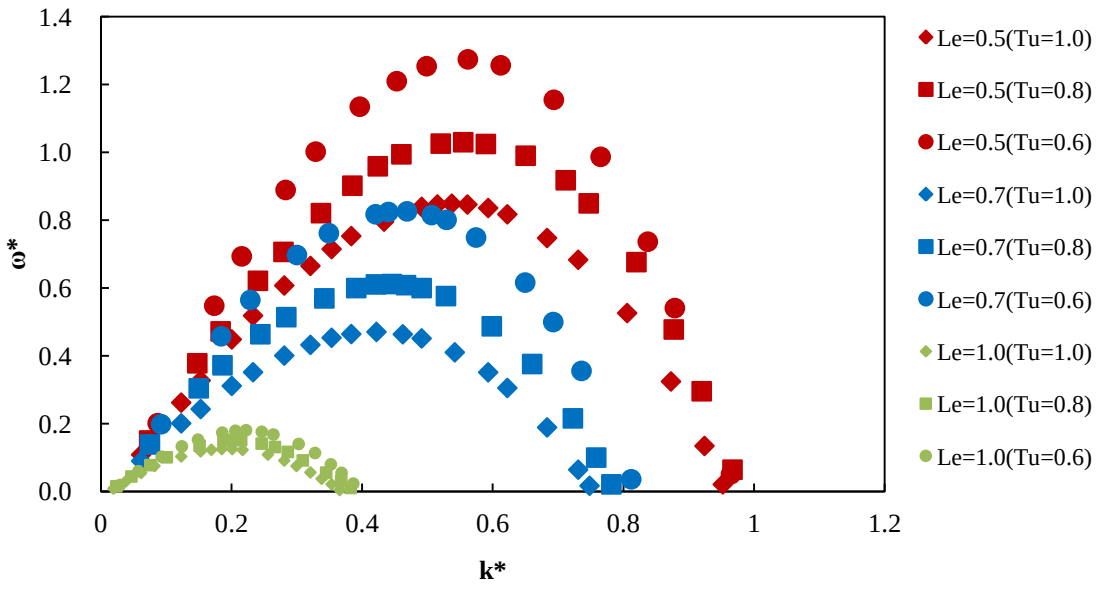

Figure 4.7: Normalized dispersion relation at Le = 0.5~1.0 and T_u = 1.0~0.6.

Table 4.3: Zeldovich numbers for T_u = 1.0~0.6.

T_u	T_b	β
1.0	1.0	8.57
0.8	6.8	9.08
0.6	6.6	9.64

4.2.1.3 Formation of cellular flame fronts

Characteristics of cellular flames induced by the intrinsic instability are investigated. To obtain the cellular flame, a disturbance with the critical wavelength is superimposed, where a_i = 1.0. Figures 4.8 (a) (b) (c) through 4.10 (a) (b) (c) illustrate the evolution of disturbed flame fronts at Le = 0.5, 0.7 and 1.0 and T_u = 1.0~0.6. The flame front is defined as the position where the reaction rate takes maximum value. The unburned gas flows in from the left at the burning velocity of a planar flame, and the burned gas flows out to the right. The superimposed disturbance evolves owing to the increase of the burning velocity due to the increase of flame-surface area. D_{cell} increases, L_{cf} and D_{cell}/λ_c become larger when the unburned-gas temperature becomes lower. This is because of the strength of hydrodynamic and diffusive-thermal instability. D_{cell}, L_{cf} and D_{cell}/λ_c at Le = 0.5~1.0 depend on the unburned-gas temperature are listed in Table 4.4.

Table 4.4: D_{cell}, L_{cf} and D_{cell}/λ_c of cellular flames at Le = 0.5~1.0 and T_u = 1.0~0.6.

T_u	D_{cell}			L_{cf}			D_{cell}/λ_c		
	Le = 0.5	Le = 0.7	Le = 1.0	Le = 0.5	Le = 0.7	Le = 1.0	Le = 0.5	Le = 0.7	Le = 1.0
1.0	5.465	4.904	9.672	1.498	1.278	1.218	0.4671	0.3291	0.2845
0.8	6.926	6.109	11.058	1.596	1.318	1.229	0.5093	0.3552	0.2880
0.6	8.811	7.846	11.476	1.697	1.368	1.259	0.5577	0.3903	0.2919

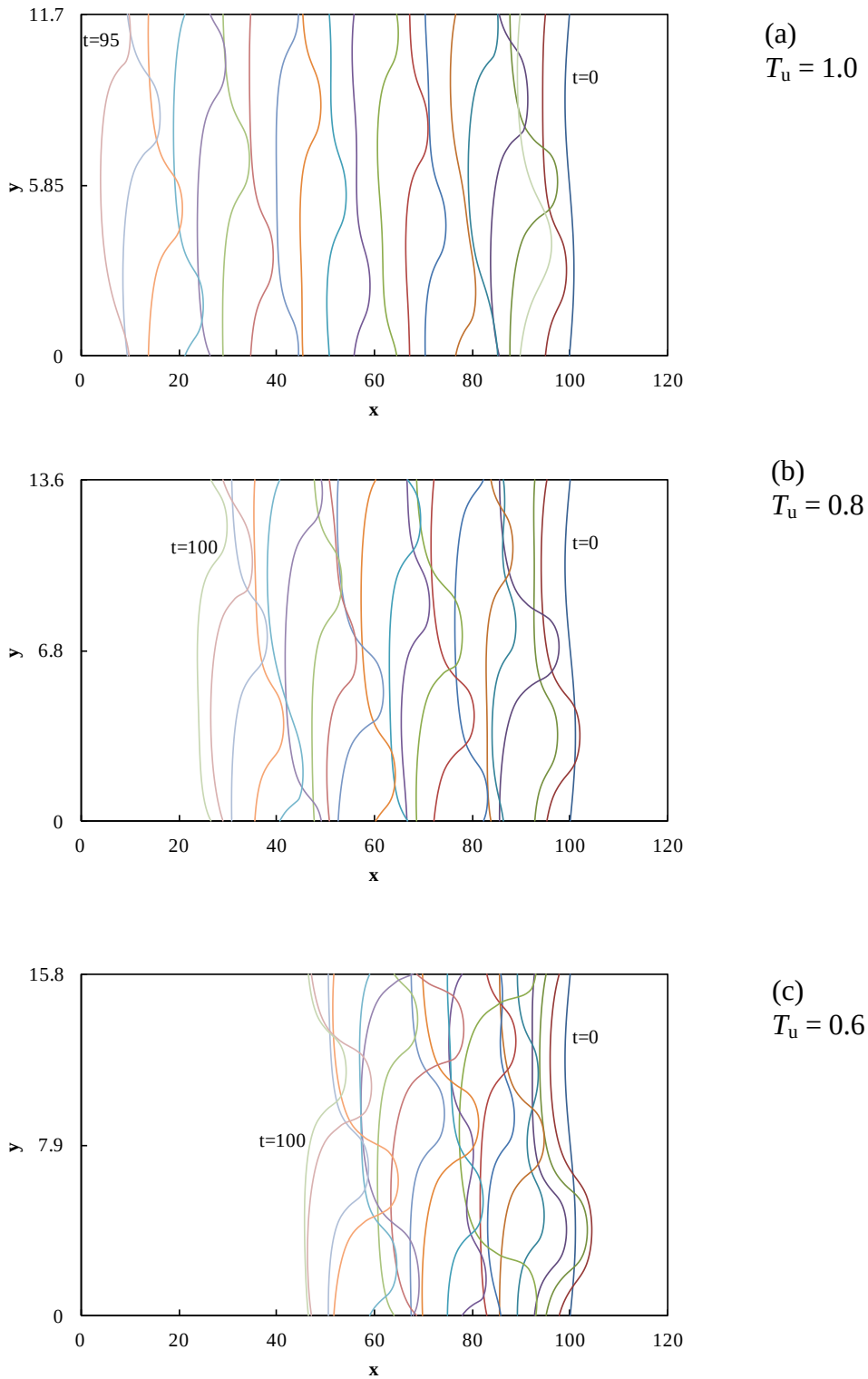

(a)
$T_u = 1.0$

(b)
$T_u = 0.8$

(c)
$T_u = 0.6$

Figure 4.8 (a) (b) (c): Evolution of disturbed flame fronts at $Le = 0.5$ and $T_u = 1.0$~0.6.

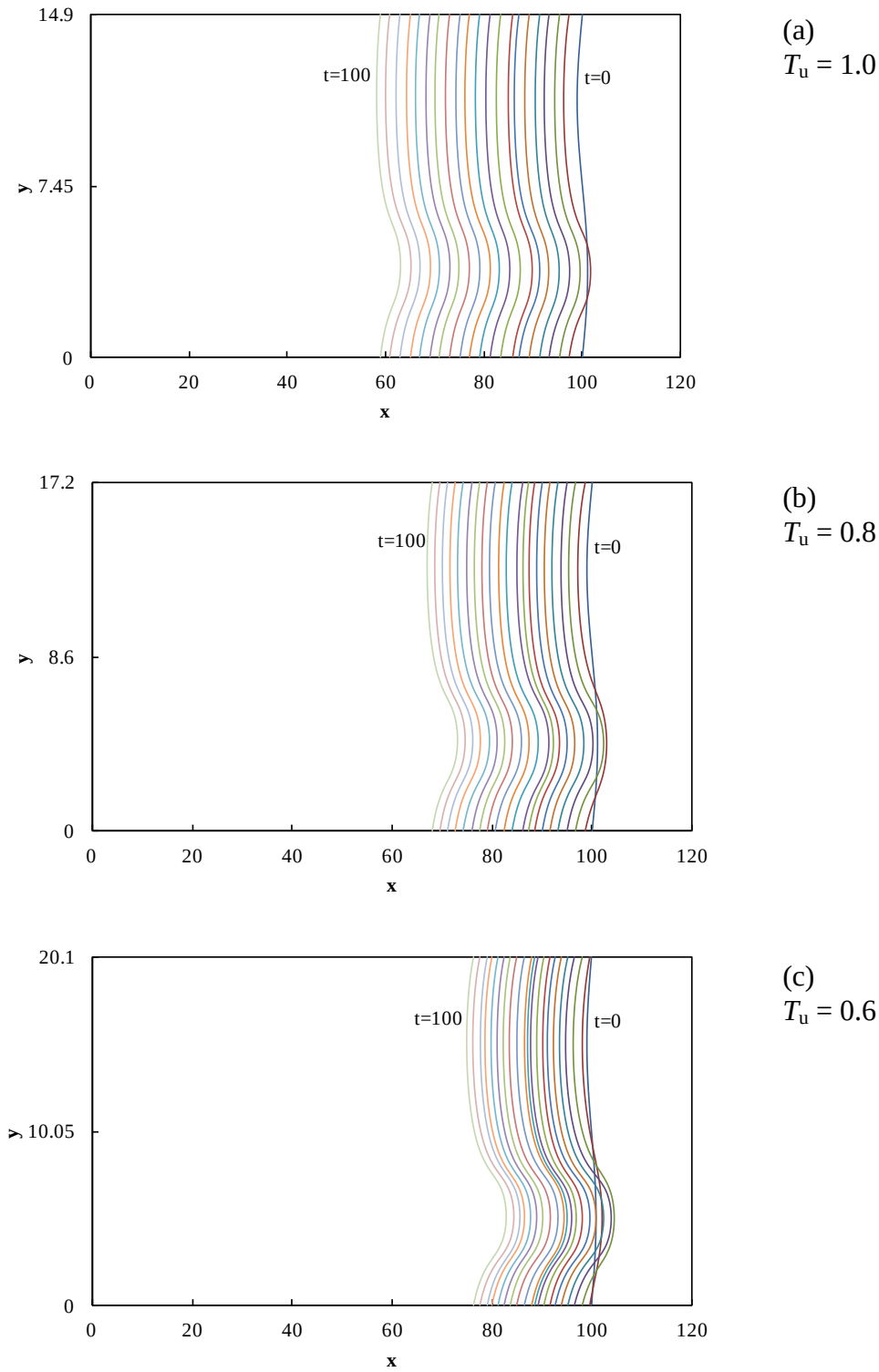

Figure 4.9 (a) (b) (c): Evolution of disturbed flame fronts at Le = 0.7 and T_u = 1.0~0.6.

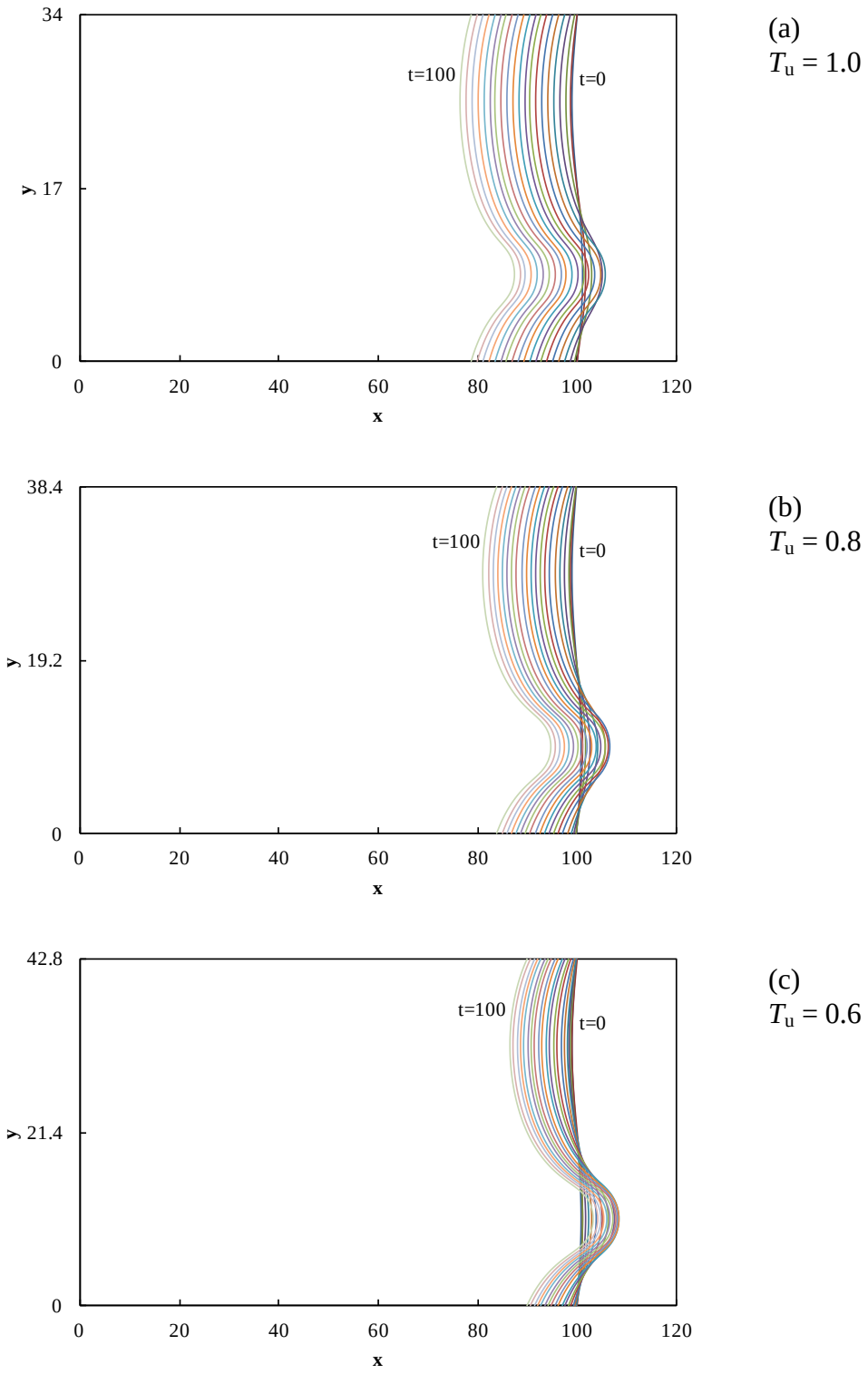

Figure 4.10 (a) (b) (c): Evolution of disturbed flame fronts at Le = 1.0 and T_u = 1.0~0.6.

Lateral movement of the cellular flame occurs at Le = 0.5 and the overshoot of temperature appears. The overshoot of the temperature causes the unstable behavior of cellular flames. [51] The unstable behavior of cellular flame at Le = 0.5 is stronger than that at Le = 0.7 and 1.0. This is because of the destabilizing effect of diffusive-thermal instability and thermal expansion. Figures 4.11 (a) (b) (c) through 4.13 (a) (b) (c) show the temperature distributions at Le = 0.5~1.0 and T_u = 1.0~0.6 for non-dimensional time t = 60. The overshoot of the temperature does not appear in Le = 1.0 flame.

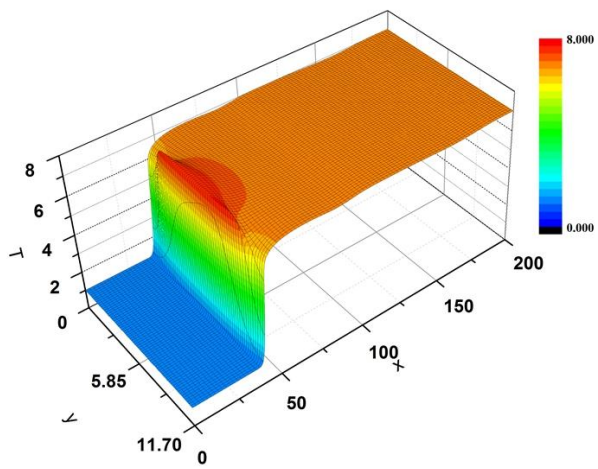

(a) T_u = 1.0

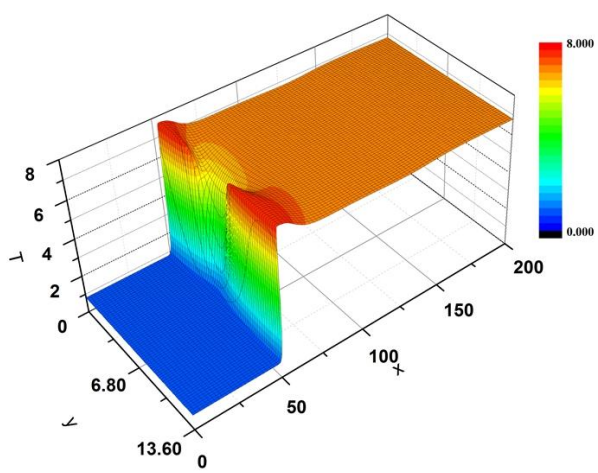

(b) T_u = 0.8

Figure 4.11 (a) (b): Temperature distribution of cellular flames at Le = 0.5 and T_u = 1.0 and 0.8.

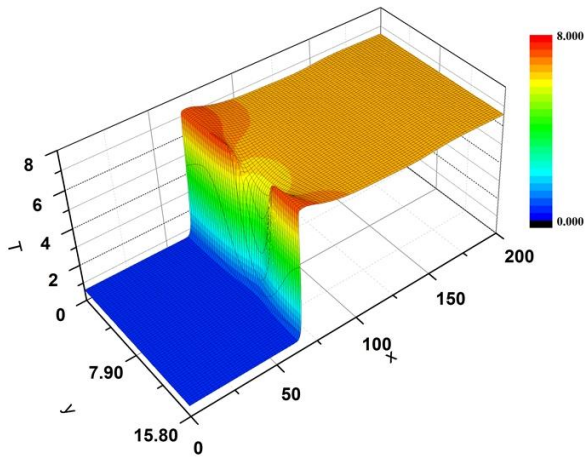

(c) T_u = 0.6

Figure 4.11 (c): Temperature distribution of cellular flames at Le = 0.5 and T_u = 0.6.

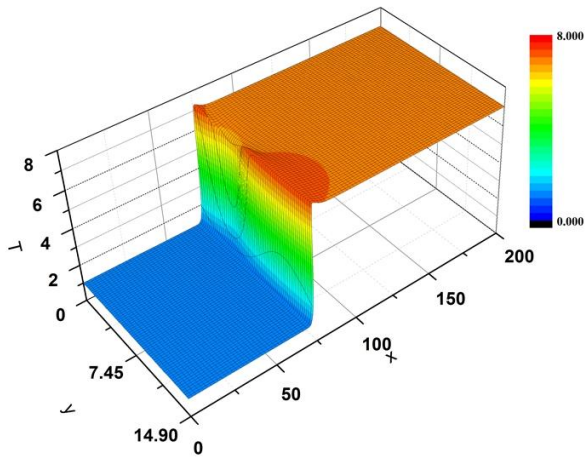

(a) T_u = 1.0

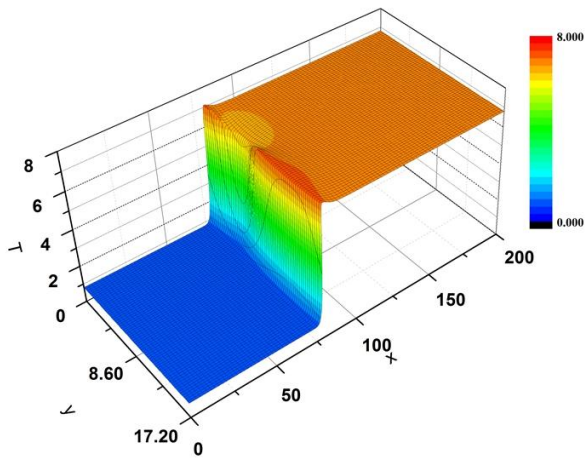

(b) T_u = 0.8

Figure 4.12 (a) (b): Temperature distribution of cellular flames at Le = 0.7 and T_u = 1.0 and 0.8.

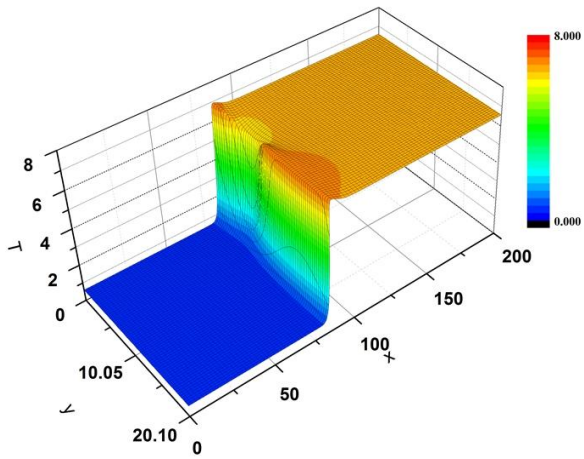

(c) $T_u = 0.6$

Figure 4.12 (c): Temperature distribution of cellular flames at $Le = 0.7$ and $T_u = 0.6$.

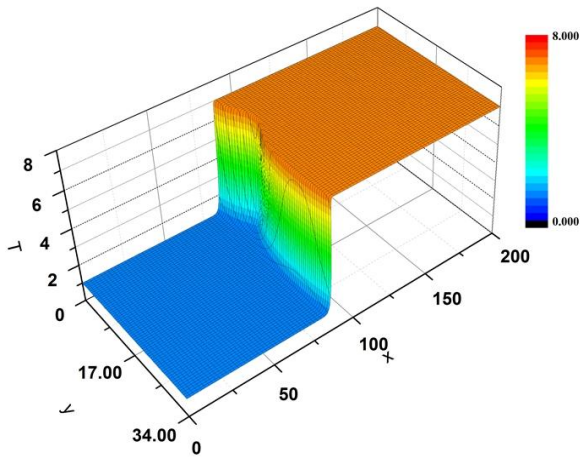

(a)T_u = 1.0

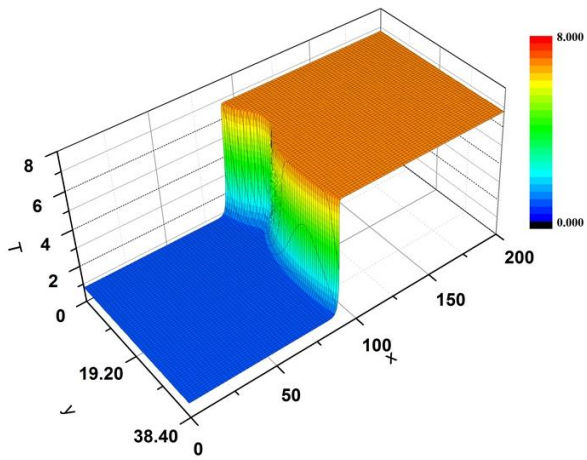

(b)T_u = 0.8

Figure 4.13 (a) (b): Temperature distribution of cellular flames at $Le = 1.0$ and $T_u = 1.0$ and 0.8.

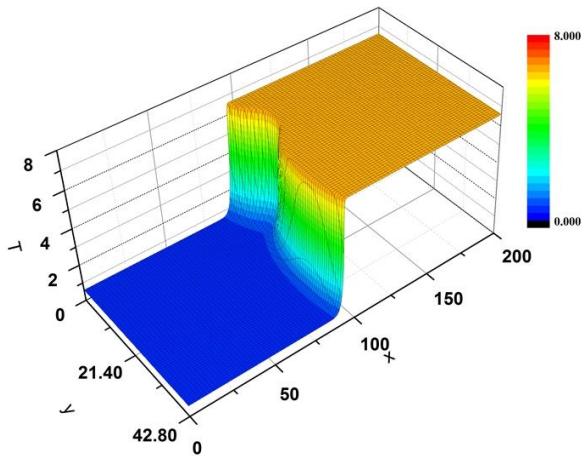

(c)T_u = 0.6

Figure 4.13 (c): Temperature distribution of cellular flames at Le =1.0 and T_u = 0.6.

4.2.1.4 Burning velocities of cellular flames

The effects of unburned-gas temperature on the burning velocity of cellular flames are investigated. The burning velocity of a cellular flame increases owing to the increase of flame surface area induced by intrinsic instability. To examine the effects of unburned-gas temperature on the intensity of instability, the burning velocity of cellular flame is normalized by that of a planar flame. Table 4.5 describes the burning velocities of cellular flames and normalized values at Le = 0.5~1.0 and T_u = 1.0~0.6. The normalized burning velocity of cellular flames increases as unburned-gas temperature becomes lower. The result shows that the intensity of intrinsic instability becomes stronger due to the enlargements of Zeldovich numbers and thermal expansion effect when unburned-gas temperature becomes lower at Le < 1.0.

Table 4.5: Burning velocities and normalized values of cellular flames at Le = 0.5~1.0 and T_u = 1.0~0.6.

T_u	S_{cf}			S_{cf}/S_u		
	Le = 0.5	Le = 0.7	Le = 1.0	Le = 0.5	Le = 0.7	Le = 1.0
1.0	2.041	1.416	1.207	2.041	1.416	1.207
0.8	1.451	0.979	0.788	2.177	1.492	1.210
0.6	0.960	0.636	0.482	2.259	1.589	1.215

4.2.2 Effect of Heat Loss

As the combustion processes are strongly affected by heat loss owing to the irreversibility, the effects of radiative heat loss on the characteristics of low temperature unburned-gas premixed flames are studied at $Le \leq 1.0$.

4.2.2.1 Numerical results for non-adiabatic stationary planar flame

Figures 4.14, 4.15 and 4.16 show the relation between the heat loss parameter A and burning velocity of non-adiabatic planar flame at Le = 0.5, 0.7 and 1.0, and T_u = 1.0~0.6.

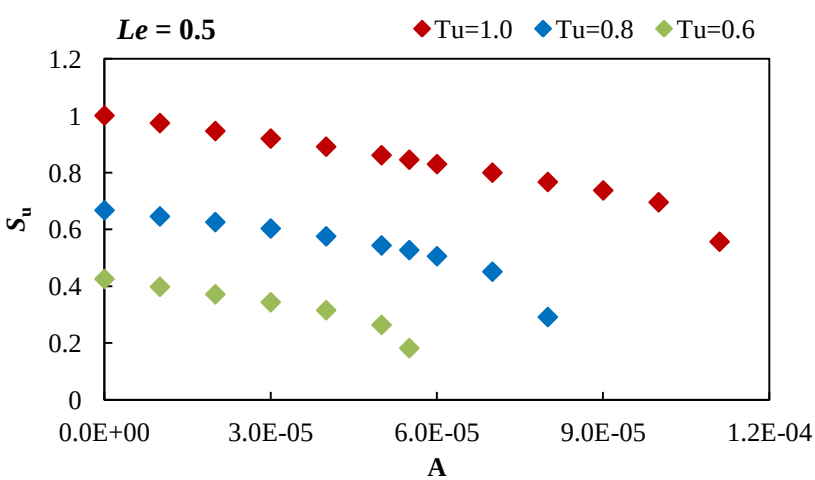

Figure 4.14: Relation between heat loss parameter and burning velocity at Le = 0.5.

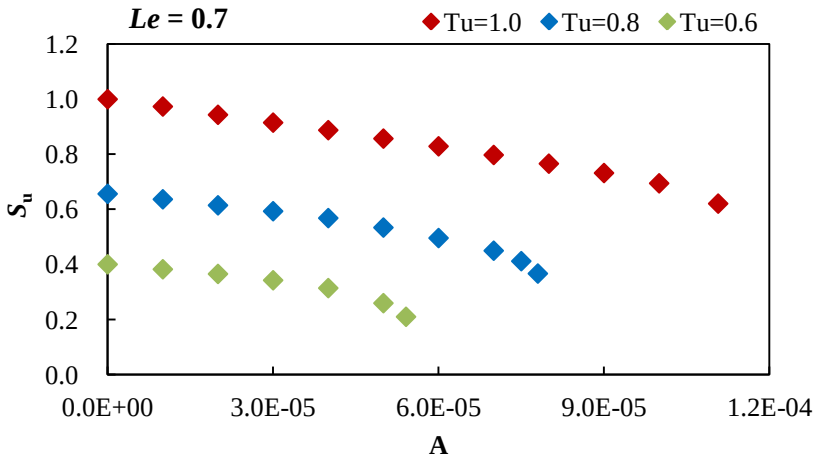

Figure 4.15: Relation between heat loss parameter and burning velocity at Le = 0.7.

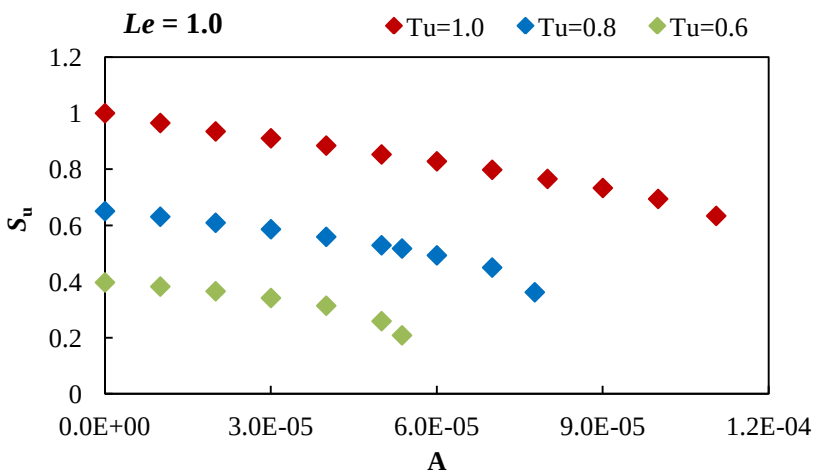

Figure 4.16: Relation between heat loss parameter and burning velocity at Le = 1.0.

The burning velocities of non-adiabatic flames are smaller than those of adiabatic flames because of the decrease in flame temperature in downstream owing to the effects of heat loss. If the heat loss parameter is larger than maximum value A_{max}, the flame will extinguish. The burning velocities depend on A at Le = 0.5~1.0 are listed in Table 4.6, 4.7 and 4.8. The distributions of density, energy, pressure, temperature and mass

fraction, ρ, e, p, T, Y at $Le = 0.5$ and $T_u = 1.0 \sim 0.6$ for $A = 4\times10^{-5}$ are shown in Figs. 4.17, 4.18 and 4.19.

Table 4.6: Burning velocity of planar flame depends on A at $Le = 0.5$.

A	S_u		
	$T_u = 1.0$	$T_u = 0.8$	$T_u = 0.6$
0	1.0000	0.6665	0.4250
0.00004	0.8905	0.5840	0.3065
0.000055	0.8446	0.5172	0.1815
0.00008	0.7615	0.2900	-
0.000111	0.5560	-	-

Table 4.7: Burning velocity of planar flame depends on A at $Le = 0.7$.

A	S_u		
	$T_u = 1.0$	$T_u = 0.8$	$T_u = 0.6$
0	1.0000	0.6564	0.4005
0.00002	0.9435	0.6148	0.3580
0.00004	0.8876	0.5625	0.2978
0.0000541	0.8449	0.5198	0.2050
0.000078	0.7740	0.3604	-
0.0001107	0.6210	-	-

Table 4.8: Burning velocity of planar flame depends on A at $Le = 1.0$.

A	S_u		
	$T_u = 1.0$	$T_u = 0.8$	$T_u = 0.6$
0	1.0000	0.6510	0.3970
0.00002	0.9350	0.6096	0.3655
0.00004	0.8845	0.5594	0.3140
0.0000537	0.8465	0.5178	0.2085
0.0000777	0.7738	0.3620	-
0.0001105	0.6340	-	-

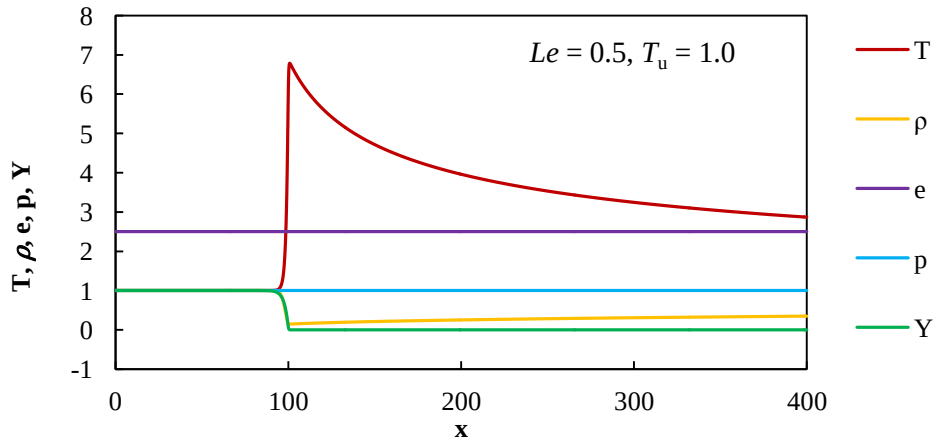

Figure 4.17: Distribution of T, ρ, e, p, Y at $Le = 0.5$ and $T_u = 1.0$ ($A = 4\times10^{-5}$).

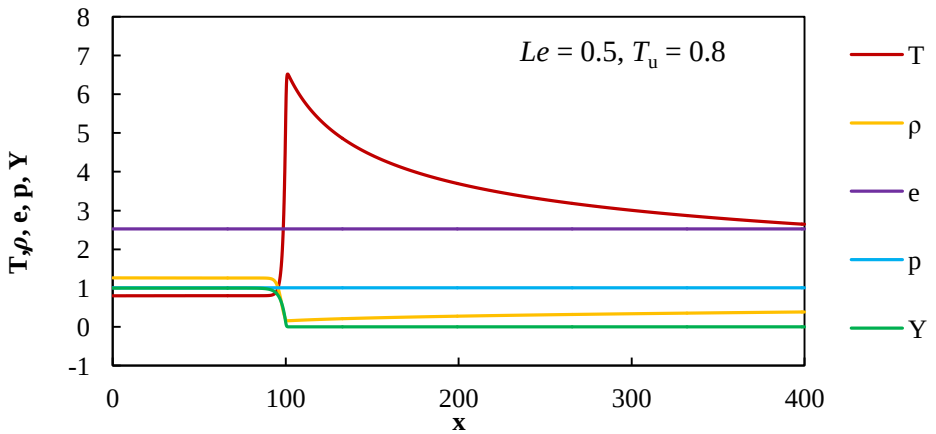

Figure 4.18: Distribution of T, ρ, e, p, Y at $Le = 0.5$ and $T_u = 0.8$ ($A = 4\times10^{-5}$).

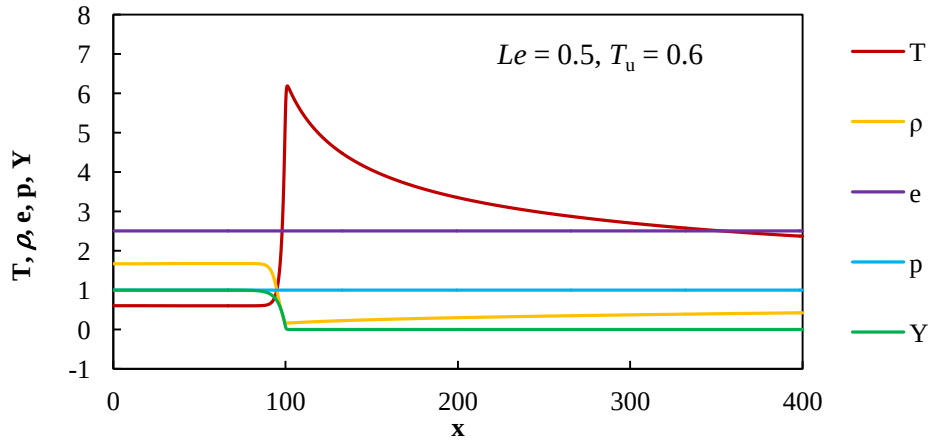

Figure 4.19: Distribution of T, ρ, e, p, Y at $Le = 0.5$ and $T_u = 0.6$ ($A = 4\times10^{-5}$).

4.2.2.2 Dispersion relations

To perform the numerical calculations of dispersion relation, i.e. the relation between the growth rate and wave number, with taking into account the radiative heat loss, initial conditions are provided by the solutions from one dimensional calculation and heat loss parameter is set to 4×10^{-5}. To obtain the dispersion relation, an initial amplitude $a_i = 0.1$ is superimposed on a stationary planar flame. The displacement of the flame front in the x-direction due to the superimposed disturbance is a_i {sin $(2\pi y/\lambda)$}. Flame surface is the site where the reaction takes a maximum value. The unburned gas flows into the left with the burning velocity of a stationary planar flame and the burned gas flows out from the right. The superimposed disturbance grows with time. The amplitude growth rate increases linearly with time. The growth rate of the disturbance depends on the wavelength, i.e. on the wave number. By changing the wavelength, the dispersion relation is obtained.

The dispersion relations at $Le = 0.5\sim1.0$ and $A = 4\times10^{-5}$are described in Fig. 4.20. The growth rate decreases and unstable range narrows as the decrease of burning velocity of planar flame owing to the heat loss effect, and the former increases and the latter widens when Lewis number becomes lower, which is due to the increase of the strength of diffusive-thermal instability and thermal expansion effect at $Le < 1$. Heat loss reduces the temperature of the flames and thus burning velocity decreases. The burning velocity of a planar flame affects the dispersion relation. Thus, the growth rate and wave number are normalized by the burning velocity of a planar flame. The normalized growth rate increases when heat loss parameter increases and unburned-gas temperature decreases. Figure 4.21 shows the normalized growth rate at $Le = 0.5\sim1.0$. The results show that the heat loss has a pronounced influence on the intrinsic instability. The linearly most unstable wave number corresponding to the maximum growth rate is obtained, and which

is referred to the critical wave number, k_c. The critical wavelength λ_c (= $2\pi/k_c$) increases when the heat loss parameter becomes larger. The obtained critical wavelengths are listed in Table.4.9.

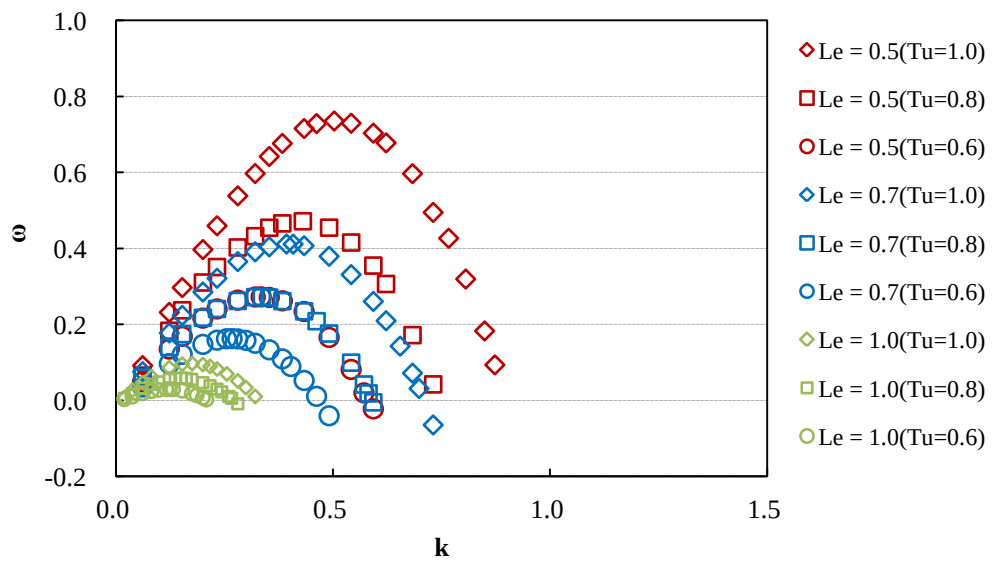

Figure 4.20: Dispersion relation at Le = 0.5~1.0 and T_u = 1.0~0.6 ($A = 4\times10^{-5}$).

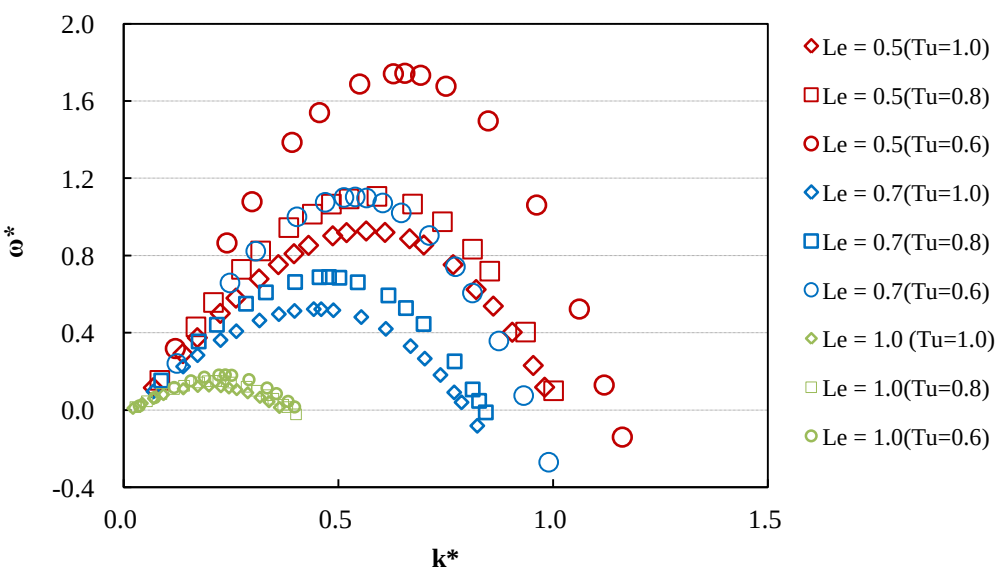

Figure 4.21: Normalized dispersion relation at Le = 0.5~1.0 and T_u = 1.0~0.6 ($A = 4\times10^{-5}$).

Table 4.9: Critical wavelengths at Le = 0.5~1.0 ($A = 4\times10^{-5}$).

T_u	T_b	Y_u	λ_c		
			Le = 0.5	Le = 0.7	Le =1.0
1.0	7.0	1.0	12.5	16.0	35.8
0.8	6.8	1.0	14.6	18.7	41.8
0.6	6.6	1.0	18.8	23.5	50.8

4.2.2.3 Formation of cellular flame fronts

Characteristics of cellular flames induced by the intrinsic instability, considering heat loss are investigated. To obtain the cellular flame, a disturbance with the critical wavelength is superimposed, where a_i = 1.0. Figures 4.22 (a) (b) (c) through 4.24 (a) (b) (c) illustrate the evolution of disturbed flame fronts at Le = 0.5, 0.7 and 1.0 and T_u = 1.0~0.6. The flame front is defined as the position where the reaction rate takes maximum value. The superimposed disturbance evolves owing to the increase of the burning velocity due to the increase of flame-surface area. The cell depth D_{cell} increases, and L_{cf} and D_{cell}/λ_c become larger especially at Le < 1, when heat loss parameter increases. This is because of the strength of hydrodynamic and diffusive-thermal instabilities owing to heat loss. Heat loss promotes the unstable behavior of the flames when Lewis number is lower than unity. When the Lewis number is unity, the effect of heat loss is weak. $D_{cell,}$ L_{cf} and D_{cell}/λ_c of non-adiabatic cellular flames at Le = 0.5~1.0 are listed in Table 4.10. Figures 4.25 (a) (b) (c) through 4.27 (a) (b) (c) show the temperature distributions at Le = 0.5~1.0 and T_u = 1.0~0.6 for non-dimensional time t = 60.

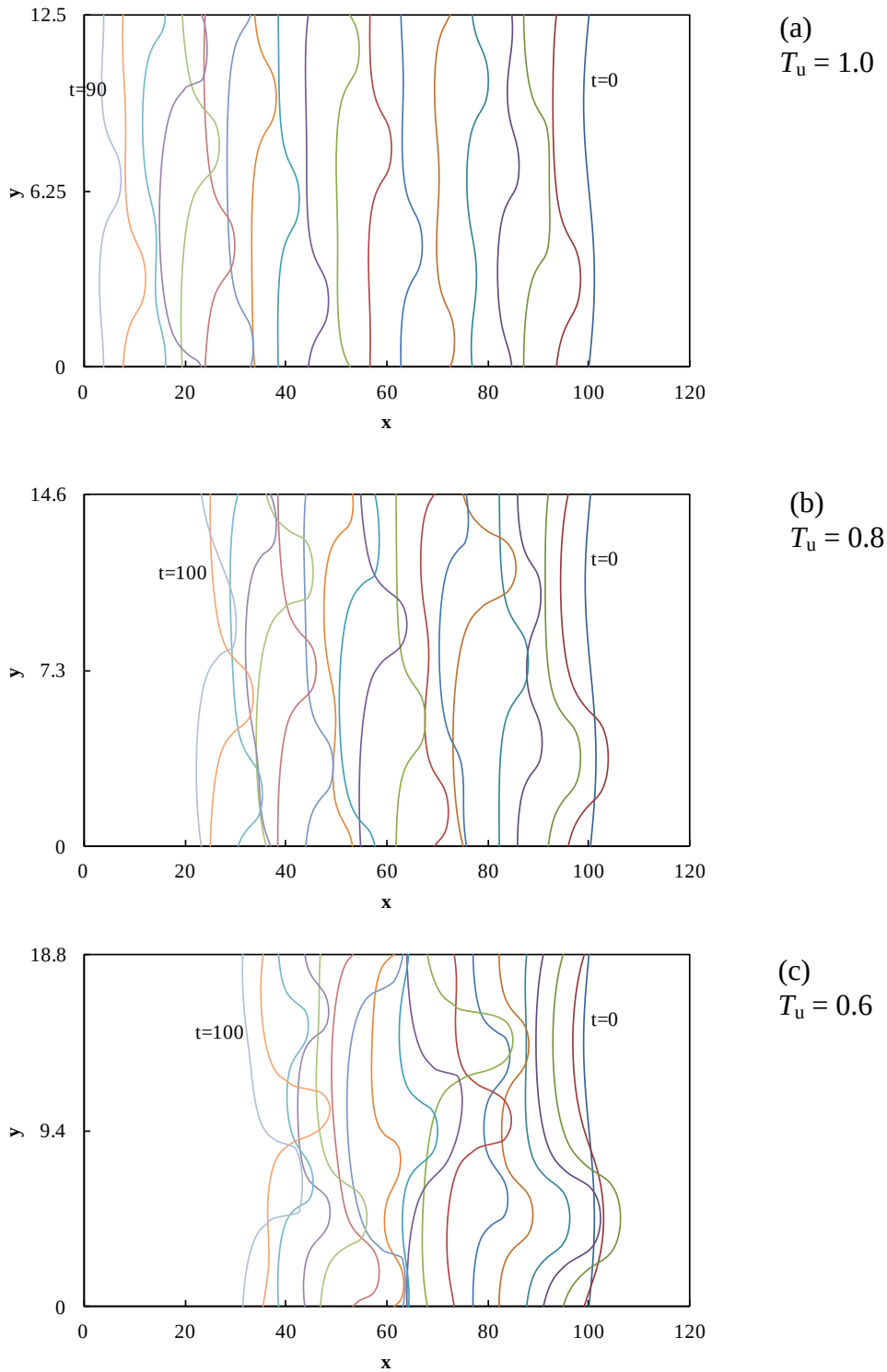

Figure 4.22 (a) (b) (c): Evolution of disturbed flame fronts at $Le = 0.5$ and $T_u = 1.0$~0.6 ($A = 4\times10^{-5}$).

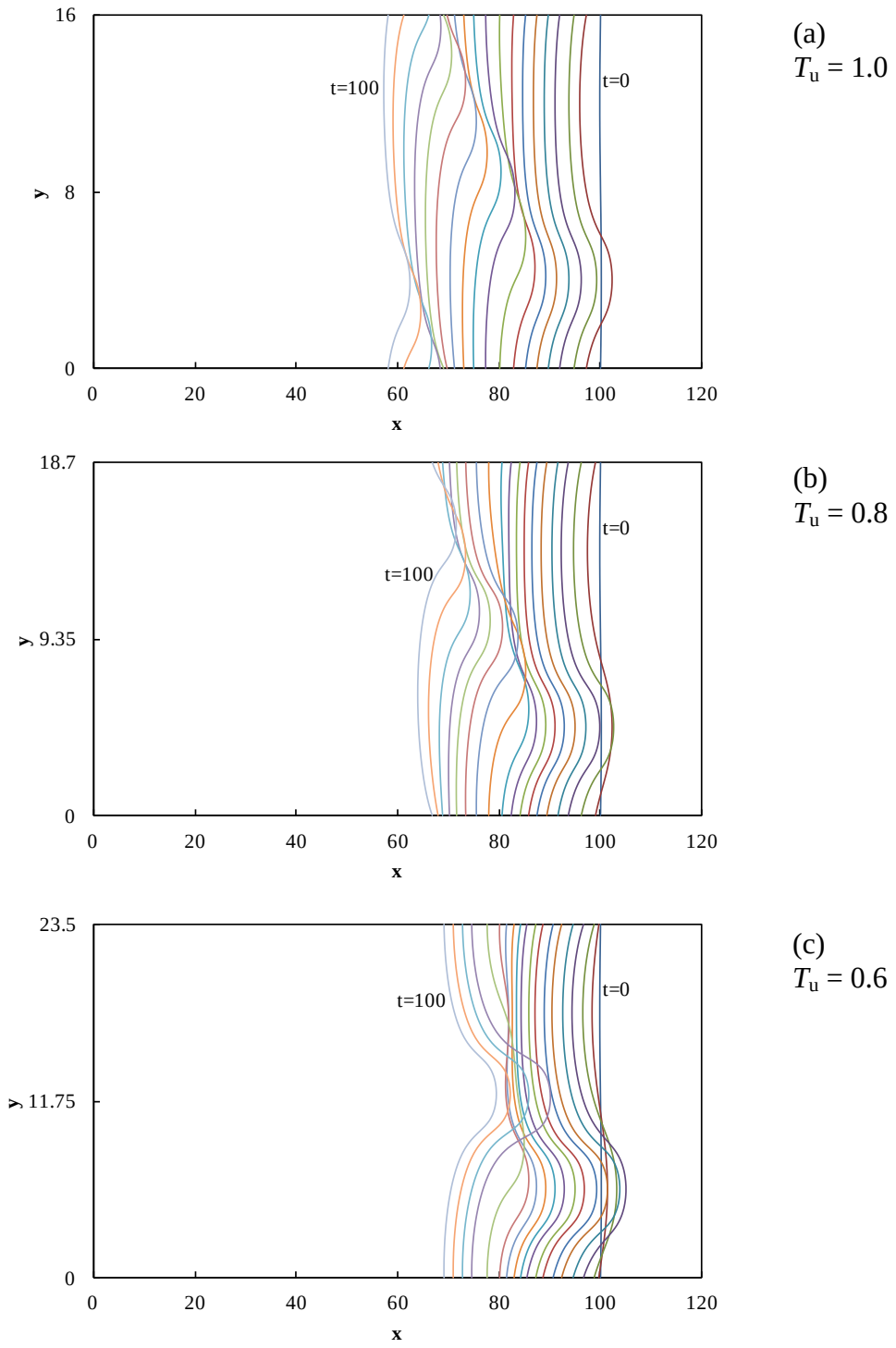

Figure 4.23 (a) (b) (c): Evolution of disturbed flame fronts at $Le = 0.7$ and $T_u = 1.0$~0.6 ($A = 4\times10^{-5}$).

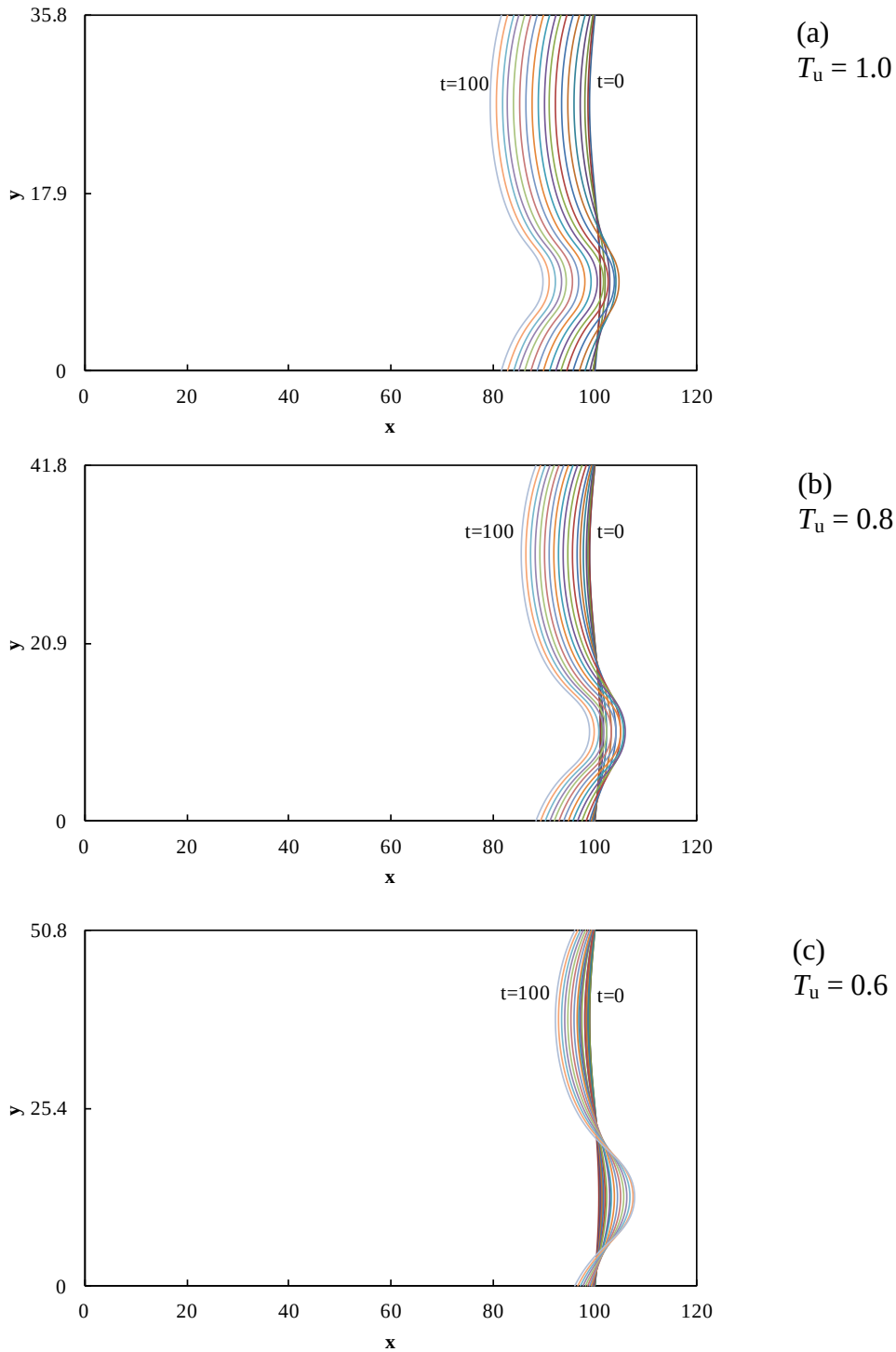

Figure 4.24 (a) (b) (c): Evolution of disturbed flame fronts at Le = 1.0 and T_u = 1.0~0.6 (A = 4×10^{-5}).

Table 4.10: D_{cell}, L_{cf} and D_{cell}/λ_c of cellular flames at Le = 0.5~1.0 and T_u = 1.0~0.6 (A = 4×10^{-5}).

T_u	D_{cell}			L_{cf}			D_{cell}/λ_c		
	Le = 0.5	Le = 0.7	Le = 1.0	Le = 0.5	Le = 0.7	Le = 1.0	Le = 0.5	Le = 0.7	Le = 1.0
1.0	5.846	5.296	10.337	1.542	1.281	1.212	0.4677	0.3310	0.2887
0.8	7.484	6.676	12.144	1.625	1.324	1.226	0.5128	0.3570	0.2905
0.6	10.541	9.536	14.935	1.776	1.414	1.303	0.5607	0.4058	0.2939

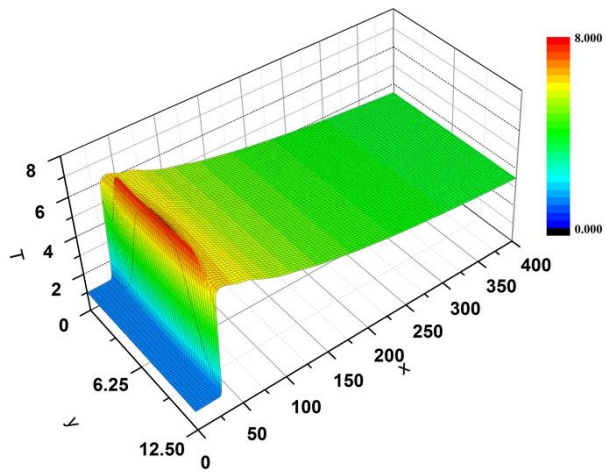

(a) T_u = 1.0

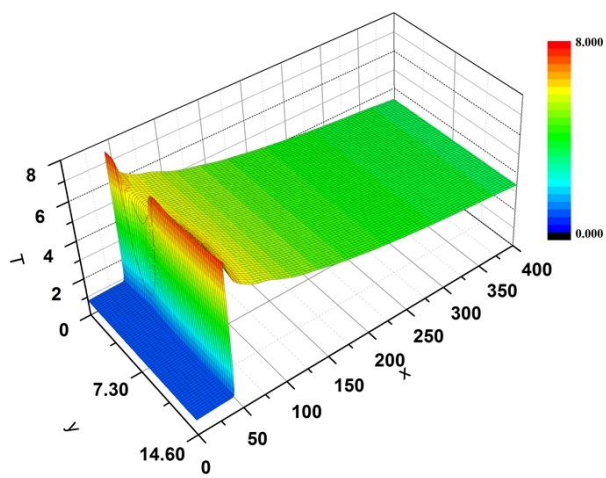

(b) T_u = 0.8

Figure 4.25 (a) (b): Temperature distribution of cellular flame fronts at Le = 0.5, T_u=1.0 and 0.8 (A = 4×10^{-5}).

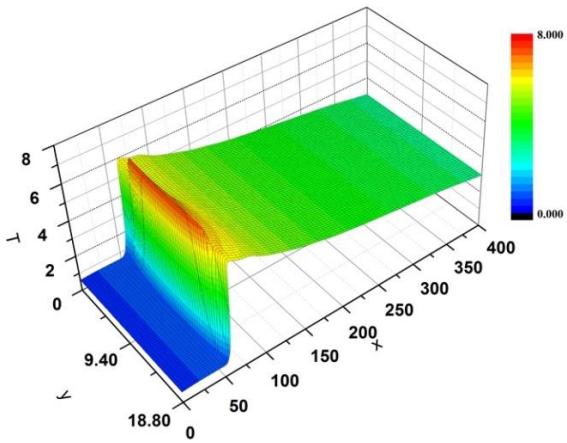

(c) T_u = 0.6

Figure 4.25 (c): Temperature distribution of cellular flame fronts at Le = 0.5, T_u=0.6 (A = 4×10^{-5}).

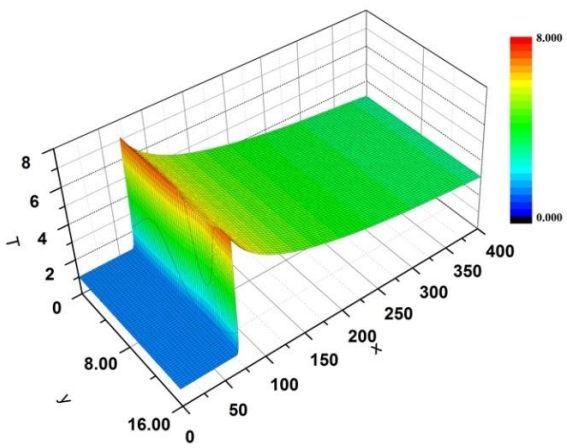

(a) T_u = 1.0

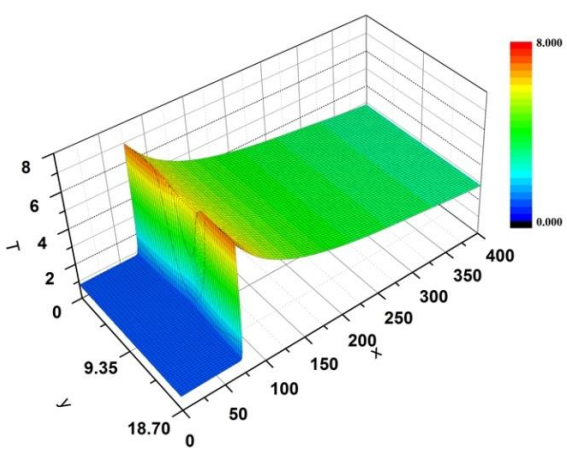

(b) T_u = 0.8

Figure 4.26 (a) (b): Temperature distribution of cellular flame fronts at Le = 0.7, T_u=1.0 and 0.8 (A = 4×10^{-5}).

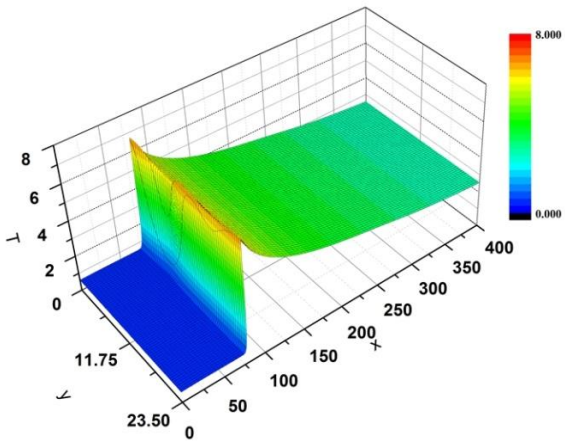

(c) T_u = 0.6

Figure 4.26 (c): Temperature distribution of cellular flame fronts at Le = 0.7, T_u=0.6 (A = 4×10^{-5}).

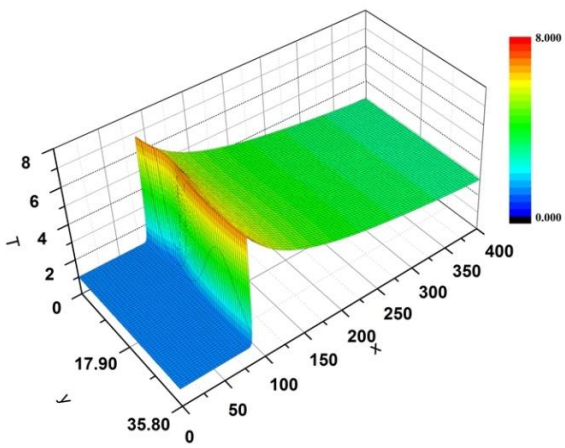

(a) T_u = 1.0

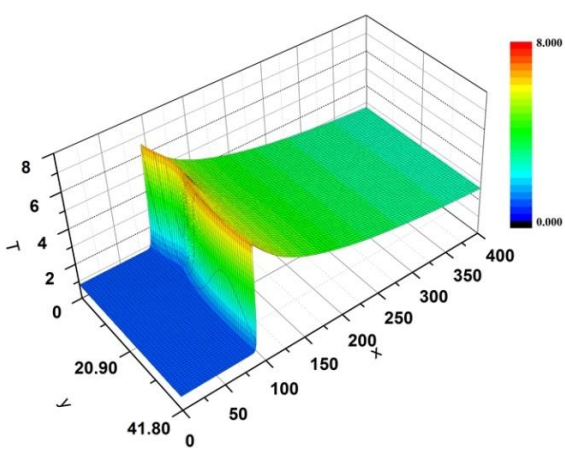

(b) T_u = 0.8

Figure 4.27 (a) (b): Temperature distribution of cellular flame fronts at Le = 1.0, T_u=1.0 and 0.8 (A = 4×10^{-5}).

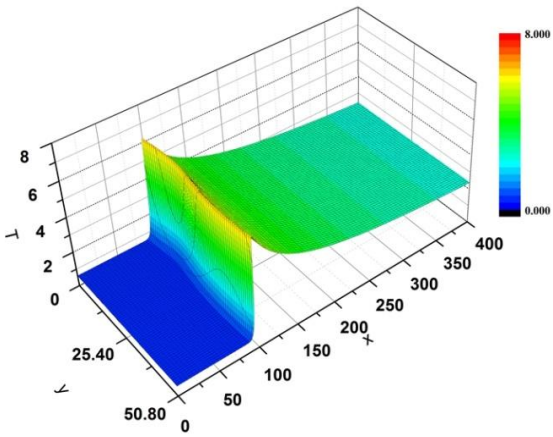

(c) T_u = 0.6

Figure 4.27 (c): Temperature distribution of cellular flame fronts at Le = 1.0, T_u=0.6 (A = 4×10^{-5}).

4.2.2.4 Burning velocities of cellular flames

The effect of heat loss on the burning velocity of cellular flame is investigated. The burning velocity of a cellular flame increases owing to the increase of flame surface area induced by intrinsic instability. The burning velocity of cellular flame is normalized by the planar flame velocity. Normalized burning velocity increases because of the effect of heat loss. The burning velocities of cellular flames and normalized values at Le = 0.5~1.0 and T_u = 1.0~0.6 (A = 4×10^{-5}) are listed in Table 4.11. Comparing with the normalized burning velocities of adiabatic flames, the normalized values in non-adiabatic flames are large. This result shows that the intensity of intrinsic instability becomes stronger as the heat loss parameter becomes larger especially at Le < 1.0.

Table 4.11: Burning velocities and normalized values of cellular flames at Le = 0.5~1.0 and T_u = 1.0~0.6 (A = 4×10^{-5}).

T_u	S_{cf}			S_{cf}/S_u		
	Le = 0.5	Le = 0.7	Le = 1.0	Le = 0.5	Le = 0.7	Le = 1.0
1.0	2.011	1.358	1.068	2.258	1.530	1.207
0.8	1.431	0.921	0.677	2.451	1.637	1.210
0.6	0.949	0.605	0.382	3.097	2.030	1.217

4.3 COMPARISON OF THEORETICAL AND NUMERICAL RESULTS

The effect of unburned-gas on the hydrodynamic instability of premixed flames at Le = 1.0 is theoretically studied and compared with the numerical results. The asymptotic method of Kadowaki, S. (2010) [53] is adopted, and we have taken some assumptions as the following:

(1) the chemical reaction is a one-step irreversible exothermic reaction

(2) the reaction rate obeys the Arrhenius law

(3) the temperature difference between the unburned and burned gases is constant

(4) the unburned and burned gases have the same molecular weights and same Lewis numbers, and the ideal gas equation of state is satisfied

(5) the effect of heat loss is neglected

(6) the specific heat and transport coefficients are constant throughout the whole region

(7) Mach number is assumed as sufficiently low.

The unburned-gas temperature is set to 2.5, 2.0, 1.5, 1.0, 0.8 and 0.6 under the condition of constant pressure.

Table 4.12 shows the theoretical and numerical results of burning velocities of planar flames depend on the unburned-gas temperature at Le = 1.0 under the adiabatic condition. The results of numerical calculation are almost equal to the theoretical results. When the unburned-gas temperature becomes lower, the burning velocity decreases.

Table 4.12: Theoretical and numerical results of burning velocities of planar flames at *Le* = 1.0.

T_u	T_b	S_u (theoretical)	S_u (numerical)
2.5	8.5	8.084	8.0000
2.0	8.0	4.565	4.5575
1.5	7.5	2.322	2.3080
1.0	7.0	1.000	1.0000
0.8	6.8	0.661	0.6510
0.6	6.6	0.406	0.3970

Figure 4.28 shows the theoretical (Th) and numerical (N) results of dispersion relations at *Le* = 1.0 under adiabatic condition and T_u = 2.5, 2.0, 1.5, 1.0 and 0.6. The dashed lines represent the theoretical results of dispersion relations. The numerical results are in agreement with the theoretical ones for the adequate small wave number ranges. This is because that sufficiently thin flame is assumed in theoretical method. [53]

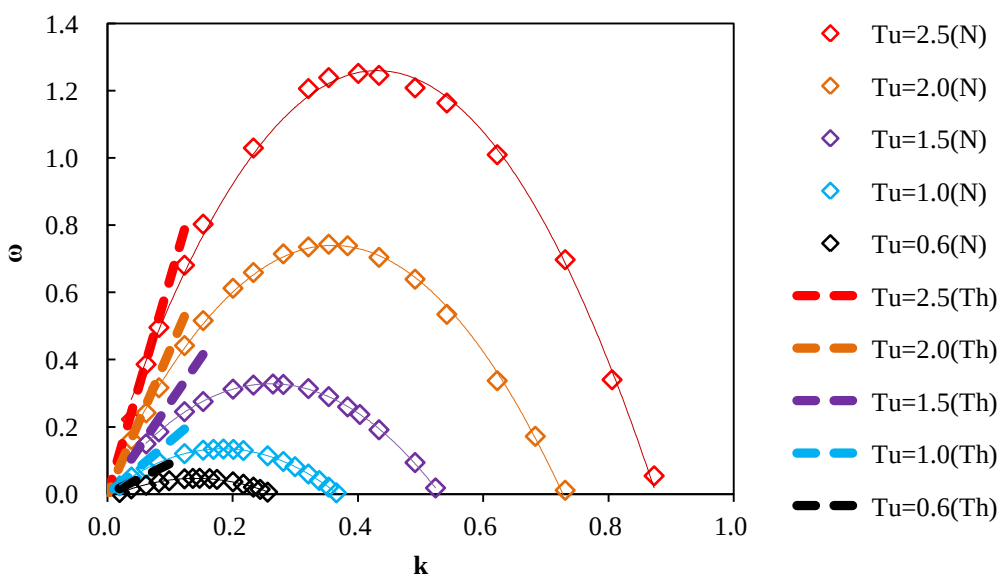

Figure 4.28: Theoretical and numerical results of dispersion relations at *Le* = 1.0.

4.4 CONCLUDING REMARKS

The effects of unburned-gas temperature and radiative heat loss on the intrinsic instability of low temperature unburned-gas premixed flame are studied numerically, based on the compressible Navier-Stokes equation under the condition of constant temperature jump. The obtained results are as follows:

When the Lewis number is less than or equal to unity, as the unburned-gas temperature decreases, the burning velocity of a planar flame decreases; the growth rate decreases and the unstable range narrows; the normalized growth rate increases.

Unstable behavior of cellular flames at $Le = 0.5$ is stronger than those at $Le = 0.7$ and 1.0, due to the strength of diffusive-thermal and hydrodynamic instabilities. Critical wavelength λ_c, D_{cell}, L_{cf} and D_{cell}/λ_c become larger. Burning velocity of cellular flame decreases, normalized burning velocity increases, and unstable behavior of the cellular flame becomes intense at $Le < 1$.

When heat loss is taken into account, especially at $Le < 1$, burning velocity of a planar flame decreases and then growth rate becomes lower. The normalized growth rate increases. The burning velocity of cellular flame decreases and normalized burning velocity increases.

Chapter 5: Conclusions

5.1 CONCLUSIONS

The effects of unburned-gas temperature and heat loss on the intrinsic instabilities of premixed flames are studied numerically as a contributing work for using hydrogen-air or methane-air premixed combustion to reduce pollutant emissions.

To investigate the diffusive-thermal instability, two-dimensional unsteady numerical calculations of reactive flows based on the diffusive-thermal model equation at Lewis numbers less than unity are performed under the condition of constant temperature jump, where thermal-expansion effects are neglected. Stationary planar flames with high- and low-temperature combustible mixtures are treated under the adiabatic and non-adiabatic conditions to provide the initial conditions for the two-dimensional calculations. Obtaining the burning velocity of a stationary planar flame depending on the heat loss parameter, the two-dimensional reactive flow is initiated to study the characteristics of diffusive-thermal instability.

The growth rate increases (decreases) as the unburned-gas temperature becomes higher (lower). The normalized growth rate decreases (increases) as the unburned-gas temperature increases (decreases). This is because of the reduction (enlargement) of Zeldovich numbers for high- (low-) temperature unburned gases at $Le < 1.0$. D_{cell}, L_{cf} , D_{cell}/λ_c and λ_c decreases (increases) as the unburned-gas temperature increases (decreases), and the unstable behavior of cellular flames induced by diffusive-thermal instability becomes weaker (stronger). When the Lewis number approaches to unity, the diffusive-thermal instability in premixed flames with high- and low- temperature unburned gases becomes weaker.

To investigate the hydrodynamic instability, numerical calculations are performed based on the compressible Navier-Stokes equations with chemical reactions. When thermal expansion effect is taken into account, the burning velocities of planar and cellular flames increase, and the intensity of intrinsic instability becomes significantly greater. As the unburned-gas temperature becomes lower, intrinsic instability becomes stronger because of the thermal expansion effects. When the Lewis number is less than unity, the intensity of intrinsic instability becomes stronger owing both to diffusive-thermal and thermal-expansion effects.

When the radiative heat loss is considered, the burning velocity of a planar flame decreases when the heat loss parameter increases. The normalized growth rate increases at $Le < 1.0$ owing to the effects of heat loss, and the unstable behavior of the cellular flame becomes intense. The burning velocity of a cellular flame decreases, and the normalized velocity increases due to the heat loss effect at $Le < 1.0$. Thus, radiative heat loss promotes the intrinsic instabilities of premixed flames.

From this study, it can be concluded that high unburned-gas temperature reduces the strength of intrinsic instability. Conversely, low unburned-gas temperature and heat loss promote the intensity of instabilities in premixed flames at Lewis numbers less than unity.

5.2 FUTURE WORK

In the current study, we performed the numerical calculations to examine the effects of unburned-gas temperature and heat loss on the intrinsic instabilities, and theoretical results on burning velocity of a planar flame at $Le = 1.0$ for different unburned-gas temperatures were compared with the numerical results. To analyze the combustion phenomena, it is important to find the burning velocity of planar flame. Thus, we desire to perform the extensive studies to obtain the information on burning velocities of lean hydrogen-air or methane-air premixed flames with high- and low- temperature unburned gases.

We have taken the assumption that the chemical reaction is a one-step irreversible exothermic reaction in the current study. In real, there are many intermediate steps during the chemical process from the reactants to the products in the combustion of hydrogen and hydrocarbon fuels. Thus, to study the intermediate steps and structure of the real flames, we will perform the numerical calculations by improving the existing one-step models to two-step models in the future.

Moreover, we will investigate the characteristics of the premixed flames of hydrogen-air or methane-air numerically by the detailed chemical kinetic model with various equivalence ratios and different unburned-gas temperatures under the adiabatic and non-adiabatic conditions.

In addition, it is interesting to extensively study the premixed flames of hydrogen-hydrocarbon-air. Since hydrogen has high reactivity and diffusivity, adding hydrogen to hydrocarbon fuels in lean premixed combustion gives the increase in flammability limit. Thus, ultra-lean premixture of hydrocarbon fuels such as methane or propane, especially in gas turbines, will be possibly fueled by adding hydrogen.

Furthermore, the burning velocities of adiabatic planar flames for various equivalence ratios with different unburned-gas temperatures of premixed flames are able to evaluate by using the CHEMKIN PRO software package. Thus, the measurements of burning velocities for hydrogen-air or methane-air or hydrogen-hydrocarbon-air premixed flames will be conducted by experiments with the support of the results from CHEMKIN code.

In near future, the instabilities of lean hydrogen-air or methane-air premixed flames will be studied experimentally by using flat burner in order to compare with the current numerical results.

References

(1) Air Pollution: Current and Future Challenges, United States Environmental Protection Agency, http://www.epa.gov/air/caa/challenges.html

(2) 2014 Key World Energy Statistics, International Energy Agency, http://www.iea.org/publications/freepublications/publication/KeyWorld2014.pdf

(3) CO2 Emissions from Fuel Combustion Highlights 2014 http://www.iea.org/publications/freepublications/publication/CO2EmissionsFromFuelCombustionHighlights2014.pdf

(4) Glassman, I. and Yetter, R.A., Combustion, 4th Ed., Academic Press, (2008), Reading, pp. 409-417

(5) Water for Life Decade: Water Scarcity, http://www.un.org/waterforlifedecade/scarcity.shtml

(6) Energy Predicament, http://pictorial-guide-to-energy.blogspot.jp/2011/03/world-population-and-energy-demand.html

(7) Gonzalez, M. and Lucky, M., Fossil Fuel Dominate Primary Energy Consumption, Article, (2013), http://www.worldwatch.org/fossil-fuels-dominate-primary-energy-consumption-1

(8) Poinsot, T., Master Course on Combustion, University of Toulouse, http://elearning.cerfacs.fr/combusiton/n7masterCourses/introduction/index.php

(9) Dunn-Rankin, D., Lean Combustion Technology and Control, Academic Press, (2008), Reading, pp. 1-17

(10) Williams, F.A., Combustion Theory, 2nd Ed., Addison-Wesley Pub., (1985), pp. 349-359

(11) Poinsot, T. and Veynante, D., Theoretical and Numerical Combustion, 2nd Ed., R.T. Edwards, Inc, (2005), p 80

(12) Law, C.K., Combustion Physics, Cambridge Press, (2006), pp. 456-471

(13) Kuo, K. K., Principles of Combustion, 2nd Ed., John Wiley & Sons, (2005), pp. 4-6

(14) Drysdale, D., An Introduction to Fire Dynamics, 3rd Ed., John Wiley & Son, (2011), pp. 101-102

(15) Som, S.K., and Datta, A., Thermodynamic irreversibilities and exergy balance in combustion processes, Progress in Energy and Combustion Science, Vol.34, (2008), p 351

(16) Cavaliere, A. and Jonnon, M.d., Mild Combustion, Progress in Energy and Combustion Science, Vol. 30, (2004), pp. 329-366

(17) Weinberg, F.J., Combustion temperature: the future?, Nature, Vol.233, (1971), pp. 239-241

(18) Jones, A. R. Lioyd, S. A. and Weinberg, F.J., Combustion in heat exchangers, Proc. Roy. Soc. (London), Vol. A36, (1978), p 97

(19) Kawamura, T., Asato, K. and Ito, S., An Experimental Study on Combustion of an Ultralean-Fuel and Air Mixture by Heat Recirculation, Vol.32, (1989), pp. 252-259

(20) Takeno, T., Sato, K. and Hase, K., A theoretical study on excess enthalpy flame, Proceedings of the Combustion Institute, Vol.18, (1981), pp. 465-472

(21) Yoshizawa, Y., Sasaki, K. and Echigo, R., Analytical study of the structure of radiation controlled flame, International Journal of Heat and Mass Transfer, Vol. 31, (1988), pp. 311-319

(22) Hanamur, K., Echigo, R. and Zhdanok, S. A., Superadiabatic combustion in a porous medium, International Journal of Heat and Mass Transfer, Vol.36, (1993), pp. 3201-3209

(23) Katsuki, M. and Hasegawa, T., The science and technology of combustion in highly preheated air, Proceeding of the Combustion Institute, Vol. 27, (1998), pp. 3135-3146

(24) Niioka, T., Fundamentals and applications of high temperature air combustion, Proceedings of Fifth ASME/JSME Joint Thermal Engineering Conference, San Diego (1997)

(25) Osino, S., Weber, R. and Bollettini, U., Numerical Simulation of Combustion of Natural Gas with High-Temperature Air, Combustion Science and Technology, Vol. 170, (2001), p 1

(26) Weber, J., Smart, J. P. and Kamp, W. vd., On the (MILD) combustion of gaseous, liquids, and solid fuels in high temperature preheated air, Proceeding of the Combustion Institute, Vol. 30, (2005), pp. 2623-2629

(27) Kadowaki, S., Asymptotic analysis on high-temperature premixed flames: Instability of flame fronts under the constant-enthalpy conditions, Journal of Thermal Science and Technology, Vol. 5, (2010), pp. 1-10

(28) Kadowaki, S., Yahata, M. and Kobayashi, H., Effects of the unburned-gas temperature and Lewis number on the intrinsic instability of high-temperature premixed flames, Journal of Thermal Science and Technology, Vol. 6, (2011), pp. 376-390

(29) Joulin, G. and Clavin, P., Linear stability analysis of nonadiabatic flames: diffusional-thermal model, Combustion and Flame, Vol. 35, (1979), pp. 139-153

(30) Sohrab, S.H. and Chao, B.H., Combustion Science and Technology, Vol.38, (1984), p 245

(31) Kagan, L. and Sivashinsky, G., Self-Fragmentation of Nonadiabatic Cellular Flames, Combustion and Flame, Vol.108, (1997), pp. 220-226

(32) Buckmaster, J. and Jackson, T. L., The effects of radiation on the thermal-diffusive stability boundaries of premixed flames, Combustion Science and Technology, Vol.103, (1994), p.299

(33) Bechtold, J.K., Cui, C. and Matalon, M., The role of radiative losses in self-extinguishing and self-wrinkling flames, Proceedings of Combustion Institute, Vol.30, (2004), pp.177-184

(34) Kadowaki, S., The effects of heat loss on the burning velocity of cellular premixed flames generated by hydrodynamic and diffusive-thermal instabilities, Combustion and Flames, Vol.143, (2005), pp.174-182

(35) Sharp, G. J. and Falle, S.A.E.G., Nonlinear cellular instabilities of planar premixed flames: numerical simulations of the Reactive Navier-Stokes equations, Combustion Theory and Modeling, Vol.10, (2006), pp. 483-514

(36) Matalon, M. and Bechtold, J. K., A multi-scale approach to the propagation of non-adiabatic premixed flames, Journal of Engineering Mathematics, Vol.63, (2009), pp.309-326.

(37) Kadowaki, S., Takahashi, H. and Kobayashi, H., The effects of radiation on the dynamic behavior of cellular premixed flames generated by intrinsic instability, Proceedings of the Combustion Institute, Vol.33, (2011), pp.1153-1162.

(38) Kadowaki, S. and Thwe Thwe Aung, The effects of radiative heat loss on the diffusive-thermal instability of high-temperature premixed flames, Proceedings of the 7th International Symposium on Turbulence, Heat and Mass Transfer, (2012), p 713, DOI: 10.1615/ICHT.2012.ProcSevIntSympTurbHeatfPal.2170

(39) Block, W., Terrestrial ecosystems: Antarctica, Polar Biology, Vol.14, (1994), pp.293-300

(40) Yoon, H. I., Park, B. K., Kim, Y. and Kang, C. Y., Glaciomarine sedimentation and its palaeoclimatic implications on the Antarctic Peninsula shelf over the last 15000 years, Palaeogeography, Palaeoclimatology, Palaeoecology, Vol.185 (2002), pp.235-254.

(41) Burton, M. G., Astronomy in Antarctica, Astronomy and Astrophysics Review, Vol.18, (2010), pp.417-469, DOI: 10.1007/s00159-010-0032-2.

(42) Aprea, J. L., Two years experience in hydrogen production and use in Hope bay, Antarctica, International Journal of Hydrogen Energy, Vol.37 (2012), pp.14773-14780.

(43) Obara, S., Morizane, Y. and Morel, J., A study of small-scale energy networks of the Japanese Syowa Base in Antarctica by distributed engine generators, Applied Energy, Vol.111 (2013), pp.113-128.

(44) Tin, T., Sovacool, B. K., Blake, D., Magill, P., Naggar, S. El., Lidstrom, S., Ishizawa, K. and Berte, J., Energy efficiency and renewable energy under extreme conditions: Case studies from Antarctica, Renewable Energy, Vol.35, (2010), pp.1715-1723.

(45) Boccaletti, C., Felice, P. D. and Sanini, E., Integration of renewable power systems in an Antarctic Research station, Renewable Energy, Vol.62, (2014), pp.582-591.

(46) Thwe Thwe Aung and Kadowaki, S., The effects of unburned-gas temperature and heat loss on the diffusive-thermal instability of premixed flames, Journal of Thermal Science and Technology, Vol.8, (2013), pp.323-335.

(47) Thwe Thwe Aung and Kadowaki, S., Intrinsic instability of premixed flames in cryogenic environment (effects of unburned-gas temperature and heat loss), Transactions of the JSME (in Japanese), Vol.81, (2015), No.15-00030

(48) Sivashinsky, G.I., Diffusional-Thermal Theory of Cellular Flames, Combustion Science and Technology, Vol.15, (1977), pp. 137-146

(49) Anderson, D.A., Tannehill, J.C. and Pletcher, R.H., Computational Fluid Mechanics and Heat Transfer, Hemisphere Pub. Corp., NY, (1984), pp. 482-488

(50) Denet, B. and Haldenwang, P., Numerical Study of Thermal-Diffusive Instability of Premixed Flames, Combustion, Science and Technology, Vol. 86, (1992), pp. 199-221

(51) Kadowaki, S. and Hasegawa, T., Numerical simulation of dynamics of premixed flames: Flame instability and vortex-flame interaction, Progress in Energy and Combustion Science, Vol. 31, (2005), pp. 193-241

(52) Sivashinsky, G.I., Instabilities, pattern formation, and turbulence in flames, Annual Review of Fluid Mechanics, Vol. 15, (1983), pp. 179-199

(53) Kadowaki, S., Asymptotic analysis on high-temperature premixed flames: Instability of flame fronts under the constant-enthalpy conditions, Journal of Thermal Science and Technology, Vol. 5, pp. 1-10 (2010)

Record of Publication/Presentation after Enrollment to NUT

Name: Thwe Thwe Aung

Student ID: 10507289

	Title	Author(s)	About the Journal				Note (if any)
			Name of Journal	Volume & Page No. (for publication)	Name of Organization	Date of Issue	
1	The Effects of Unburned-gas Temperature and Heat Loss on the Diffusive-thermal Instability of Premixed Flames	Thwe Thwe Aung and Satoshi Kadowaki	Journal of Thermal Science and Technology	Vol.8, No.1, pp. 323-335	Japan Society of Mechanical Engineering and Heat Transfer Society of Japan	2013年07月10日	
2	極低温環境における予混合火炎の固有不安定性(未燃ガス温度と熱損失の影響)	トエ トエ アウン、門脇 敏	日本機械学会論文集	Vol.81, No.824, 15_00030	The Japan Society of Mechanical Engineering	2015年 04月25日	
3	The diffusive-thermal instability of premixed flames with low unburned-gas temperature under the adiabatic and non-adiabatic conditions	Thwe Thwe Aung and Satoshi Kadowaki	Mechanical Engineering Jounal		The Japan Society of Mechanical Engineering		Under review

Record of Publication/Presentation after Enrollment to NUT

Name: Thwe Thwe Aung

Student ID: 10507289

	Title	Author(s)	About the Conference				Note (if any)
			Name of Conference	Place (for presentation)	Name of Organization	Date of Issue	
1	The effects of radiative heat loss on the diffusive-thermal instability of high-temperature premixed flames	Thwe Thwe Aung and Satoshi Kadowaki	7th International Symposium on Turbulence, Heat and Mass Transfer	Sicily, Italy	International Centre for Heat and Mass Transfer	2012年09月24-27日	
2	The Effects of Unburned-Gas Temperature and Lewis Number on the Diffusive-Thermal Instability of Premixed Flames under the Low Temperature Environment: Numerical Calculations Based on the Model Equation	Thwe Thwe Aung and Satoshi Kadowaki	1st International Conference of Energy, Environment and Human Engineering	Yangon, Myanmar	Myanmar Maritime University (MMU) Nagaoka University of Technology (NUT) Nihon University (NU) Saitama University (SU) Association of Japan Myanmar Mutual Cooperation	2013年12月21-23日	
3	Effects of unburned-gas temperature and heat loss on the diffusive-thermal instability of premixed flames under the low temperature environment	Thwe Thwe Aung and Satoshi Kadowaki	The 3rd International GIGAKU Conference in Nagaoka (IGCN-2014)	Nagaoka, Japan	Nagaoka University of Technology	2014年06月20-23日	
4	The Effects of Intermediate Product on the Intrinsic Instability of Premixed Flames with High Lewis Number Reactant	Satoshi Kadowaki, Thwe Thwe Aung, Wataru Yamazaki and Hideaki Kobayashi	11th Interantional Conference on Flow Dynamics	Sendai, Japan	Institute of Fluid Science, Tohoku University	2014年10月8-10日	